# HIDRAULICA

HYDRAULICS-PNEUMATICS-TRIBOLOGY-ECOLOGY-SENSORICS-MECHATRONICS

2024
December
No. 4

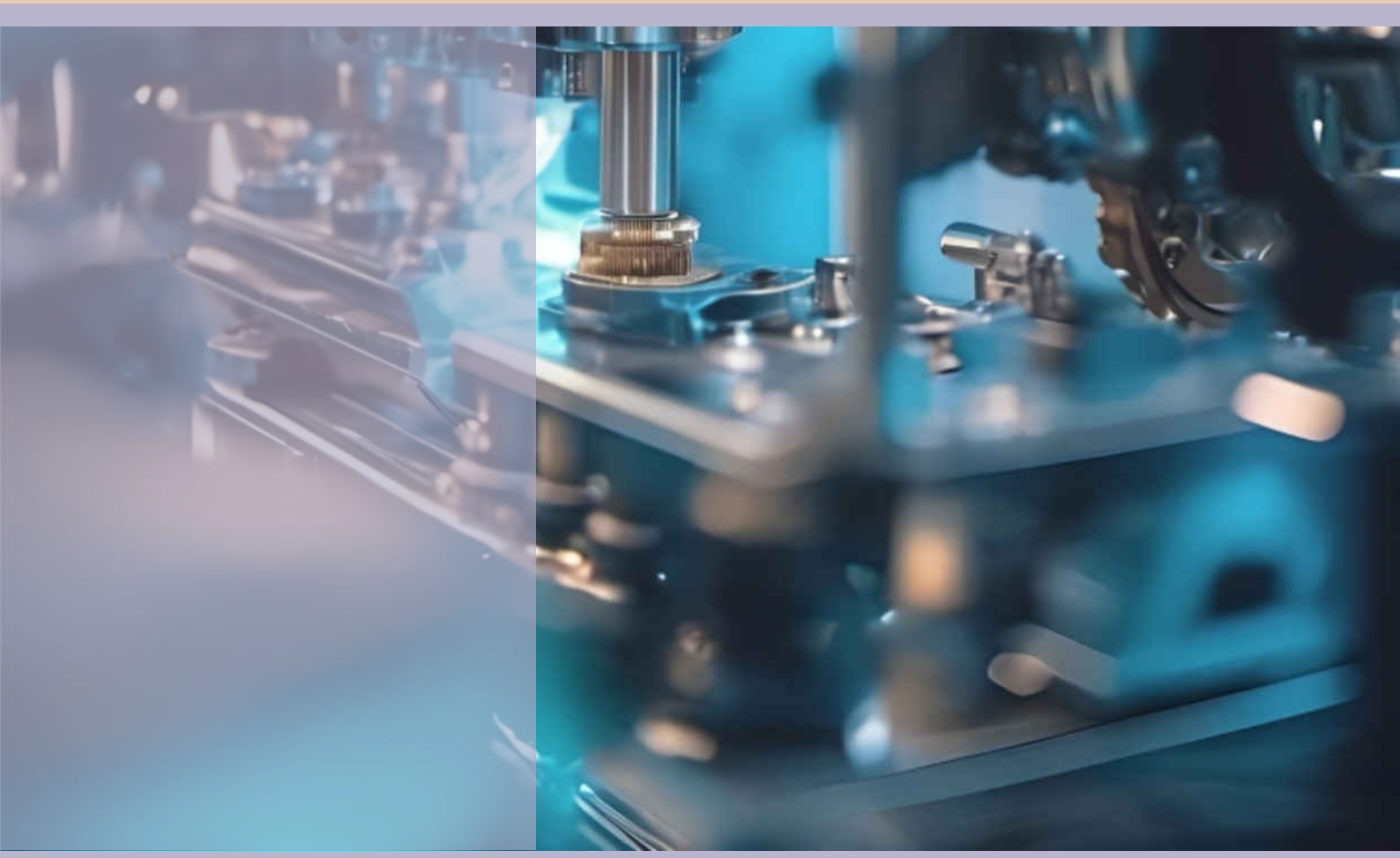

ISSN 1453 - 7303
ISSN-L 1453 - 7303

https://hidraulica.fluidas.ro

## CONTENTS

***Published by:***
***Hydraulics and Pneumatics Research Institute, Bucharest-Romania***
Address: 14 Cuţitul de Argint, district 4, Bucharest, 040558, Romania
Phone: +40 21 336 39 91; Fax: +40 21 337 30 40; e-Mail: ihp@fluidas.ro; Web: www.ihp.ro
***with support from:***
***National Professional Association of Hydraulics and Pneumatics in Romania - FLUIDAS***
e-Mail: fluidas@fluidas.ro; Web: www.fluidas.ro

**HIDRAULICA Magazine** is indexed by international databases

**ISSN 1453 – 7303; ISSN – L 1453 – 7303**

## EDITORIAL

# Automatizarea Industrială Avansată și Colaborativă – Transformarea Industriei din România

Dr. Ing. Gabriela Matache
REDACTOR ȘEF

Industria contemporană se află într-un proces de transformare profundă, în care automatizarea joacă un rol central, redefinind standardele de eficiență și adaptabilitate. În România, numeroase companii din diverse sectoare integrează tehnologii avansate de automatizare, utilizând soluții hidraulice și pneumatice care contribuie la optimizarea proceselor și la adaptarea acestora la cerințele dinamice ale pieței.

O tendință emergentă și promițătoare în acest context este utilizarea sistemelor colaborative, concepute pentru a funcționa în sinergie cu operatorii umani, menținând standarde ridicate de siguranță și performanță.

Un exemplu relevant din peisajul industrial românesc este reprezentat de utilizarea roboților colaborativi în zone industriale precum Pitești, Cluj-Napoca sau Timișoara. În sectorul auto, de exemplu, acești roboți, echipați cu sisteme pneumatice de înaltă precizie, sunt folosiți pentru asamblarea componentelor sensibile, cum ar fi circuitele electronice sau piesele pentru sisteme de direcție asistată. Implementarea acestor tehnologii nu doar că minimizează erorile de fabricație, dar oferă și o flexibilitate sporită în liniile de producție. În cadrul uzinei Dacia de la Mioveni, automatizarea avansată a permis reducerea timpului de asamblare, menținând în același timp standarde riguroase de calitate.

În domeniul echipamentelor grele și al construcțiilor, soluțiile hidraulice rămân elemente fundamentale. Integrarea automatizării cu senzori și tehnologii de conectivitate a facilitat dezvoltarea utilajelor inteligente, capabile să răspundă în mod adaptiv la condiții variabile de operare. De exemplu, în producția de tractoare forestiere din România, exista companii care au implementat sisteme hidraulice avansate, contribuind la creșterea eficienței operaționale și la reducerea consumului de combustibil.

Totodată, automatizarea colaborativă și utilizarea actuatoarelor pneumatice precise au înregistrat progrese remarcabile în industrii precum cea alimentară și farmaceutică. În unitățile de procesare a produselor alimentare, roboții colaborativi, echipați cu tehnologii pneumatice, sunt folosiți pentru ambalarea și manipularea produselor, asigurând conformitatea cu standardele stricte de igienă și siguranță.

Deși implementarea automatizării industriale avansate în România cunoaște progrese semnificative, există și provocări notabile. Principalele dificultăți sunt reprezentate de lipsa personalului calificat pentru operarea și întreținerea acestor sisteme, precum și de investițiile inițiale considerabile, care pot fi un obstacol pentru întreprinderile mici și mijlocii.

Cu toate acestea, perspectivele sunt încurajatoare. Instituții de învățământ superior, precum universitățile tehnice din București și Cluj-Napoca, colaborează cu mediul industrial pentru formarea specialiștilor în domeniile mecatronicii și automatizării. În plus, accesul la fondurile europene destinate digitalizării industriei creează oportunități semnificative pentru companiile care doresc să adopte soluții moderne și să-și modernizeze procesele de producție.

În concluzie, automatizarea industrială avansată și colaborativă reprezintă un pilon esențial pentru viitorul industriei românești. Prin utilizarea roboților colaborativi, a sistemelor hidraulice și pneumatice inteligente, țara noastră dispune de premisele necesare pentru a deveni un hub regional de inovație tehnologică. Susținerea unei educații tehnice de calitate și implementarea unor politici care să stimuleze modernizarea industriei vor accelera această tranziție, conturând o industrie mai eficientă, sigură și sustenabilă.

## EDITORIAL

# Advanced and Collaborative Industrial Automation – Transforming Romania's Industry

Ph.D.Eng. Gabriela Matache
EDITOR-IN-CHIEF

The contemporary industry is undergoing a profound transformation, with automation playing a central role in redefining standards of efficiency and adaptability. In Romania, numerous companies across various sectors are integrating advanced automation technologies, leveraging hydraulic and pneumatic solutions that optimize processes and adapt them to the dynamic demands of the market.

A promising emerging trend in this context is the adoption of collaborative systems designed to work in synergy with human operators while maintaining high standards of safety and performance.

A relevant example from the Romanian industrial landscape is the use of collaborative robots in industrial hubs such as Pitești, Cluj-Napoca, and Timișoara. In the automotive sector, for instance, these robots, equipped with high-precision pneumatic systems, are utilized for assembling sensitive components, such as electronic circuits or parts for power steering systems. The implementation of such technologies not only minimizes manufacturing errors but also provides enhanced flexibility in production lines. At the Dacia plant in Mioveni, advanced automation has enabled the reduction of assembly times while upholding rigorous quality standards.

In the field of heavy equipment and construction, hydraulic solutions remain fundamental. The integration of automation with sensors and connectivity technologies has facilitated the development of intelligent machinery capable of adaptively responding to variable operating conditions. For example, in the production of forestry tractors in Romania, there are companies that have implemented advanced hydraulic systems, contributing to increased operational efficiency and reduced fuel consumption.

Moreover, collaborative automation and the use of precise pneumatic actuators have achieved remarkable progress in industries such as food processing and pharmaceuticals. In food processing facilities, collaborative robots equipped with pneumatic technologies are employed for packaging and handling products, ensuring compliance with strict hygiene and safety standards.

Although the implementation of advanced industrial automation in Romania has seen significant progress, notable challenges persist. The primary difficulties include a lack of skilled personnel to operate and maintain these systems, as well as substantial initial investments, which can pose a barrier for small and medium-sized enterprises.

However, the outlook is encouraging. Institutions of higher education, such as the technical universities in Bucharest and Cluj-Napoca, collaborate with the industrial sector to train specialists in mechatronics and automation. Furthermore, access to European funds dedicated to industry digitization creates significant opportunities for companies seeking to adopt modern solutions and upgrade their production processes.

In conclusion, advanced and collaborative industrial automation represents a cornerstone for the future of Romanian industry. By employing collaborative robots and intelligent hydraulic and pneumatic systems, the country has the necessary prerequisites to become a regional hub for technological innovation. Supporting quality technical education and implementing policies that encourage industrial modernization will accelerate this transition, shaping an industry that is more efficient, safer, and more sustainable.

# New Developments in Intelligent Diagnostic Methods for Hydraulic Piston Pumps Faults

Assoc. Prof. PhD. Eng. **Ștefan ŢĂLU**[1,*]

[1] Technical University of Cluj-Napoca, The Directorate of Research, Development and Innovation Management (DMCDI), Constantin Daicoviciu Street, no. 15, Cluj-Napoca, 400020, Cluj county, Romania

* stefan_ta@yahoo.com

***Abstract:*** *As industries increasingly embrace digital transformation, the need for effective fault diagnosis in hydraulic piston pumps (HPPs) has grown in importance. HPPs are critical components across various sectors, including aerospace and manufacturing, where their reliability directly impacts system performance. The reliability of these pumps affects not only operational productivity but also the safety of the entire system. As a result, the development of diagnostic methods for identifying and addressing faults in HPPs has become a crucial area of research. This article explores the latest advancements in intelligent diagnostic techniques for fault detection in HPPs, highlighting their effectiveness and limitations. By providing insights into these advancements, this review aims to contribute to safer and more reliable hydraulic systems in modern operational environments.*

***Keywords:*** *Diagnostic methods, hydraulic piston pump, intelligent maintenance, intelligent fault detection and diagnosis*

## 1. Introduction

Hydraulic systems are essential to industrial production and manufacturing, and mathematical modeling and simulation of these systems provide valuable insights into their performance [1-4]. At the heart of these systems, the hydraulic pump plays a critical role by converting mechanical energy into hydraulic energy to deliver pressurized oil throughout the system [5-7].
Hydraulic piston pumps (HPPs) are crucial components in various industrial applications, including construction, manufacturing, and automotive systems, where they are utilized to convert mechanical energy into hydraulic energy [8]. The fundamental principle of operation for HPPs lies in the movement of pistons within cylinders, which creates pressure through the displacement of hydraulic fluid. This mechanism allows for efficient power transmission over considerable distances, making HPPs an essential element in hydraulic systems.
HPPs consist of numerous intricate components, including valves, drive mechanisms, cylinders and pistons, seals and gaskets, fluid ports, and a supporting structure. Recent developments in materials technology, along with innovations in precision machining techniques, contemporary design processes, and simulation methods, have greatly improved the performance, durability, and resistance of hydraulic piston pumps to wear and corrosion. On the other hand, these pumps operate under challenging conditions characterized by high temperatures, significant pressure levels, and fluctuating loads, which can put considerable stress on their internal components. These extreme operational environments often lead to typical failures that are difficult to diagnose quickly, as pinpointing the exact cause and location of faults can be complex. Common issues include wear and tear, cavitation, leakage, and contamination of the hydraulic fluid. These faults can lead to significant downtime, reduced performance, and increased maintenance costs.
As the industry advances, HPPs are being designed with greater precision and increasingly intricate structures, underscoring the need for efficient, accurate, and intelligent fault diagnosis technologies. However, challenges remain in fault identification due to environmental influences, multiple interfering factors, and the inherent complexity of various operational tasks. Traditional diagnostic methods often relied on visual inspections and routine maintenance checks; however, these approaches can be time-consuming and may not detect early signs of failure. Recent advancements in diagnostic technologies have introduced new methodologies and innovations that enhance the ability to detect and diagnose faults in HPPs.

Over the past few decades, a multitude of studies have focused on reviewing and analyzing the methodologies employed in the recognition of faults within hydraulic piston pumps (HPPs). These studies have made significant strides in categorizing fault diagnosis approaches according to the various types of signals utilized, including vibration, acoustic, thermal, and pressure signals. Despite this progress, there is a notable deficiency in detailed classifications and comparative analyses that critically evaluate the efficacy and applicability of these diagnostic methods across different contexts, as well as delineate the strengths and weaknesses of current diagnostic techniques. In light of these considerations, this review aims to provide a comprehensive overview of the latest developments in intelligent diagnostic techniques for HPPs, examining existing methodologies, evaluating their effectiveness in various operational contexts, and discussing future directions for research and implementation.

## 2. Research methodology

Hydraulic piston pumps (HPPs) can be categorized based on their structural designs into two primary types: radial piston pumps and axial piston pumps [8,9]. Within these broad classifications, axial piston pumps are of two types namely swash plate type and bent axis type (fig. 1). This classification highlights the variations in design and function that influence the performance and application of HPPs across various industrial contexts. A survey was conducted on diagnostic methods for hydraulic piston pump faults in the scientific literature from 2011 to 2024.

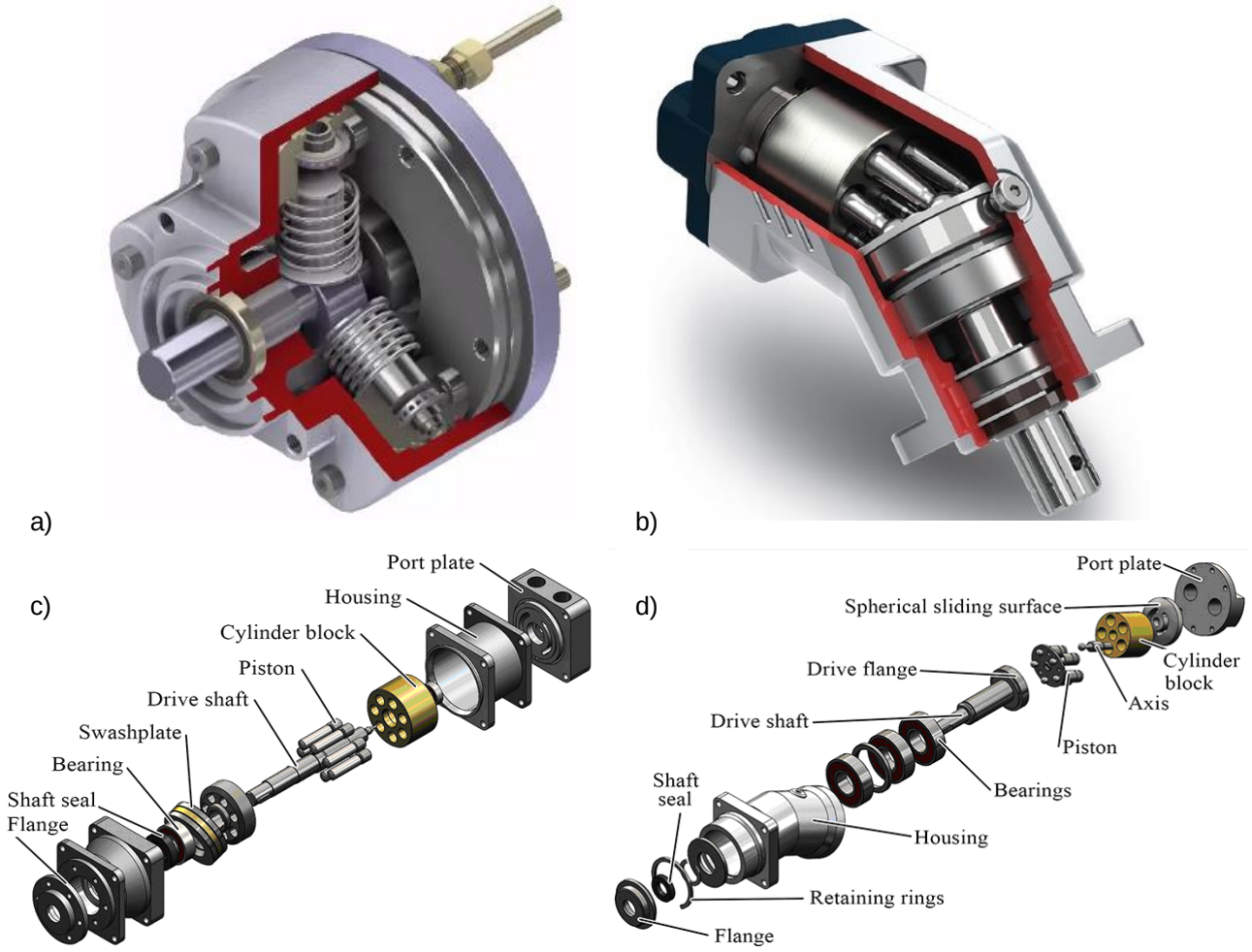


**Fig. 1.** a) Radial piston pump, b) axial piston pump, c) axial piston pump - swash plate type, d) axial piston pump – bent axis type.

### 2.1 The fault diagnosis methods of hydraulic piston pumps

Fault diagnosis methods for hydraulic piston pump faults focus on identifying, classifying, and evaluating various types of pump malfunctions by analyzing the system's signals and operating data. Currently, fault identification methods can be divided into three main categories: a) traditional

intelligent fault diagnosis methods; b) modern intelligent fault diagnosis methods; and c) combined intelligent fault diagnosis methods [9].

a) Traditional intelligent fault diagnosis method rely on well-established techniques that often use physical models, statistical analysis, and signal processing to identify faults [9,10-13]. Key approaches include: vibration analysis, acoustic emission, pressure signal analysis, thermal analysis. Traditional methods often use threshold-based decision-making, where measurements are compared to predefined limits. Deviations beyond these thresholds trigger alerts for potential faults. While effective, these methods may have limitations in detecting complex faults, particularly when multiple faults are present [14-17].

b) Modern intelligent fault diagnosis methods harness advanced computing power and data analytics, using machine learning, deep learning, and artificial intelligence (AI) to enhance fault detection and diagnosis accuracy [18-20]. Some key techniques include: machine learning algorithms, deep learning techniques, data-driven models, signal feature extraction and processing. Modern methods can recognize intricate fault patterns and adapt over time as new data becomes available. However, they require large datasets and computational resources, and implementation can be complex [21-24].

c) Combined intelligent fault diagnosis methods integrate traditional and modern techniques to improve fault diagnosis accuracy and robustness. By combining the strengths of physical models with data-driven approaches, these methods offer a balanced solution [25-29]. Some key techniques include: model-based and data-driven fusion, multi-sensor data fusion, ensemble learning, adaptive thresholding. Combined methods are particularly valuable in situations where high fault-diagnosis accuracy is required but data availability or computational resources are limited. They offer a comprehensive approach by leveraging both theoretical knowledge and real-world data, making them suitable for complex fault scenarios in hydraulic piston pumps [30-34].

### 2.2 Advanced techniques for intelligent fault detection and diagnosis of hydraulic piston pumps

Intelligent fault detection and diagnosis methods, leveraging deep learning and machine learning algorithms, enable the automatic identification of faults in hydraulic piston pumps through the analysis of complex signal data. With capabilities like adaptive learning, feature extraction, and model optimization, these methods enhance diagnostic accuracy and reliability, even in challenging conditions such as small sample sizes and noisy environments.

The fault diagnosis method utilizing Siamese neural networks proposed by Gao et al. [20] aimed to overcome the challenges of low accuracy and underfitting often encountered in traditional deep neural networks, particularly when applied to small sample sizes. The Siamese subnetwork was constructed with convolutional and pooling layers, automatically extracting meaningful low-dimensional features from the raw vibration signals. By using Euclidean distance to quantify the similarity between input sample pairs, this method effectively augmented the training dataset, facilitating the training of the SNN model to differentiate accurately among health states, and improving diagnostic accuracy even in scenarios with limited data.

Wang et al. [19] introduced a fault detection method based on Deep Belief Networks (DBNs) to enhance reliability in axial piston pumps, specifically targeting the complex issue of identifying multiple, often ambiguous fault types. This approach begins by processing raw signal data from the time, frequency, and time-frequency domains, enabling the extraction of robust features for both training and testing samples. These samples are then classified using DBNs, which are constructed from stacked Restricted Boltzmann Machines (RBMs) designed to automatically learn intricate fault features. By using this deep learning structure, the method reduces reliance on manually engineered features, allowing for more accurate fault pattern recognition in challenging diagnostic conditions. The classification results demonstrated a high accuracy rate of 97.40%, which significantly outperformed conventional models such as Support Vector Machines (SVM) and Artificial Neural Networks (ANN). This approach proved effective in cases where the underlying fault mechanisms were poorly understood, showcasing its potential as a robust tool for complex fault detection in hydraulic systems.

Xiao et al. [24] proposed an innovative hybrid approach, Multipoint Optimal Minimum Entropy Deconvolution Adjusted - Teager Energy Operator (MOMEDA-TEO) method, specifically

developed to isolate fault impulses from axial piston pump bearings, where periodic vibrations often mask fault signals. This method enhances periodic impulses through an optimized MOMEDA framework, enabling fault frequency extraction via Teager Energy Operator (TEO) demodulation. On the other hand, MOMEDA has been adopted for its ability to directly yield an optimal filter solution without requiring iterative procedures. Unlike Maximum Correlated Kurtosis Deconvolution (MCKD), MOMEDA employs a maximum D-norm rule, allowing it to analyze vibration signals with a non-integer fault period, thus eliminating the need for resampling. Experimental validation indicated that this hybrid approach significantly improved both accuracy and processing speed compared to traditional techniques, demonstrating its effectiveness in extracting fault impulses and advancing fault diagnostics in hydraulic systems.

Tang et al. [21] proposed a novel integrated intelligent method for fault diagnosis of hydraulic axial piston pumps. The approach begins with the transformation of vibration signals into time-frequency images using continuous wavelet transform (CWT), which enables the effective extraction of key features. These transformed images serve as the input for a newly designed deep Convolutional Neural Network (CNN) model aimed at accurately classifying fault types. To better understand the potential learning dynamics within the various layers of the CNN, t-distributed stochastic neighbor embedding (t-SNE) was applied to visualize the reduced features, offering insights into the relationships between fault patterns captured by the network. Experimental testing validated the proposed method's effectiveness and stability, showing high accuracy in identifying various fault types in hydraulic axial piston pumps.

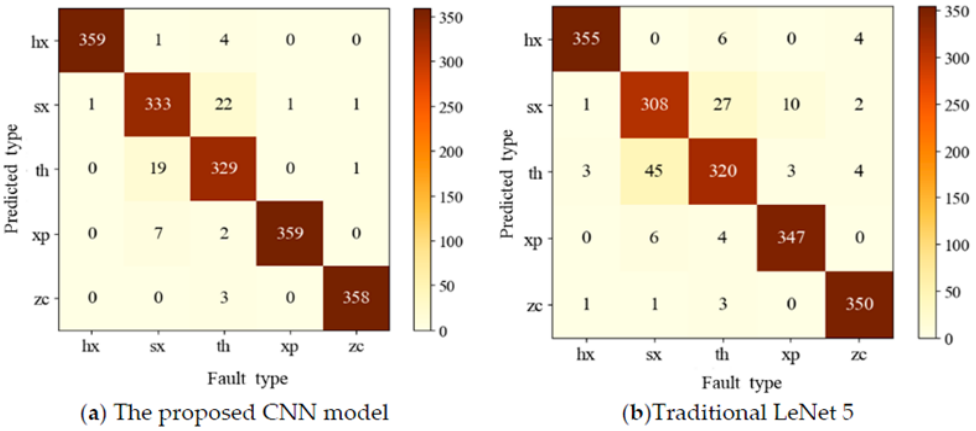


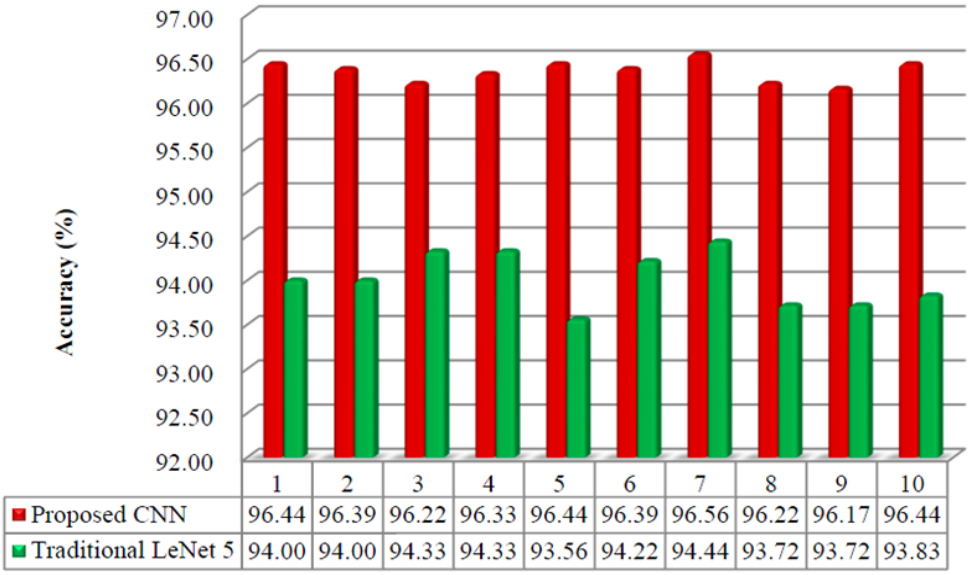


| | 1 | 2 | 3 | 4 | 5 | 6 | 7 | 8 | 9 | 10 |
|---|---|---|---|---|---|---|---|---|---|---|
| Proposed CNN | 96.44 | 96.39 | 96.22 | 96.33 | 96.44 | 96.39 | 96.56 | 96.22 | 96.17 | 96.44 |
| Traditional LeNet 5 | 94.00 | 94.00 | 94.33 | 94.33 | 93.56 | 94.22 | 94.44 | 93.72 | 93.72 | 93.83 |

**Fig. 2.** The confusion matrix of the testing samples on CNN in the seventh trial: a) The proposed CNN model, b) Traditional LeNet 5. c) The comparison between the proposed CNN and traditional LeNet 5. Reprinted from ref. [21] with permission of MDPI AG publisher.

Zhu et al. [35] introduced an innovative approach to hydraulic pump fault diagnosis using stacked autoencoders (SAE), a type of deep learning architecture renowned for its robust learning and representation capabilities. This method addresses the challenge of manual feature extraction, which is not only time-consuming but also prone to subjective bias. By leveraging SAE, the process is fully automated, with the model trained directly on raw vibration signals, eliminating the need for manually crafted features. To enhance the model's performance, especially when working with small training datasets, the researchers integrated the rectified linear unit (ReLU) activation function and a Dropout strategy. These additions help mitigate issues like gradient vanishing and overfitting, allowing the model to generalize better and learn more effectively from limited data. The SAE's ability to learn hierarchical representations of the vibration signals ensures that it can automatically capture complex patterns associated with various fault conditions in the hydraulic pump. Through experimental validation, the proposed method demonstrated superior fault recognition capabilities when compared to traditional machine learning techniques, such as backpropagation (BP) and support vector machine (SVM). In particular, SAE proved effective in situations where the training dataset was small, achieving high accuracy in recognizing hydraulic pump conditions. This is a significant advancement in the field, as it ensures reliable diagnosis even in real-world scenarios where data is often limited. Moreover, the SAE's ability to operate without the need for prior feature extraction makes it a more efficient and less error-prone alternative to conventional methods. These results highlight the SAE's potential to improve the reliability and accuracy of hydraulic pump fault diagnosis, making it a promising tool for engineering applications.

Tang et al. [36] proposed an advanced intelligent fault diagnosis method for hydraulic piston pumps, utilizing a CNN enhanced with an adaptive learning rate strategy. This approach is designed to improve diagnostic accuracy by overcoming the limitations of traditional CNN models in handling diverse fault types. The first step in the process involves transforming three raw signals - vibration, pressure, and sound - into two-dimensional time-frequency images using CWT. This transformation allows the model to better capture the complex characteristics of these signals, which are critical for accurate fault detection. Next, the researchers developed a modified CNN architecture that incorporates an adaptive learning rate mechanism to optimize the training process. This improvement enhances the model's ability to converge efficiently while maintaining high performance, particularly when dealing with varying fault conditions. To further enhance the interpretability of the learned features, t-distributed stochastic neighbor embedding (t-SNE) is employed to visualize the feature distribution across the main layers of the CNN model. This visualization helps in understanding how the CNN distinguishes between different fault types. The effectiveness of the proposed method was evaluated using a confusion matrix, which provides a comprehensive analysis of the classification accuracy for each fault type. Experimental results demonstrated that the CNN model with the adaptive learning rate outperforms the original CNN model, achieving higher diagnostic accuracy.

Tang et al. [37] proposed an innovative method for fault diagnosis in hydraulic piston pumps by combining Bayesian optimization (BO) with an improved CNN for fault feature extraction and classification. In this approach, acoustic signals were initially transformed into time-frequency distributions using CWT, allowing for a more detailed representation of the signal characteristics essential for accurate fault detection. The process began with the construction of a preliminary CNN model, where the initial hyperparameters (HPs) were set, and the range of each hyperparameter to be optimized was identified. Subsequently, BO was applied to intelligently search for the optimal combination of hyperparameters, aiming to improve the CNN's performance by fine-tuning the learning process. This step ensured that the model was well-suited to handle the complexities of hydraulic piston pump fault diagnosis. The resulting model, referred to as CNN-BO, integrated the strengths of both CNNs for feature extraction and BO for hyperparameter optimization, yielding a more efficient and effective fault detection system. The diagnostic performance of the CNN-BO model was thoroughly evaluated using a confusion matrix, which provided insights into the accuracy of fault classification for various fault types. Additionally, t-distributed stochastic neighbor embedding (t-SNE) was employed to visualize the learned features and assess the model's ability to distinguish between different fault conditions. The comparative

analysis demonstrated that CNN-BO significantly outperformed traditional models, offering both higher classification accuracy and greater robustness in fault diagnosis.
Tables 1–4 provide detailed insights into various intelligent fault diagnosis methods, covering the types of algorithms, fault categories, and unique features or enhancements associated with each approach. These tables highlight advancements in adaptive learning, feature extraction, and model optimization techniques, showcasing how these methods perform under specific operational conditions.

**Table 1:** Algorithm performance and application scope

| Algorithm type | Fault type | Accuracy (%) | Application complexity | Optimal conditions | Suitable signal types |
|---|---|---|---|---|---|
| Spatial alignment algorithm. (Ref. [18]). | Loose slippers, sliding wear | 94 | Moderate | High-frequency data | Vibration |
| Twin neural networks. (Ref. [20]). | Sliding wear, valve plate wear | 91 | High | Small dataset environments | Acoustic |
| Deep forest. (Ref. [38]). | Bearing faults | 95 | Moderate | High-dimensional feature data | Sensor fusion |
| Deep confidence network. (Ref. [19]). | Multiple fault types | 93 | High | Multi-fault diagnosis | Acoustic, vibration |
| Minimum entropy deconvolution. (Ref. [24]). | Bearing faults | 90 | Low | Low signal-to-noise ratio | Vibration |
| Stacked self-encoder. (Ref. [35]). | Cylinder faults, valve plate wear | 89 | Moderate | Imbalanced data distribution | Vibration, temperature |
| Sparse self-encoder. (Ref. [39]). | Leakage faults | 88 | High | High-dimensional signals | Pressure, temperature |
| Convolutional neural network. (Ref. [22,23,37]). | Various mechanical faults | 96 | High | Complex fault patterns | Multi-sensor data |

**Table 2:** Fault sensitivity and detection accuracy

| Algorithm type | Sensitivity (%) | Detection accuracy (%) | Robustness (%) | Noise mitigation techniques | Noise tolerance level |
|---|---|---|---|---|---|
| Spatial alignment algorithm | 92 | 94 | 85 | Low-pass filtering | Low |
| Twin neural networks | 90 | 91 | 88 | Data augmentation | Medium |
| Deep forest | 94 | 95 | 90 | Ensemble techniques | High |
| Deep confidence network | 93 | 93 | 92 | Signal processing pre-training | High |
| Minimum entropy deconvolution | 89 | 90 | 87 | Deconvolution | Medium |
| Stacked self-encoder | 91 | 89 | 89 | Feature extraction optimization | High |
| Sparse self-encoder | 88 | 88 | 90 | Sparse representation | High |
| Convolutional neural network | 96 | 96 | 93 | Adaptive learning techniques | Very high |

**Table 3:** Adaptability to different industrial applications

| Algorithm type | Applicable industry | Adaptation to environmental changes | Adaptability score | Key strengths in application | Real-world application examples |
|---|---|---|---|---|---|
| Spatial alignment algorithm | Automotive | Medium | 7 | High alignment accuracy | Railway axles, car suspension systems |
| Twin neural networks | Aerospace | High | 8 | Handles small datasets well | Aircraft hydraulic systems, pumps |
| Deep forest | Manufacturing | Very High | 9 | Strong feature extraction | Industrial robots, conveyor belts |
| Deep confidence network | Oil and gas | High | 8 | Handles multi-fault scenarios | Power plants, wind turbines |
| Minimum entropy deconvolution | Energy | Medium | 6 | Low computational load | Large motor machinery, generators |
| Stacked self-encoder | Industrial machinery | Medium | 7 | Suitable for imbalanced data | Factory automation, mechanical presses |
| Sparse self-encoder | Hydraulics | High | 8 | High robustness | Oil rigs, hydraulic presses |
| Convolutional neural network | Multi-industry | Very high | 9 | Strong adaptive learning | Automobile engines, marine engines |

**Table 4:** Algorithm compatibility with data sources

| Algorithm type | Primary data source | Secondary data sources | Data compatibility (%) | Data preprocessing requirement | Scalability to large datasets |
|---|---|---|---|---|---|
| Spatial alignment algorithm | Vibration sensors | Optical sensors | 85 | Minimal (filtering only) | Moderate |
| Twin neural networks | Acoustic sensors | Pressure sensors | 90 | High (data augmentation needed) | High |
| Deep forest | Vibration and acoustic sensors | Visual inspections | 87 | Moderate (feature selection) | Moderate |
| Deep confidence network | Multi-sensor data | Environmental condition sensors | 92 | High (normalization and scaling) | High |
| Minimum entropy deconvolution | Vibration sensors | Speed sensors | 80 | Low (signal filtering) | Moderate |
| Stacked self-encoder | Temperature sensors | Vibration and thermal sensors | 88 | Moderate (dimensional reduction) | High |
| Sparse self-encoder | Pressure sensors | Flow rate sensors | 89 | Moderate (feature extraction) | High |
| Convolutional neural network | Multi-sensor arrays | Optical, thermal, pressure sensors | 94 | High (complex data transformation) | Very high |

Table 1 details algorithm performance and application scope, presenting a range of methods -such as spatial alignment, twin neural networks, and deep forest - that cater to specific fault types and application complexities. For instance, CNNs excel in handling complex fault patterns across multi-sensor data with an accuracy of 96%, making them suitable for diverse mechanical faults in multi-industry settings. Meanwhile, methods like minimum entropy deconvolution, with lower computational requirements, are particularly effective in vibration data analysis under low signal-to-noise conditions.
Table 2 compares fault sensitivity and detection accuracy among these algorithms, emphasizing their robustness and noise mitigation capabilities. CNNs lead in noise tolerance and detection accuracy at 96%, aided by adaptive learning techniques, whereas spatial alignment algorithms, though highly accurate at 94%, exhibit lower noise tolerance, mitigated by low-pass filtering. This table highlights how specific noise mitigation techniques - like ensemble methods in deep forest algorithms - enhance robustness in complex industrial environments.
Table 3 assesses the adaptability of these algorithms to various industrial applications. CNNs and deep forest algorithms show exceptional adaptability, with applications spanning automotive engines, manufacturing robots, and hydraulic systems. In contrast, spatial alignment algorithms, while beneficial in automotive applications, achieve a moderate adaptability score due to limited alignment with rapidly changing conditions. This table underscores the versatility of deep learning methods in adapting to environmental shifts, such as those encountered in the aerospace and oil and gas industries.
Table 4 focuses on algorithm compatibility with different data sources and their scalability to large datasets. CNNs and deep confidence networks demonstrate high compatibility with multi-sensor data, requiring advanced preprocessing but offering scalability in handling large datasets. In contrast, algorithms like minimum entropy deconvolution, which primarily rely on vibration sensors, offer lower data compatibility and scalability, suitable for moderate applications with minimal preprocessing needs.

## 3. Future challenges in predicting intelligent fault detection and diagnosis for hydraulic piston pumps

Predicting intelligent fault detection in hydraulic piston pumps presents unique challenges due to the complexity of their mechanical structure. One primary challenge is managing the wide variety of potential faults, including wear, leakage, and cavitation, each requiring specialized detection methods. Hydraulic piston pumps operate under varying loads and speeds, creating fluctuations that can obscure early fault indicators. As a result, developing algorithms that can accurately diagnose faults despite environmental noise and signal interference is crucial. Existing algorithms often require high-quality, labeled data, which can be challenging to obtain consistently in industrial settings, especially when small sample sizes are common in real-world data for hydraulic systems. This leads to difficulties in training robust, generalizable models that can reliably detect faults across different operating conditions. Achieving a balance between high detection accuracy and computational efficiency is essential for real-time fault diagnosis. Another challenge is improving the scalability of intelligent fault detection algorithms to accommodate large datasets from multi-sensor systems, which are increasingly being deployed to monitor HPPs. As the number of sensors used in hydraulic systems grows, managing and integrating data from diverse sources becomes progressively more complex. Additionally, real-world hydraulic systems face non-stationary conditions that affect fault symptoms over time, further complicating the prediction accuracy. Ensuring the adaptability of fault diagnosis models across different HPPs models and operating environments remains a critical challenge that requires continuous refinement. Integrating predictive maintenance insights with fault diagnosis systems will require advancements in data analytics and real-time processing. Moreover, fault diagnosis models must become more robust to handle sudden fluctuations in hydraulic systems without misclassifying normal operations as faults. This is especially important when considering the deployment of intelligent diagnosis in harsh environments, such as high-temperature or high-pressure conditions, which requires durable sensor technology that can withstand these extreme conditions. Improving fault detection for complex faults, where multiple components degrade simultaneously, is another crucial area for

future research. Real-time, in-situ fault detection will depend on reducing the computational load of algorithms without sacrificing accuracy. To meet the demands of advancing hydraulic systems, fault detection methods must incorporate machine learning techniques that require minimal retraining for sustained accuracy. Integrating these systems within industrial IoT networks will necessitate secure, interoperable data transfer, fostering a comprehensive strategy for predictive maintenance and fault management across diverse industries.

## 4. Conclusions

This review has underscored recent advancements in intelligent diagnostic methods for hydraulic piston pump faults, which have notably enhanced fault detection accuracy, predictive capabilities, and real-time monitoring. By leveraging machine learning, advanced sensor technologies, and data analytics, these methods are better able to diagnose issues such as wear, leakage, and cavitation in hydraulic systems, driving improvements in operational efficiency. However, challenges remain, particularly in managing noise interference, handling limited data in rare-fault scenarios, and scaling algorithms for broader industrial applications. Future research must address these limitations by focusing on increasing model adaptability across diverse and dynamic operating conditions, optimizing computational efficiency to facilitate real-time applications, and integrating data from multiple sensors to enhance robustness. Additionally, the incorporation of intelligent diagnostic methods into industrial IoT ecosystems will be critical, as this integration enables seamless predictive maintenance, fostering more efficient, automated maintenance strategies.

**Conflicts of Interest**: The author declares no conflict of interest.
**ORCID**: Ştefan Ţălu, https://orcid.org/0000-0003-1311-7657.

### References

[1] Diaconu, Mihai, Tiberiu Axinte, Cătălin Frățilă, Paul Bocănete, and Remus Cojocaru. "Design and study of hydraulic systems." *Hidraulica Magazine*, no. 2 (June 2021): 49-56.
[2] Bucureșteanu, Anca. "Mathematical modeling and simulation of the operation of hydraulic systems with resistive adjustment." *Hidraulica Magazine*, no. 2 (June 2022): 15-22.
[3] Debeleac, Carmen Nicoleta. "About computer tools available for dynamic analysis of mechanic and hydraulic systems of the loader bucket." *Hidraulica Magazine*, no. 4 (December 2022): 19-24.
[4] Marinescu, Alexandru-Daniel, Teodor Costinel Popescu, Alina-Iolanda Popescu, and Carmen-Anca Safta. "Approaches of the best maintenance strategies applied to hydraulic drive systems." *Hidraulica Magazine*, no. 4 (December 2016): 63-68.
[5] Ţălu, Mihai, Ştefan Ţălu, and Mircea Rădulescu*. Fluid Mechanics. Volumetric and hydrodynamic machines. Theory and simulation*. Craiova, Universitaria Publishing House, 2011.
[6] Darshan, Katgeri, and Basavaraj Hubballi. "A review & progress on digital hydraulic pumps and valves." *Hidraulica Magazine*, no. 1 (2019): 116-123.
[7] Ţălu, Ştefan. "Assessing the remaining useful life of hydraulic pumps: a review." *Hidraulica Magazine*, no. 3 (September 2024): 7-18.
[8] Zhang, Qin. *Basics of Hydraulic Systems*, 2nd Edition. Boca Raton, CRC Press, 2019.
[9] Zhu, Yong, Qingyi Wu, Shengnan Tang, Boo Cheong Khoo, and Zhengxi Chang. "Intelligent Fault Diagnosis Methods for Hydraulic Piston Pumps: A Review." *Journal of Marine Science and Engineering* 11, no. 8 (2023): 1609. https://doi.org/10.3390/jmse11081609.
[10] Wen, C., F. Lv, Z. Bao, and M. Liu. "A review of data driven-based incipient fault diagnosis." *Acta Automatica Sinica* 42 (2016): 1285–1299.
[11] Ma, Zhonghai, Shaoping Wang, Jian Shi, Tongyang Li, and Xingjian Wang. "Fault diagnosis of an intelligent hydraulic pump based on a nonlinear unknown input observer." *Chinese Journal of Aeronautics* 31, no. 2 (February 2018): 385–394.
[12] Li, Weijun, Hui Li, Sai Gu, and Tao Chen. "Process fault diagnosis with model- and knowledge-based approaches: Advances and opportunities." *Control Engineering Practice* 105 (December 2020): 104637. https://doi.org/10.1016/j.conengprac.2020.104637.
[13] Shao, Y., X. Yuan, C. Zhang, Y. Song, and Q. Xu. "A novel fault diagnosis algorithm for rolling bearings based on one-dimensional convolutional neural network and INPSO-SVM." *Applied Sciences* 10, no. 12 (2020): 4303.
[14] Bedotti, A., M. Pastori, F. Scolari, and P. Casoli. "Dynamic modelling of the swash plate of a hydraulic axial piston pump for condition monitoring applications." *Energy Procedia* 148 (August 2018) 266–273.

[15] Bensaad, D., A. Soualhi, and F. Guillet. "A new leaky piston identification method in an axial piston pump based on the extended Kalman filter." *Measurement* 148 (December 2019): 106921.
[16] Chao, Qun, Junhui Zhang, Bing Xu, Qiannan Wang, Fei Lyu, and Kun Li. "Integrated slipper retainer mechanism to eliminate slipper wear in high-speed axial piston pumps." *Frontiers of Mechanical Engineering* 17 (2022): 1.
[17] Tang, H., Y. Ren, J. Xiang, and A. Kumar. "Numerical and experimental analysis of rotor-bearing system for axial piston pump with misalignment–rubbing coupling fault." *Journal of Sound and Vibration* 559 (2023): 117786.
[18] Fang, L., Y. Lü, Q. Zhang, and Z. Qi. "Fault diagnosis based on semi-supervised neighborhood adaptive LLTSA." *Journal of Vibration and Shock* 36 (2017): 189–194.
[19] Wang, S., J. Xiang, Y. Zhong, and H. Tang. "A data indicator-based deep belief networks to detect multiple faults in axial piston pumps." *Mechanical Systems and Signal Processing* 112 (2018): 154–170.
[20] Gao, H., Q. Chao, Z. Xu, J. Tao, M. Liu, and C. Liu. "Piston pump fault diagnosis based on Siamese neural network with small samples." *Journal of Beijing University of Aeronautics and Astronautics* 49 (2022): 155–164.
[21] Tang, Shengnan, Yong Zhu, Shouqi Yuan, and Guangpeng Li. "Intelligent diagnosis towards hydraulic axial piston pump using a novel integrated CNN model." *Sensors* 20, no. 24 (2020): 7152.
[22] Xu, C., J. Huang, Y. Lan, B. Wu, C. Niu, X. Ma, and B. Li. "Fault diagnosis of axial piston pump based on D-1DCNN." *Journal of Mechanical & Electrical Engineering* 55 (2021): 108–118.
[23] Tang, Shengnan, Yong Zhu, and Shouqi Yuan. "An improved convolutional neural network with an adaptable learning rate towards multi-signal fault diagnosis of hydraulic piston pump." *Advanced Engineering Informatics* 50 (October 2021): 101406.
[24] Xiao, C., H. Tang, Y. Ren, J. Xiang, and A. Kumar. "Adaptive MOMEDA based on improved advance-retreat algorithm for fault features extraction of axial piston pump." *ISA Transactions* 128, Part B (September 2022): 503–520.
[25] Jiang, W., C. Lu, and Y. Zhu. "HHT and fuzzy C-means clustering-based fault recognition for axial piston pump." *Journal of Jilin University* 45 (2015): 429–436.
[26] Wu, Z., C. Xiao, H. Tang, Y. Ren, and Y. He. "Fault diagnosis of axial piston pump based on polynomial Chirplet transform and variational mode decomposition under variable speed conditions." *Chinese Hydraulics & Pneumatics* 45 (2021): 77–82.
[27] He, Y., H. Tang, Y. Ren, and A. Kumar. "A deep multi-signal fusion adversarial model based transfer learning and residual network for axial piston pump fault diagnosis." *Measurement* 192 (2022): 110889.
[28] Xiao, C., H. Tang, Y. Ren, and A. Kumar. "Fuzzy entropy assisted singular spectrum decomposition to detect bearing faults in axial piston pump." *Alexandria Engineering Journal* 61 (2022): 5869–5885.
[29] Jiang, W., P. Zhang, M. Li, and S. Zhang. "Axial piston pump fault diagnosis method based on symmetrical polar coordinate image and fuzzy C-means clustering algorithm". *Shock and Vibration*, no. 1 (2021): 6681751.
[30] Wang, S., and J. Xiang. "A minimum entropy deconvolution-enhanced convolutional neural networks for fault diagnosis of axial piston pumps." *Soft Computing* 24 (2019): 2983–2997.
[31] Tang, S., S. Yuan, Y. Zhu, and G. Li. "An integrated deep learning method towards fault diagnosis of hydraulic axial piston pump." *Sensors* 20 (2020): 6576.
[32] Wei, X., Q. Chao, J. Tao, C. Liu, and L. Wang. "Cavitation fault diagnosis of high-speed axial piston pump based on spectrum analysis and convolutional neural network." *Chinese Hydraulics & Pneumatics*, 45 (2021): 7–13.
[33] Zhou, Y., A. Kumar, C. Parkash, G. Vashishtha, H. Tang, A. Glowacz, A. Dong, and J. Xiang. "Development of entropy measure for selecting highly sensitive wavelet packet transform band to identify defective components of an axial piston pump." *Applied Acoustics* 203 (2023): 109225.
[34] Zhu, Y., T. Zhou, S. Tang, and S. Yuan. "Failure analysis and intelligent identification of critical friction pairs of an axial piston pump." *Journal of Marine Science and Engineering* 11 (2023): 616.
[35] Zhu, H., T. Rui, X. Wang, Y. Zhou, and H. Fang. "Fault diagnosis of hydraulic pump based on stacked autoencoders." Paper presented at the 2015 12th IEEE International Conference on Electronic Measurement & Instruments, Qingdao, China, July 16–18, 2015.
[36] Tang, S., Y. Zhu, and S. Yuan. "An improved convolutional neural network with an adaptable learning rate towards multi-signal fault diagnosis of hydraulic piston pump." *Adv. Eng. Inform.* 50 (2021): 101406.
[37] Tang, S., Y. Zhu, and S. Yuan. "A novel adaptive convolutional neural network for fault diagnosis of hydraulic piston pump with acoustic images." *Advances in Engineering Informatics* 52 (2022): 101554.
[38] Jiang, W., M. Li, P. Zhang, Y. Zhao, and S. Zhang. "Intelligent fault diagnosis method for rotating equipment based on full vector enhanced deep forest." *China Mechanical Engineering* 33 (2022): 1324–1335.
[39] Chen, L., Y. He, and S. Dong. "Recognition of hydraulic pump leakage status based on deep neural network." *Chinese Journal of Scientific Instruments* 41, no. 4 (2020): 86–94.

# Optimizing the Flow through the Hydraulic Installation of a Port Crane

Prof. PhD.Eng. **Mariana PANAITESCU**[1,*], Prof. PhD.Eng. **Fănel-Viorel PANAITESCU**[1], Senior Lecturer PhD. Eng. **Ionuț VOICU**[1]

[1] Constanta Maritime University, Faculty of Marine Engineering, Department of Engineering Sciences in the Mechanical Field and Environment

* panaitescumariana1@gmail.com

***Abstract:*** *The lifting installations with cranes have a much higher productivity than the big ones and come into operation without preliminary preparations, but compared to the big ones, they are constructively more complex and more expensive. They can have manual (very rare), electric (currently the most widespread) and electrohydraulic (with greater possibilities of adjusting the working speeds) actuation. The primary condition and the basis of the economic growth of the port activity is the provision of appropriate performances and in particular the activities of operating ships and handling goods, which constitute the main function of a port. As a result, the optimization of the flows through the hydraulic installations of the port equipment is very important in the operational processes. The current work presents the structural and operational characteristics of a harbour crane in order to optimize the performance of hydraulic installations.*

***Keywords:*** *Crane, flow, harbour, optimization, plant, simulation*

## 1. Introduction about Port Cranes

Port cranes constitute the main means of trans-shipment of goods and are located along the mooring front. Superstructure works developed simultaneously with the progress made in shipbuilding. This is how specialized berths and maritime terminals appeared, equipped with the most modern operating installations, specialized in the operation of a certain type of cargo. At the same time, transport systems were developed, the most complex form of which is the door to door system. Following the analysis of the technical park in the Romanian maritime and river ports, it is found that in a general goods terminal the most common Port Operational Facilities (POF) are quay cranes.
Figures 1 and 2 show the most common port facilities, constituting the main means of trans-shipment of goods [1], [2], [3]. With the help of quay cranes, both general cargoes and some specialized ships are operated. Port practice demonstrates that in the vast majority of situations the use of quay cranes is characterized by a higher productivity than the equipment on board. Quay cranes are mainly intended for cargo handling operations from the ship to the terminal and vice versa. The lifting capacity of these cranes is variable, being dependent on the specialization or destination of the port operating berth [4].

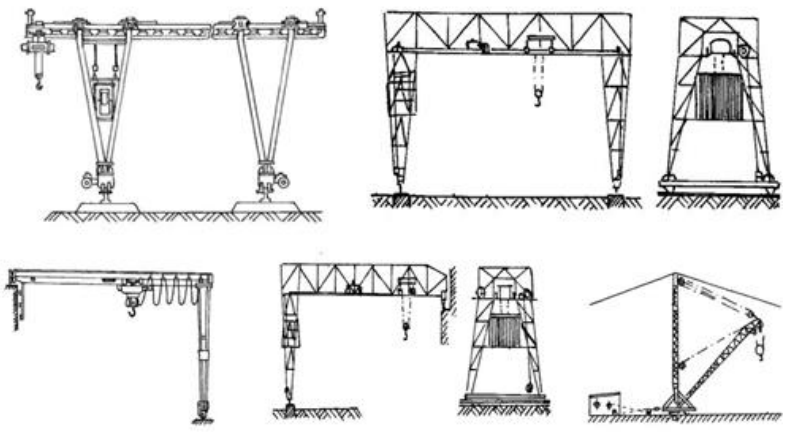

**Fig. 1.** Different types of port cranes [1]

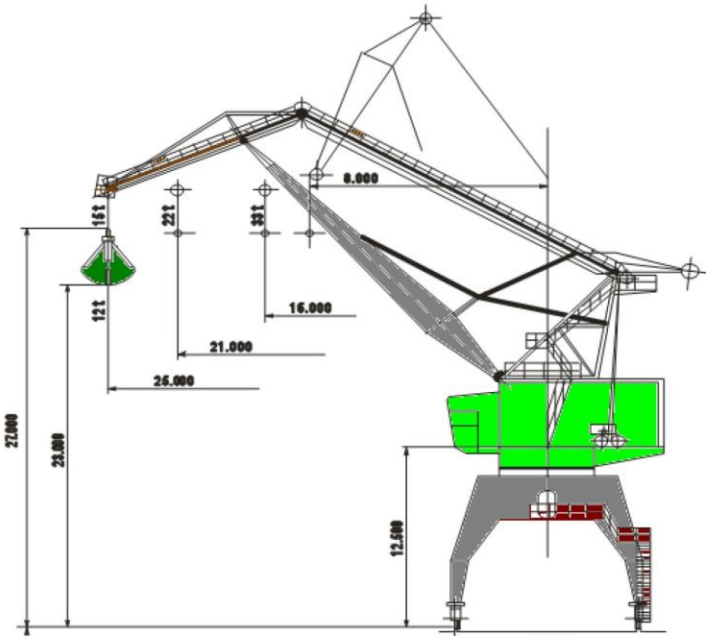


**Fig. 2.** Port crane with square jib [2]

Quay cranes can be classified into:

- gantry cranes

- semi-portal cranes.

In both types, the actual crane rests on a metal structure whose shape also gives the name of the respective type of crane. The rollers of the translation mechanism rest on a guide rail located along the magazine wall at a given height. The most widespread quayside cranes are the portal type (Fig. 3) [5].

**Fig. 2.** Hercules model quayside crane [5]

The characteristics of the port crane are (Table 1):
- Model: HC-PT
- Type: Lifting platform
- Capacity: maximum 50 tons
- Working radius: 65 m
- Brand electrical parts: Siemens, Schneider, Chnt

**Table 1:** The characteristics of the port crane

| Product specifications | Value |
|---|---|
| Lifting capacity, [t]<br><br>Radius, [m] | Main hook :<br>50 45<br>24-33 24-60<br>Auxiliary hook:<br>20<br>28-65 |
| Lifting height , [m] | 60 |
| Working radius, [m] | Max. 60... 65<br>Min. 24... 28 |
| Mechanism speed ;<br>Lifting speed , [m/min]<br><br>Descent speed, [m/min]<br>Rotation speed, [rot/min]<br>Movement speed, [m/min] | <br>Main hoo-: 7; Auxiliary hook-<br>15<br>~ 10<br>0.24<br>30 |
| Power source | 3-phase A.C.60 Hz 440V |
| Track Gauge / abatement, [m] | 13/16 |
| Portal height, [m] | ~13 |
| Chassis rolling radius, [m] | ~17 |
| Wind pressure with the crane in operation, [$N/m^2$] | 250 |
| Wind pressure with the crane on standby, [$N/m^2$] | 1000 |
| Installed capacity, [kW] | 125 |
| Starting current, [A] | 250 |

- Working environment: -20 + 45 degrees C
- Sling type: metal cables
- Power source: Electric
- Specifications: CE, CCC
- HS code: 84263000
- Certification: CE, ISO 900I: 2000
- Use: Port, constructions
- Name: Mobile jib crane
- Lifting height: 60 m
- Protection device: Limit Switch, main isolation switch
- Control mode: Cabinet / Remote Control.

The component elements of the port crane are (Fig. 3)[5]:

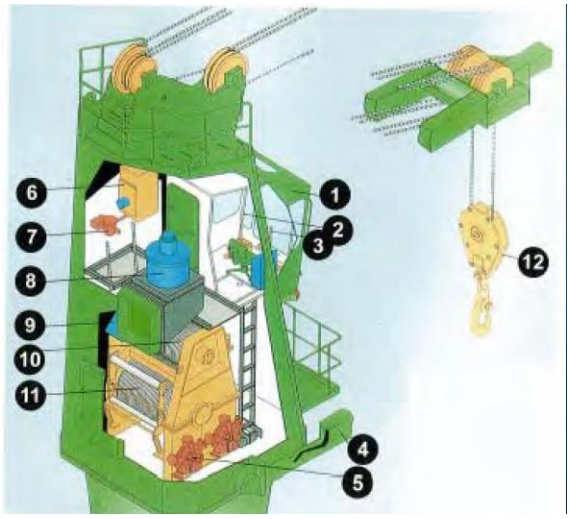


**Fig. 3.** Port crane-the components elements [5]

1. crane cabin
2. lever for arm movement and rotation
3. lift lever
4. arm
5. hydraulic motor
6. oil tank
7. oil filter
8. oil cooler
9. limit switch
10. lifting cable
11. lifting cable
12. locking pulley.

## 2. Method and research

The research consists of:
- presentation of the hydraulic actuation installation [2], [3], [4], [5], [6], 7], [8];
- flow optimization by using the ANSYS FLUENT simulation program [8], [9], [10].

### 2.1 Presentation of the general scheme and component parts

The reference crane is equipped with 2 drive cylinders (Fig. 4)[3],[6]

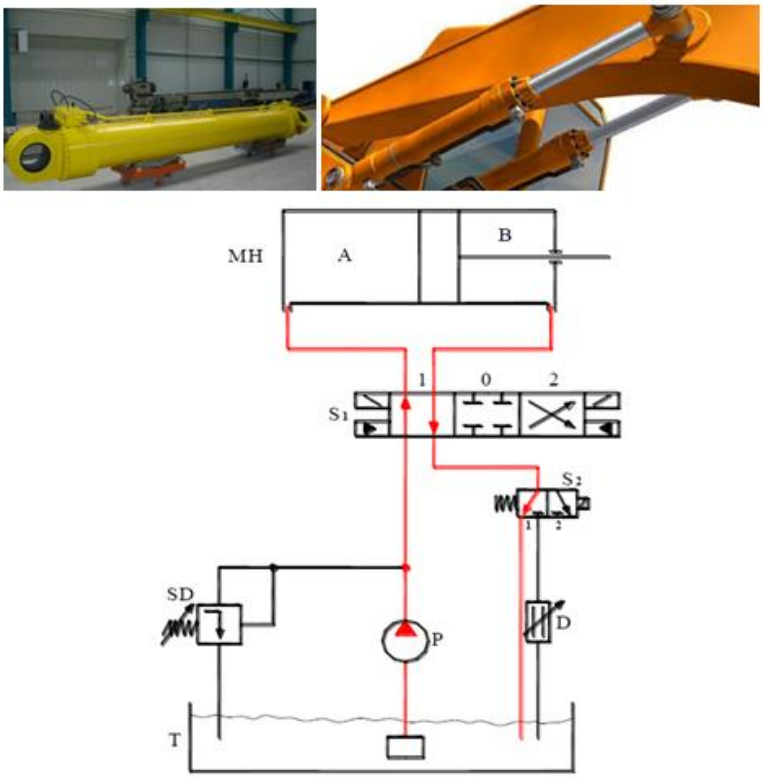


**Fig. 4.** Hydraulic cylinders and the general diagram of the operation of hydraulic cylinders [3], [6]

The diagram above comprises the hydraulic pump P, the pressure valve SD, the three-position hydraulic distributor with hydraulic steering S1, the hydraulic distributor S2, the hydraulic motor MH coupled to the working body, filters, pressure relays, throttle with flow regulator D and the tank T .

- *The destination of the hydraulic pump*

The hydraulic pump is designed to transform the mechanical energy received from the electric motor into the hydraulic energy of the fluid that is transmitted to the hydraulic system, namely the working body (Fig. 5) [4].

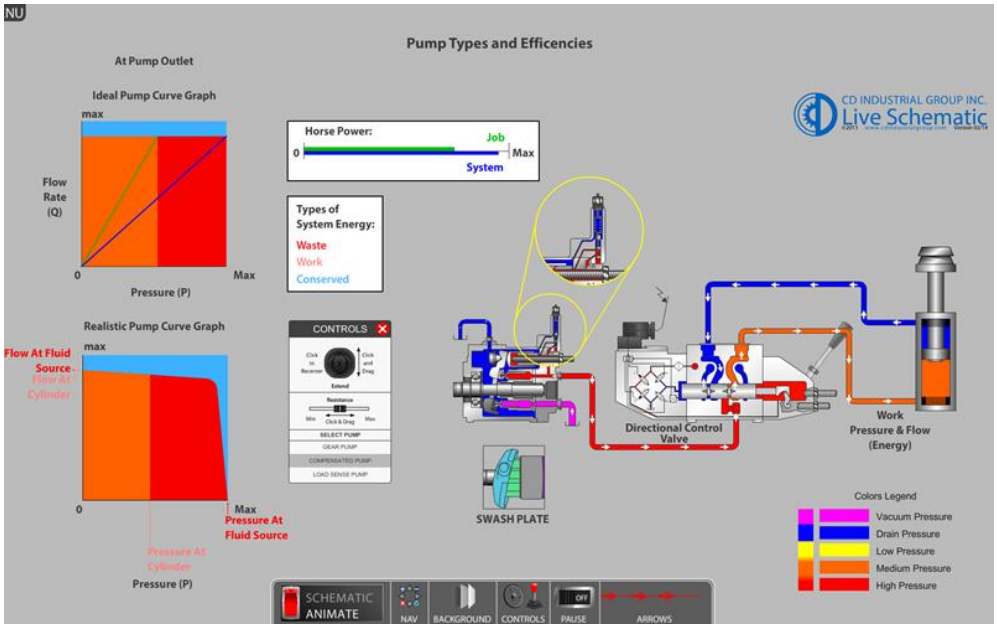


**Fig. 5.** Hydraulic pump [4]

- *The destination of the hydraulic motor*

The hydraulic motor is designed to transform the potential energy of the liquid into the mechanical energy of the working body (Fig. 6)[4].

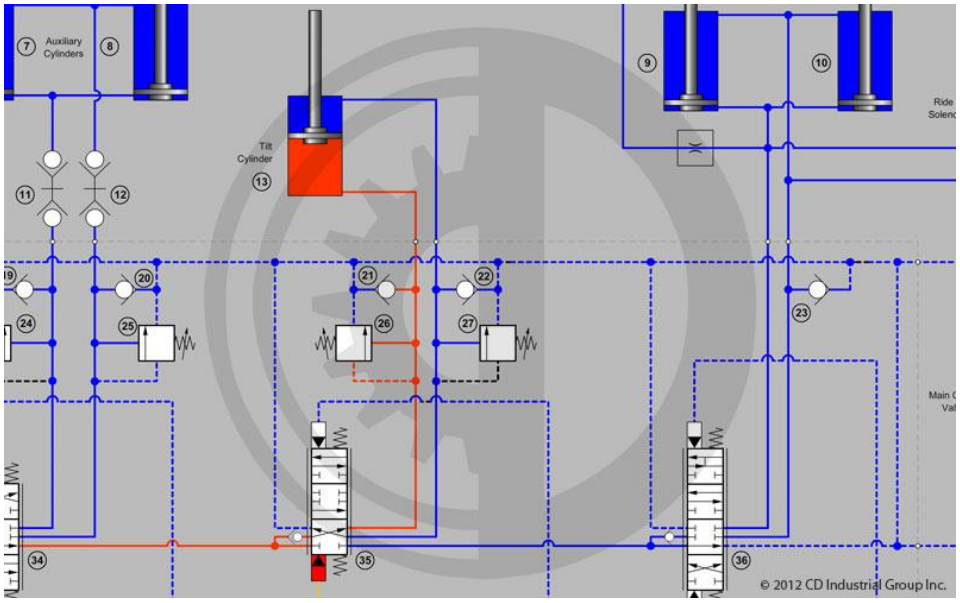


**Fig. 6.** Hydraulic motor [4]

- *The destination of distributors*

The hydraulic distributors are intended for discharging, stopping and starting the working bodies of the machine tools and the technological equipment which is performed by changing the direction of movement of the flow of the working fluid of the hydraulic system, opening and closing the system, changing the direction. The three-position hydraulic distributor (DH) is intended for starting and dumping the cycle (Fig. 7) [5].

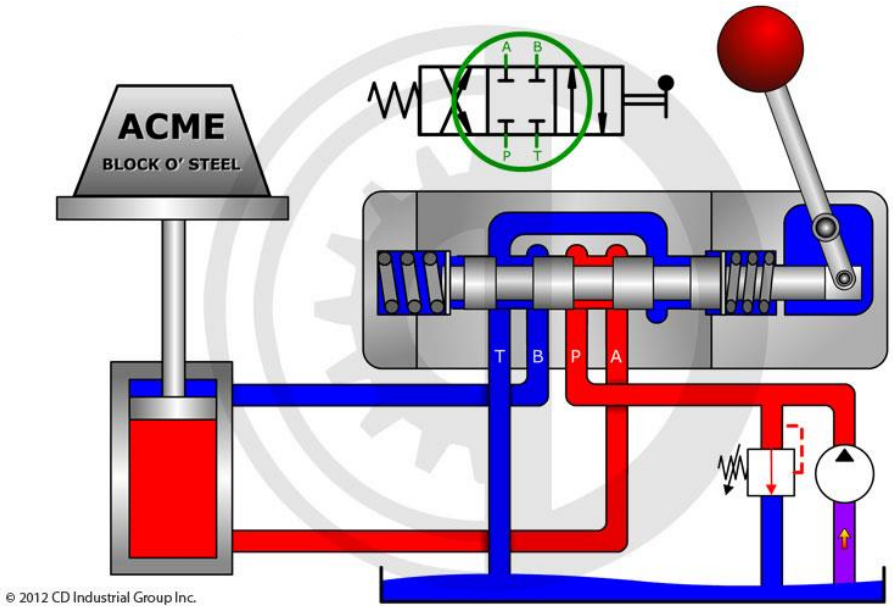


**Fig. 7.** Distributors [5]

- *The destination of the pressure device*

The pressure device is designed to protect the hydraulic system from overload and maintain a constant pressure (Fig. 8) [5].

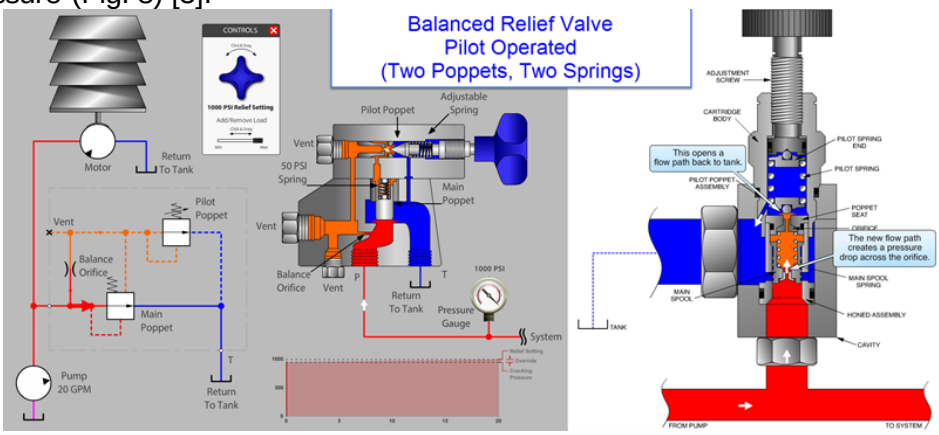


**Fig. 8.** Pressure valves [5]

- *The destination of throttles with regulator*

Throttles with regulator are designed to regulate the flow of liquid and keep it constant, therefore also the speed of the working body. In this case, chokes with a regulator are used and are installed at the output (Fig. 9) [5].

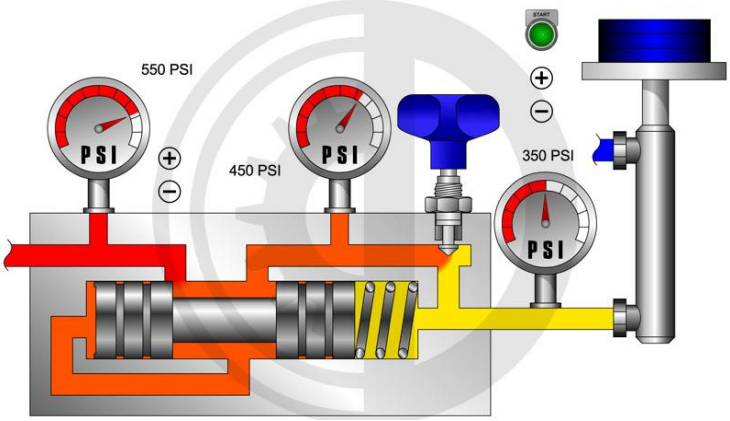


**Fig. 9.** Flow regulators [5]

- *The purpose of one-way valves*

Check valves are used in hydraulic systems to allow fluid to move through pipes in one direction only (Fig. 10) [5].

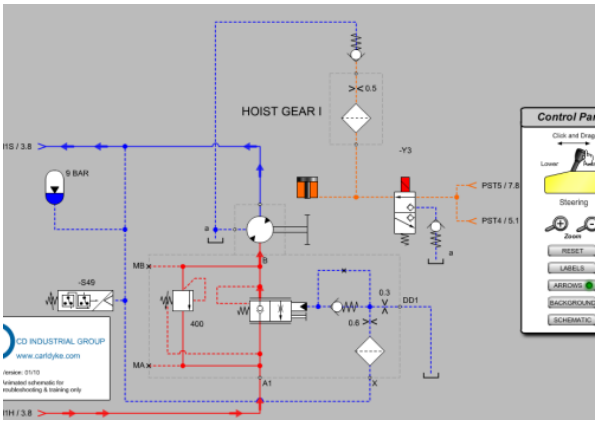


**Fig. 10.** Check valves [5]

## 2.2. Simulation of fluid flow on the hydraulic installation

To model the fluid flow system on the hydraulic installation, the Ansys program was used, namely Ansys-Fluent, the part that deals with the study of liquid flow.
With the help of the *Design Modeler* option offered by the Ansys Fluent program, the geometric construction of a sector of the hydraulic installation of the quay crane was realized (Fig. 11).

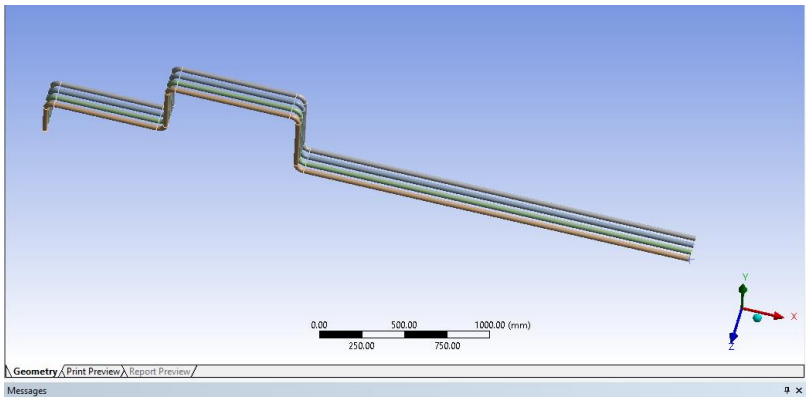


**Fig. 11.** Design of the crane hydraulic installation sector (Ox)

Given that it is equipped with 2 hydraulic lifting cylinders, we included the round-return installation sector with oil supply for the 2 cylinders (Fig. 12, Fig. 13).

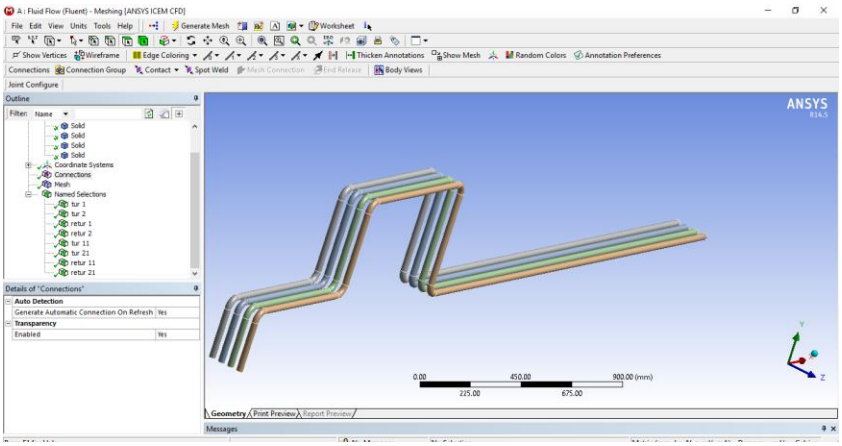


**Fig. 12.** Design of the crane hydraulic installation sector (Oy)

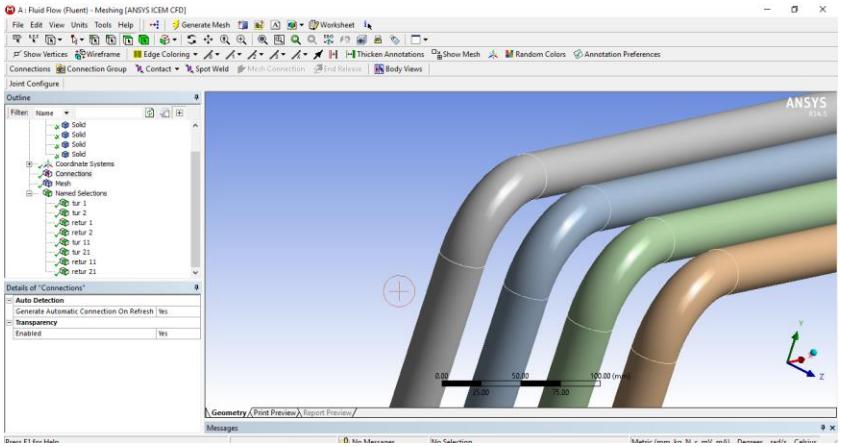


**Fig. 13.** Design of the crane hydraulic installation sector (Oz)

The fluid entry and exit points were established. Thus we noted 2 inputs and 2 outputs for the 2 actuation cylinders (Fig. 14).

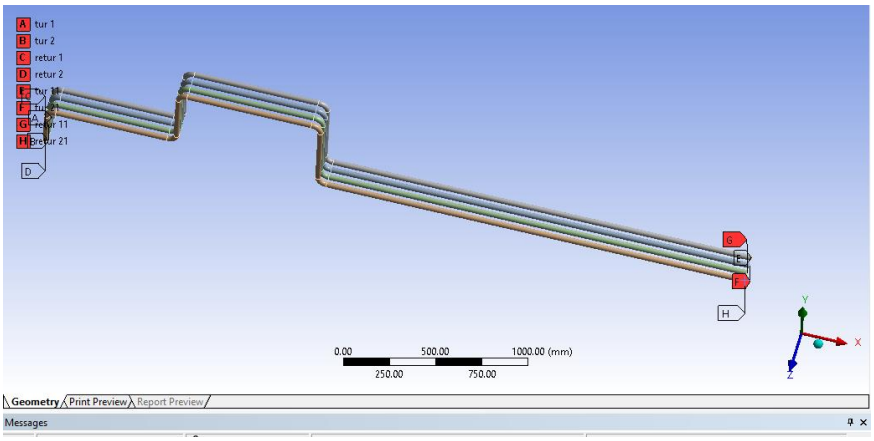


**Fig. 14.** The inlets and outlets in the hydraulic installation (return - return)

The next stage after the geometric construction, is the discretization of the installation. This process is a structural analysis of the entire pipeline segment, it being divided into a certain number of cells, with a view to the possibility of further development of the calculation on each cell, determining particular values of pressure and velocity.
The discretization was performed using the "Mesh" interface of the Ansys Fluent program. The structural analysis resulted in 1546512 cells and 243811 nodes (Fig. 15).

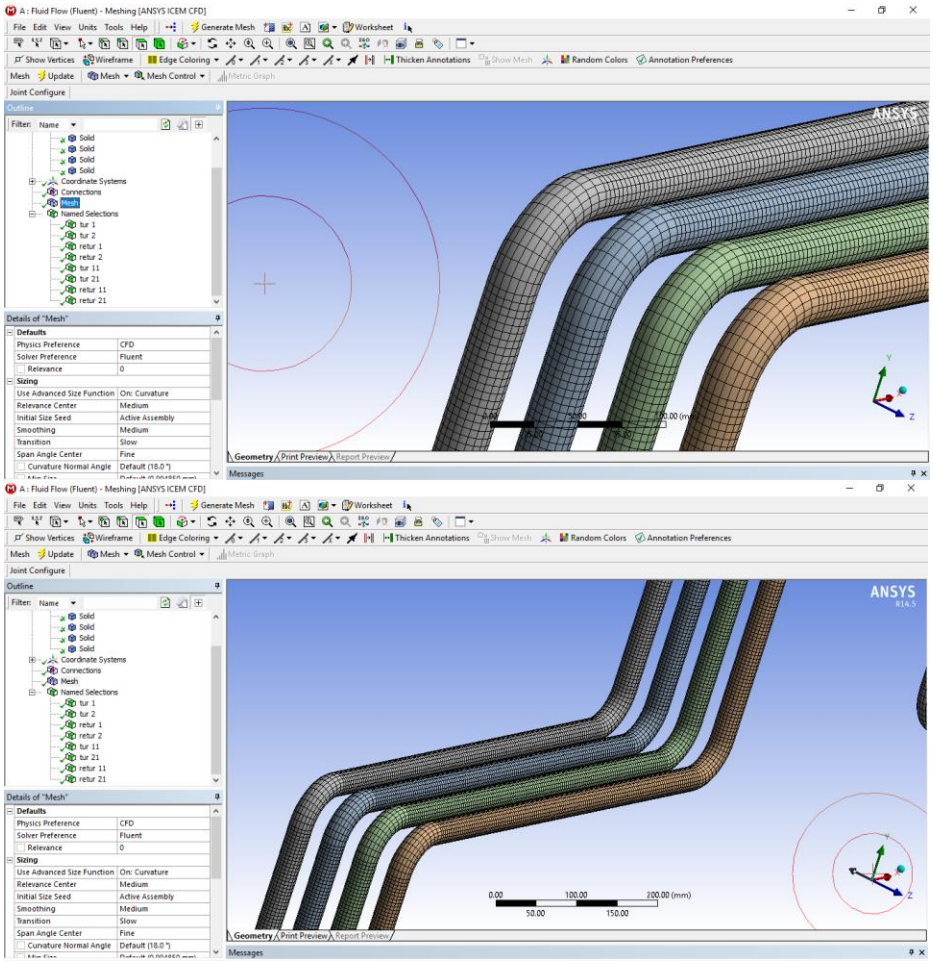


**Fig. 15.** Discretization of the installation

To visualize the results, the simulation program was run with the established working conditions.

## 3. Results and interpretations

After carrying out the simulation with the numerical program ANSYS FLUENT, the local pressure drops and speed variations on certain sectors, as well as on the entire installation, are presented in Fig. 16....Fig. 22.

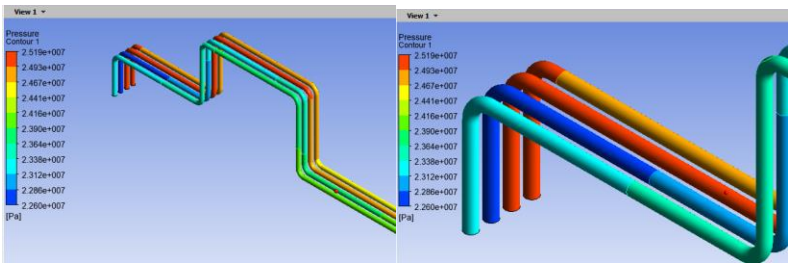


**Fig. 16.** The pressure on the contour-view 1 stream line on wall

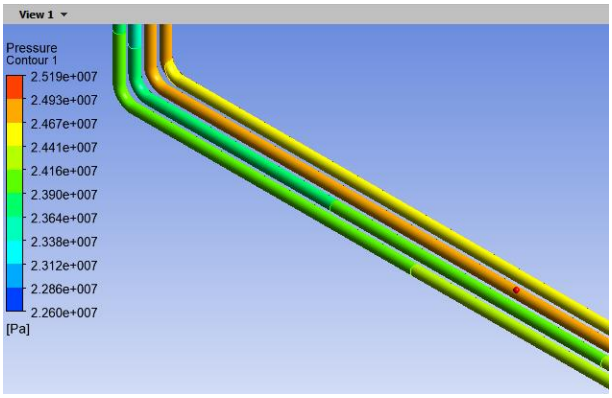


**Fig. 17.** The pressure on the contour-view 2 wireframe

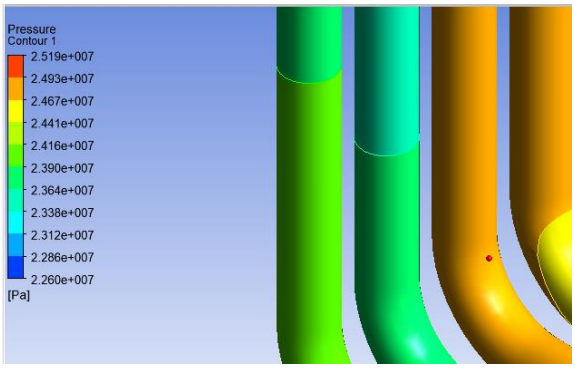


**Fig. 18.** The pressure on the bends of the installation

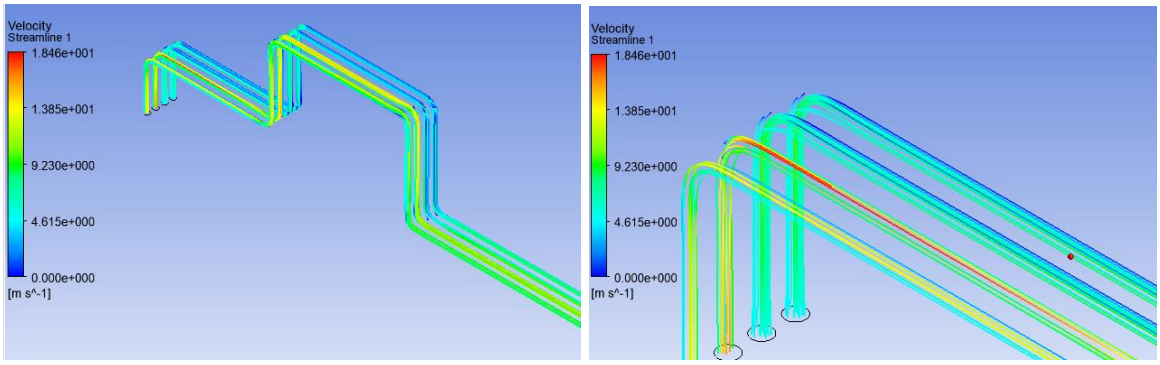


**Fig. 19.** The velocity on streamline 1

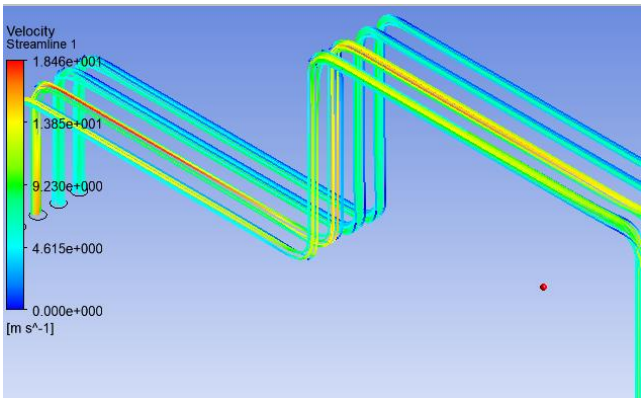


**Fig. 20.** The distribution of velocity on the frame

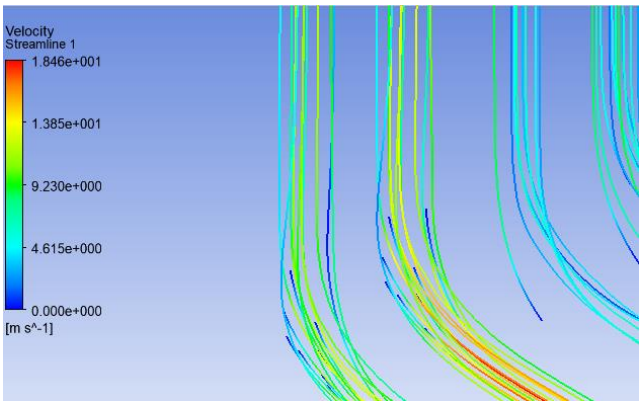


**Fig. 21.** The distribution of velocity on the bends of the installation

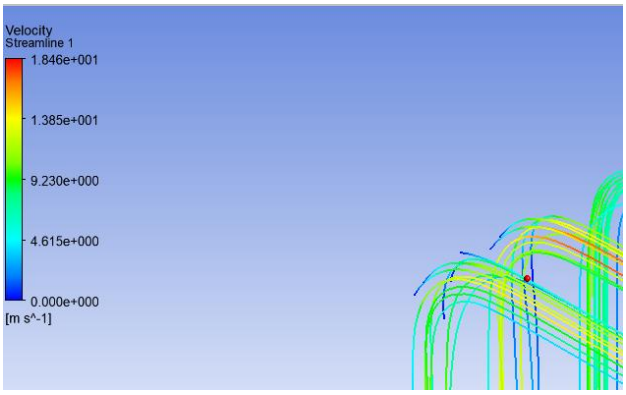


**Fig. 22.** The distribution of velocity- limit values

The main results obtained from the simulation were:

- pressure on the installation (cylinder 1 stroke): max 2.519 $\cdot 10^7$ Pa, min 2.441 $\cdot 10^7$ Pa;
- pressure on the installation (cylinder 2 stroke): max 2.519 $\cdot 10^7$ Pa, min 2.467 $\cdot 10^7$ Pa;
- pressure on the installation (return cylinder 1): max 2.441 $\cdot 10^7$ Pa, min 2.286 $\cdot 10^7$ Pa;
- pressure on the installation (return cylinder 2): max 2.441 $\cdot 10^7$ Pa, min 2.312 $\cdot 10^7$ Pa.

To optimize the design of hydraulic plant of crane, one must choose an uniform distribution of velocities during all frames [6,7,8].

## 4. Conclusions

The main quay cranes used in the naval industry were presented.

The quay cranes are the main means of trans-shipment of goods and are located along the mooring front. The actual capacity of quay cranes is not always their nominal capacity; for

example, a crane of 3-5 tf capacity can theoretically make 40 cycles/hour, which gives an average of 4.5 x 40 = 180 t/hour unloaded cargo. But for general goods, an unloading rate of 15t/h/team is quite a high average. Such cranes have a large range of action and a very small theoretical cycle, being very efficient in the operation of ships. The working cycle of the crane is the essential element in assessing the productivity of the port facility.
The quay crane with the main characteristics was presented:
- maximum load: 50 tons;
- lifting height: 60 m;
- installed power: 125 kW;
- type: Hercules.

The optimization of the flow was carried out with the help of the Design Modeller option offered by the ANSYS Fluent program: the optimization of the geometric construction of a sector of the hydraulic installation of the quay crane was analysed. Given that it is equipped with 2 hydraulic lifting cylinders, the round-return installation sector with oil supply for the 2 cylinders was included. The fluid entry and exit points were established. Thus, 2 inputs and 2 outputs were noted for the 2 actuation cylinders and the distribution of speeds on the routes of the installation was followed so that there were no discontinuities in the distributions of the current lines. Finally, the routes of the structures with the uniform hydrodynamic spectrum of speeds were chosen.

**References**

[1] Menon, Hari. "Types of Port Cranes", *Marine Insight*, November 2, 2023. Accessed October 2, 2024. https://www.marineinsight.com/naval-architecture/types-of-port-cranes/.
[2] Chopra, Karan. "Port Gantry Cranes: A General Overview", *Marine Insight,* November 20, 2018. Accessed October, 2, 2024. https://www.marineinsight.com/ports/port-gantry-cranes-a-general-overview/.
[3] Kaushik, Mohit. "What are Telescopic Cranes?" *Marine Insight,* February 25, 2024. Accessed October 2, 2024. https://www.marineinsight.com/ports/what-are-telescopic-cranes/.
[4] Hiteshk. "10 Massive Crane Ships Operating at the Sea", *Marine Insight*, January 31, 2022. Accessed October 2, 2024. https://www.marineinsight.com/types-of-ships/5-massive-crane-ships-operating-at-the-sea/.
[5] Weihua Crane Group. "STS Cranes". Accessed October 2, 2024. https://weihuaheavycrane.com/port-cranes/Quayside-Container-Crane.html.
[6] CD Industrial Group Inc. "Blast Hole Drills". Accessed October 2, 2024. https://www.cdiginc.com/courses/blast-hole-drills.
[7] Best Macarale Utilaje SRL. "Hydraulic installation for cranes / Instalația hidraulică la macarale". Accessed October 3, 2024. https://inchirieri-macara.ro/instalatia-hidraulica-la-macarale/
[8] Panaitescu, F.V., M. Panaitescu, and G. Andresoiu. *Gravitational installations* / *Instalatii gravitationale.* Constanta, DADA Publishing House, 2000.
[9] ANSYS, Inc. "Ansys Fluent. Fluid Simulation Software". https://www.ansys.com/products/fluids/ansys-fluent.
[10] Panaitescu, M., F.V. Panaitescu, and I. Omocea. *Flows in marine engineering.* Bucharest, Paideia Publishing House, 2001.

# Fluid Contamination Aspects Due to Hydraulic System Operation

Associate Professor **Fănel Dorel ȘCHEAUA**[1,*]

[1] Dunarea de Jos University of Galati

* fanel.scheaua@ugal.ro

***Abstract:*** *Fluid contamination is a significant concern in hydraulic and fluid systems, as contaminants in hydraulic, lubrication, or process fluids lead to equipment wear, corrosion and even catastrophic failures in sensitive equipment. Effective contamination control is essential for maintaining system reliability, optimizing performance and extending the life of both fluids and equipment. With advances in sensing, modelling and filtration technologies, industries are better equipped to manage fluid contamination and ensure system resilience. This paper presents the fluid contamination general aspects, main sources, the principal contaminants types, represented by different particles of solid contaminants (metallic fragments, dust and wear particles from machinery components) and its implications for system efficiency. The contaminant particles can be abrasive and cause wear on surfaces, water droplets often found in hydraulic and lubrication systems, leading to corrosion, degradation of additives and further reduced fluid operational performance, other air and gas particles entrained into hydraulic fluid volume leading to cavitation, reduced lubrication and oxidation. Main models describing the hydraulic fluid contamination are presented and further the numerical analysis results based on parameters primary considered for a hydraulic actuation type.*

***Keywords:*** *Hydraulic actuation, fluid contamination, contaminant types, mathematical model, numerical analysis*

## 1. Introduction

The degree of cleanliness of the working fluid is an essential condition for the optimal functioning of hydrostatic drive systems, as it ensures that the tasks imposed on the respective system are strictly fulfilled.
The general aspects of fluid contamination, its sources and its implications is shown through the principal contaminants types, which are represented by different particles of solid contaminants (metallic fragments, dust and wear particles from machinery components), that can be abrasive and cause wear on surfaces, water droplets often found in hydraulic and lubrication systems, leading to corrosion, degradation of additives and further reduced fluid operational performance, other air and gas particles entrained into hydraulic fluid volume leading to cavitation, reduced lubrication and oxidation. Other contaminants include chemical contaminants like acids or solvents that act to fluid properties degradation, corrosion of metal components, or react with additives.
Manufacturing residual material particles which are leftover from the manufacturing process are contaminants represented by metal shavings, dust, or paint remnants.
From the external environment contaminants are accounted all dust and dirt that enter the fluid system through seals, open reservoirs, or vents.
Over time, components such as seals, bearings and pumps generate wear particles that mix with the fluid. Also, from system maintenance activities could be introduced contaminants through improper maintenance or during refilling and topping off, while water ingress can be mainly from condensation, leaks, or improper storage of fluids.
Regarding the effects of contamination, it is demonstrated that abrasive particles generate erosion and surface wear on moving parts, leading to reduced lifespan of components. Water, acids and other contaminants cause corrosion, weakening metal components and compromising seals. Entrained air or gas bubbles can cause cavitation phenomenon, which damages pump surfaces and reduces efficiency. Fluid properties like viscosity, lubrication and heat transfer can be compromised, resulting in a drop in system performance and over time, excessive contamination can lead to clogging, component malfunctions, or even complete system failure.
It is therefore important to carry out specific measurement and analysis of contaminants, especially particle counting methods, as the main method for assessing contamination levels, as they measure the size and quantity of particles in the fluid.

Based on ISO cleanliness codes as standards, the number of particles per milliliter of fluid is classified, allowing systems to maintain specific cleanliness standards.
It is also important to measure water content using techniques such as Karl Fischer titration or relative humidity sensors that are used to measure water contamination.
Spectrographic analysis to identify specific contaminants or wear metals, especially in lubricating oils, is also a handy method.
Testing the viscosity and pH of the working fluid helps to establish the condition of the fluid when the chemical composition of the fluid has changed due to contamination.
In order to avoid contamination of the working fluid of the hydrostatic system, filtration activities of the working fluid are necessary through
filtration systems. These are presented as different types of filters (screen, depth, magnetic) that can retain and remove particles from fluid. Good filtration removes even microscopic particles but may slow fluid flow.
For water retention and removal, methods like vacuum dehydration and centrifugal separators are used.
At the level of breathers and seals, in order to prevent external contaminants, systems use breathers, seals and gaskets that protect against dirt and moisture.
Regular fluid testing and monitoring systems have the role of detecting fluid contamination early, allowing for preventive maintenance.
Using proper design standards and implementing protocols for flushing, cleaning and preventive maintenance, good results are obtained in terms of reducing contamination risks.
Standards and Guidelines that provide detailed information on hydraulic fluid contamination are mainly represented by ISO 4406 as a widely used standard for cleanliness codes in hydraulic systems, which define the allowable particle counts per milliliter, ISO 4407 which outlines particle count methods using microscopic techniques and also ASTM Standards which provide guidelines on water and particle contamination measurement and acceptable limits within hydraulic fluids.
Implications for Different Industries that use hydraulic systems to operate multiple equipment working parts should be mentioned as the main domains represented by aerospace and defense because fluid high cleanliness is essential due to the sensitivity of hydraulic components and the critical nature of equipment reliability.
Further within automotive and heavy machinery it should be highlighted that hydraulic and lubrication fluids must be kept clean in order to prevent wear in engines, transmissions and hydraulic pumps.
The Oil & Gas energy industry has high needs for fluids used in drilling and extraction face challenges from abrasive particles, water ingress, and microbial growth.
For food and pharmaceuticals there are strict requirements regarding contamination control as fluids interact with food products, requiring non-toxic, contaminant-free fluids.
Future developments in hydraulic fluid contamination control mean the use of intelligent systems that include smart sensors that have the role of monitoring fluid quality in real-time, transmitting data to control systems that alert operators when contamination levels are too high.
We are moving towards achieving a high level generically called advanced filtration technologies (AFT) which uses new filter materials and designs that improve efficiency and reduce the need for frequent filter changes, including the possible use of nano-additives and self-healing fluids, as types of fluids containing nano-additives that can bind to contaminants or heal small abrasions caused by contaminants [1-10].

## 2. Fluid Contamination Modelling

For contaminant transport models the Lagrange and Euler methods are primary used to simulate contaminants distribution within fluid systems. Each method has a unique perspective on how particles or contaminants move through the fluid field and each is suited to different types of analyzes in fluid dynamics, including hydraulic and lubrication systems.
For high filtration efficiency, mathematical models are used to calculate the filters impact on removing particles, tracking efficiency over time and across different filter types [11-15].

Numerical analysis enhances the dynamic simulation performance that accounts for factors like temperature, wear rate and filtration efficiency, making it possible to predict contamination build-up and the impact on performance based on the results obtained.
The LAGRANGE method approach, presents a perspective in which individual particles (contaminants) are tracked as they move through the fluid. Each particle's position, velocity, and other properties are followed over time, essentially "traveling" along with the contaminant in the fluid flow.
The approach is intuitive because it mimics how a contaminant might be observed if one could track its exact path through the system.
For a particle of mass *m* and velocity *v(t)* the Newton second law is written as:

$$m\frac{dv}{dt} = \sum F$$
$$\sum F = F_d + F_g + F_b + F_l + F_f \tag{1}$$

where the main forces acting on the particle are considered as drag force *(Fd)* directly dependent of drag coefficient *(Cd)*, gravity force *(Fg)*, buoyancy force *(Fb)*, lift force *(Fl) based on* lift coefficient *(Cl)* and other forces *(Ff)* represented by hydrodynamic, Van der Waals, electrostatic repulsion forces, steric and contact (elastic and frictional) forces.

$$F_d = -\frac{1}{2}A\cdot C_d\cdot\rho|v-u|(v-u)$$
$$F_g = mg$$
$$F_b = -\rho\cdot g\cdot V_p \tag{2}$$
$$F_l = C_l\cdot\mu\sqrt{\rho\cdot\nu}\cdot D_p^2\frac{(u-v)\times\nabla\times u}{|u-v|}$$

Each contaminant particle is tracked individually, showing its path and changes in velocity, pressure, and other variables over time, while it focuses on individual particles or "parcels" of fluid, capturing the transport of contaminants due to advection, diffusion and other forces acting on each particle.

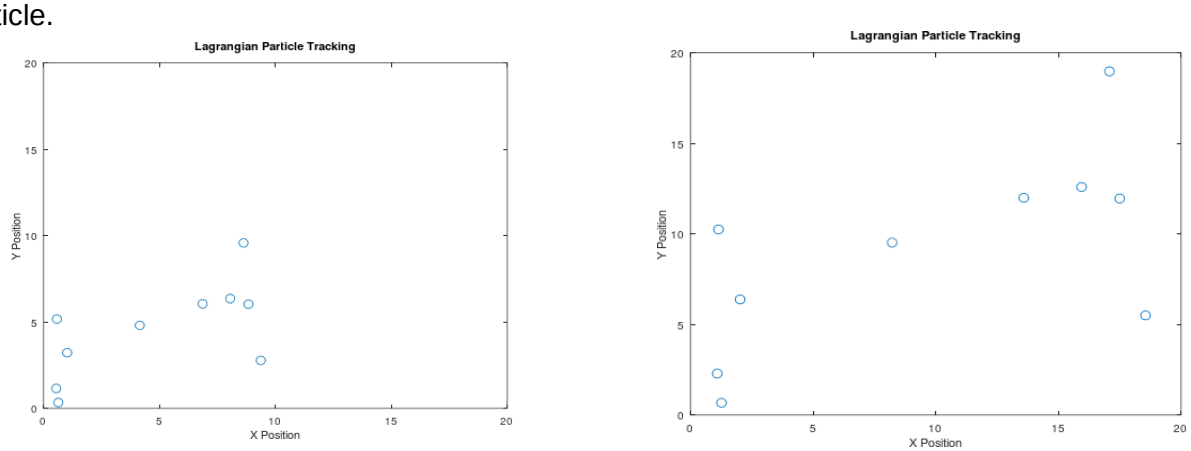


**Fig. 1.** The time distribution of particle tracking based on Lagrange method

The position of each particle *x(t)*, is updated by integrating the velocity over time:

$$v(t) = \frac{dx}{dt} \tag{3}$$

The method allows for precise modeling of particle-fluid and particle-particle interactions, such as collision, aggregation and deposition.
The main advantages offered are related to the fact that it offers highly detailed insights into the behaviour of individual particles which is useful for studying contaminant behaviour in complex flows.
The method capture localized phenomena such as particle sedimentation, aggregation and specific particle-fluid interactions.
Also, in terms of temporal and spatial details, is effective for applications where understanding the detailed trajectory of particles is essential, especially for particle deposition on surfaces or contamination hotspots.
The EULER method approach treats contaminants as a concentration field rather than individual particles. Hence, the fluid domain is divided into fixed control volumes or grid cells, and the contaminant concentration within each cell is calculated over time.
The focus is on how the contaminants concentration changes at fixed points in space due to advection, diffusion and reaction rates within the fluid.
The field-based approach has the ability to model contaminant concentration as a scalar field that varies with position and time, rather than tracking individual particles [8-17].
A fixed reference frame calculates contaminant transport at specific points in space, focusing on how contaminants diffuse, mix, and spread within the fluid field.
The contaminant transport is modelled as a concentration field *C(x, y, z, t)* within the fluid region. The main approach uses the advection - diffusion equation which describes the contaminant evolution at fixed spatial points:

$$\frac{\partial C(x,y,z,t)}{\partial t} + u\left(u_x, u_y, u_z\right) \cdot \nabla C(x,y,z,t) = D\nabla^2 C(x,y,z,t) + S(x,y,z,t) \tag{4}$$

where:
*C* – contaminant concentration field*;*
*u* – fluid velocity vector;
*D* – diffusion coefficient*;*
*S* – source or sink term for contamination sources or filters*.*

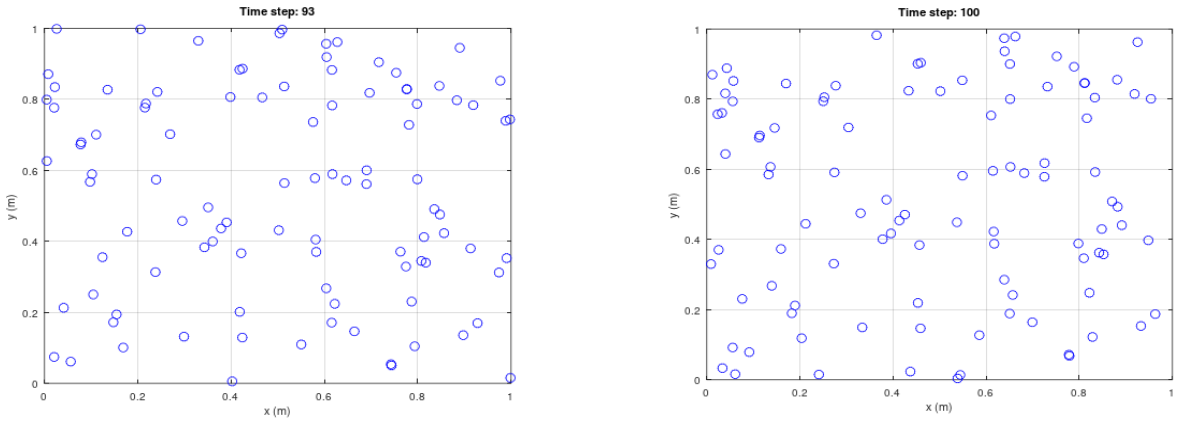


**Fig. 2.** The time distribution of particle tracking based on Euler method

As presented in figure 3, the Euler method provides a continuous view of contaminant concentration, while the Lagrange method gives specific details about individual particle movement, which is valuable for both density observation and particle tracking in fluid contamination approaches.

The continuum approach that assumes a continuous contaminant distribution is highlighted, which is particularly useful for high-density contaminant flows.

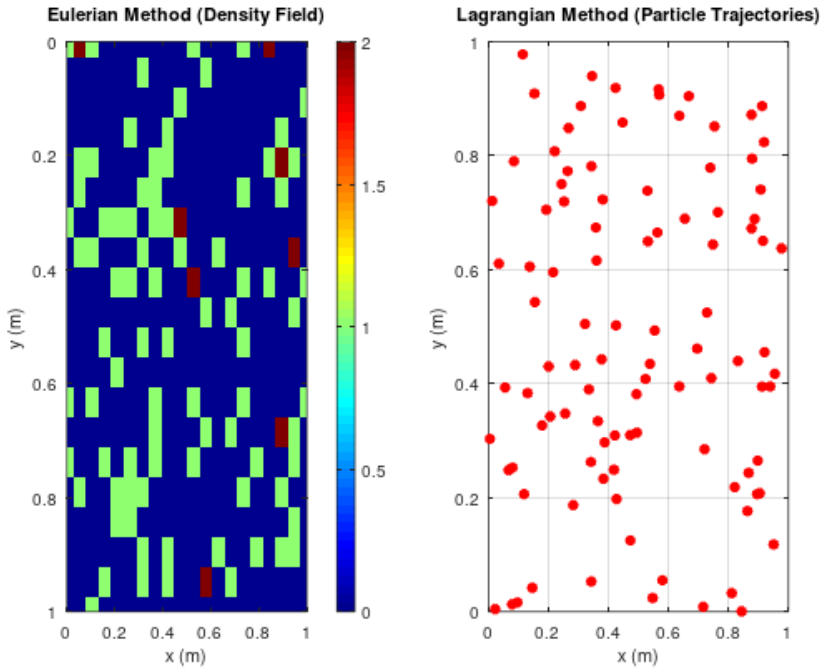


**Fig. 3.** The spatial distribution of particle tracking based on both Lagrange and Euler methods

The main advantages are related to the efficiency offered for large-scale systems, being suitable for large, complex systems with high concentrations of contaminants, as it avoids tracking individual particles. The improved computational efficiency is offered for high-contaminant densities or turbulent flows, as it works with averaged values rather than individual particle data.

The Euler method is effective at simulating processes like diffusion, convection and mixing where concentration changes are smooth over space and time, for the specific applications concerns like general contamination analysis, being mainly used for studying overall contaminant dispersion and concentration within hydraulic systems and predicting contaminant buildup over time, ideal for applications where diffusion and mixing are the main transport mechanisms, such as in large reservoirs or cooling systems and also useful in systems where contaminants are uniformly dispersed and specific particle trajectories are not critical to the analysis.

## 3. The hybrid Euler-Lagrange approach

In fluid dynamics and contaminant transport applications different models are used which combine the two methods (Euler, Lagrange) in order to take advantage of the strengths of each approach. In the case of fluid contamination modelling, this approach often seeks to balance between computational efficiency and accuracy, particularly when dealing with complex flow fields, heterogeneous contaminant transport, or both.

In the concept of the hybrid approach Euler-Lagrange method combines aspects of both methods related to existence of fixed grid points used to solve for the flow or concentration at different spatial locations, which is typically more computationally efficient for solving large-scale problems (Euler method), while individual particles or tracers are tracked as they move through the flow region, capturing detailed dynamics of individual particles, which is ideal for studying individual particle behaviour or precise tracking (Lagrange method).

In this approach, the Euler method models the continuous fluid field, while the Lagrange method tracks individual particles. The particles are registered according to the fluid flow and the contaminant concentration is updated in the Euler grid. This method is especially useful for tracking discrete contaminant particles (water droplets or particles in the fluid) in a flow field.

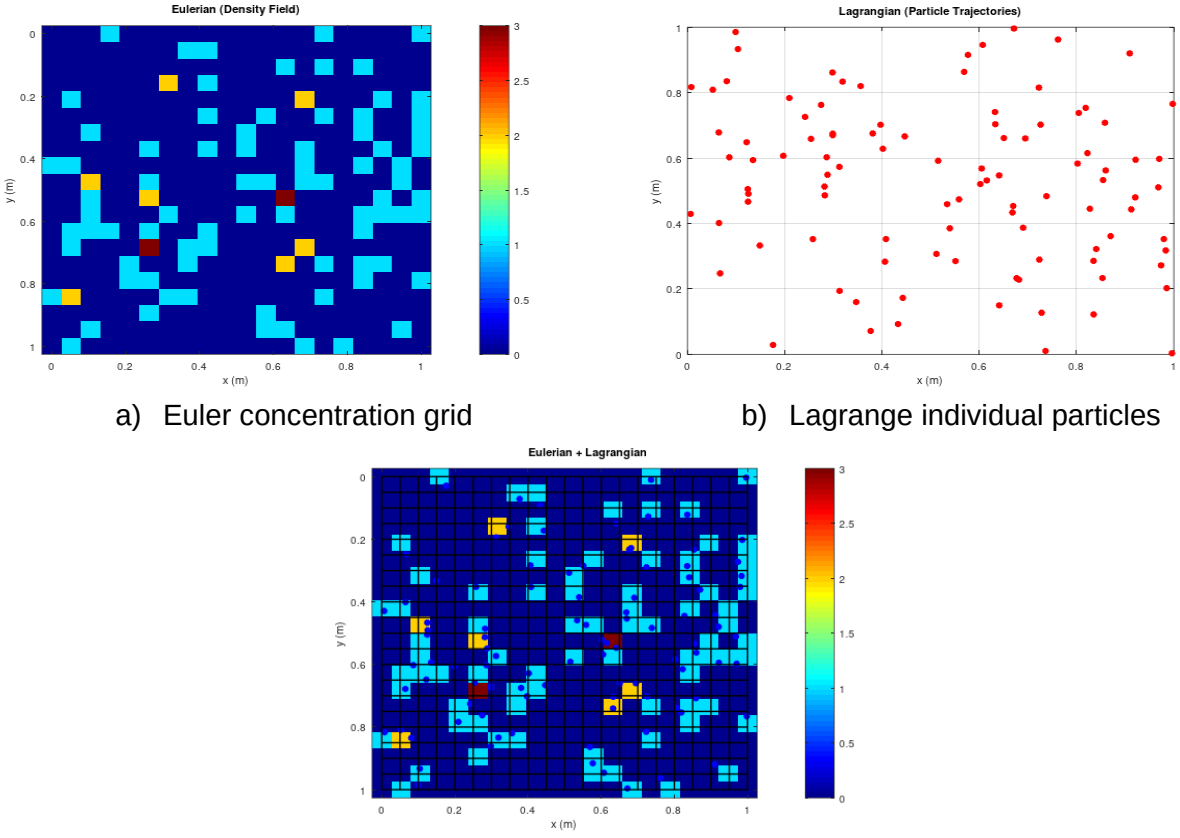


a) Euler concentration grid b) Lagrange individual particles

c) The combined view

**Fig. 4.** The spatial distribution of particle tracking based on hybrid approach (Lagrange and Euler methods)

The particles movement is calculated in the Lagrange frame and further their concentration is added to the Euler grid.
Figure 4a presents the density of contaminant particles mapped into fixed grid (Euler), where according to the legend the higher particle concentration is shown, enhancing in this manner the macroscopic contaminant distribution. In the 4b figure all individual Lagrange particles are shown with specific distribution.
This hybrid approach captures both the global distribution of contaminant (Euler) and the individual contaminant particles motion (Lagrange).

## 4. Numerical analysis for fluid contamination

A numerical approach analysis which simulates the contaminant transport within a fluid system is performed, incorporating a few additional physical parameters, represented by fluid flow velocity, particle size and filtration efficiency according with particle size (figure 5).
For hydraulic actuation systems, filtration efficiency versus particle size represents the critical aspect for maintaining the system reliability and performance over time. All contaminants such represented by dust particles, wear particles or water can severely damage the hydraulic circuit components.
The hydraulic filtering units are designed to capture particles of varying sizes, typically in the range of 1–100 micrometers (μm), while the filtration efficiency is defined as the fraction of particles removed, which is highly dependent on the filter beta ratio *(β)* and particle size.
The beta ratio *(β)* is used to describe the filtration performance, while the $\beta$=2 means 50% efficiency (1 from 2 particles is removed) and further $\beta$=200 means 99.5% efficiency (199 from 200 particles are removed by the filtration system).

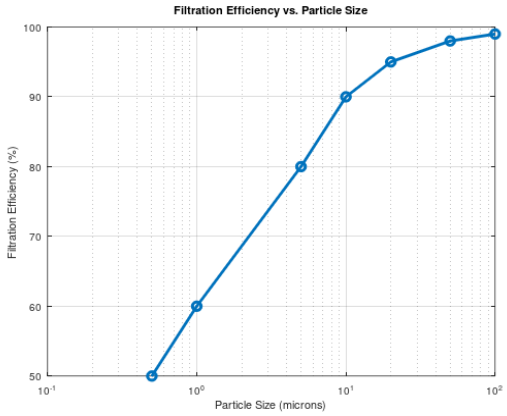


**Fig. 5.** The filtration efficiency according with the particle size (microns)

The study highlights the different conditions with impact on the contaminant's concentration and the system behaviour over time.

**Table 1.** Numerical initial values

| Crt. No. | Parameter | Value | |
|---|---|---|---|
| 1. | Fluid domain length | 1.00 (m) | |
| 2. | Fluid flow velocity for x and y coordinate components | u=0.1 m/s | v=0.05 m/s |
| 3. | Filtration efficiency | 50 – 99 % | |
| 4. | Number of particles | 100 | |
| 5. | Analysis time steps | 100 | |
| 6. | Particle size distribution | Equal size | |
| 7. | Particle initial position | Random distribution | |

Regarding the particle movement, it is considered that are entrained by the flow (Euler velocity field).
The filtration system removes particles according with filtration capacity, while the contaminant particles of constant size are in motion influenced by the fluid velocity field.

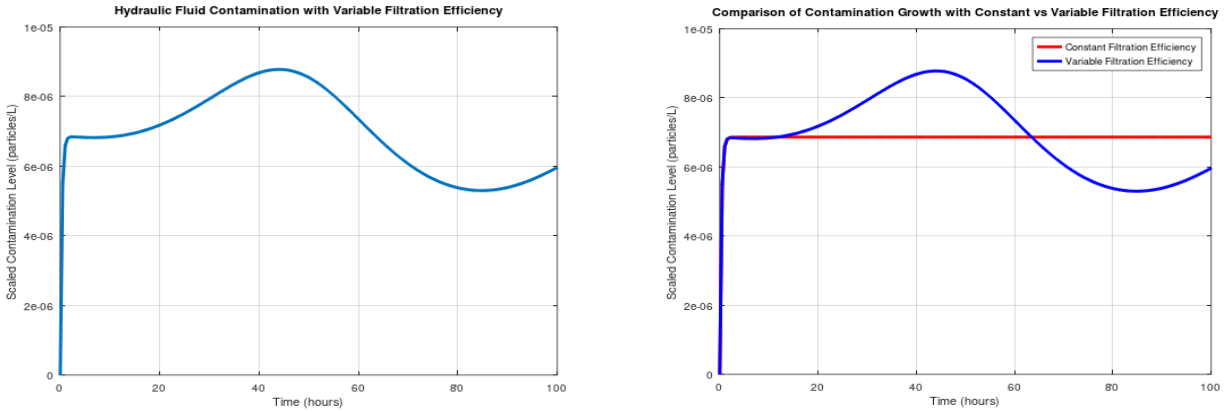


a) Fluid contamination due to variable efficiency filtration system

b) Fluid contamination due to constant and variable efficiency filtration system

**Fig. 6.** The hydraulic fluid contamination function of constant and variable filtration efficiency

For moving particles using Lagrange method is tracked the position, according with the Euler grid interactions. The contaminant concentration is calculated at each grid cell and further updated in time. The filtration system enhances the particle concentration reduction over time, with

proportional influence of filtration efficiency value. Filtering solutions with constant (theoretical) and time-variable efficiency (real condition) are highlighted in Figure 6.
The analysis results will emphasize the particle concentration field over time and contaminant dispersion and accumulation at the fluid region over time.
The obtained results are presented in figure 7, being emphasized the fluid flow

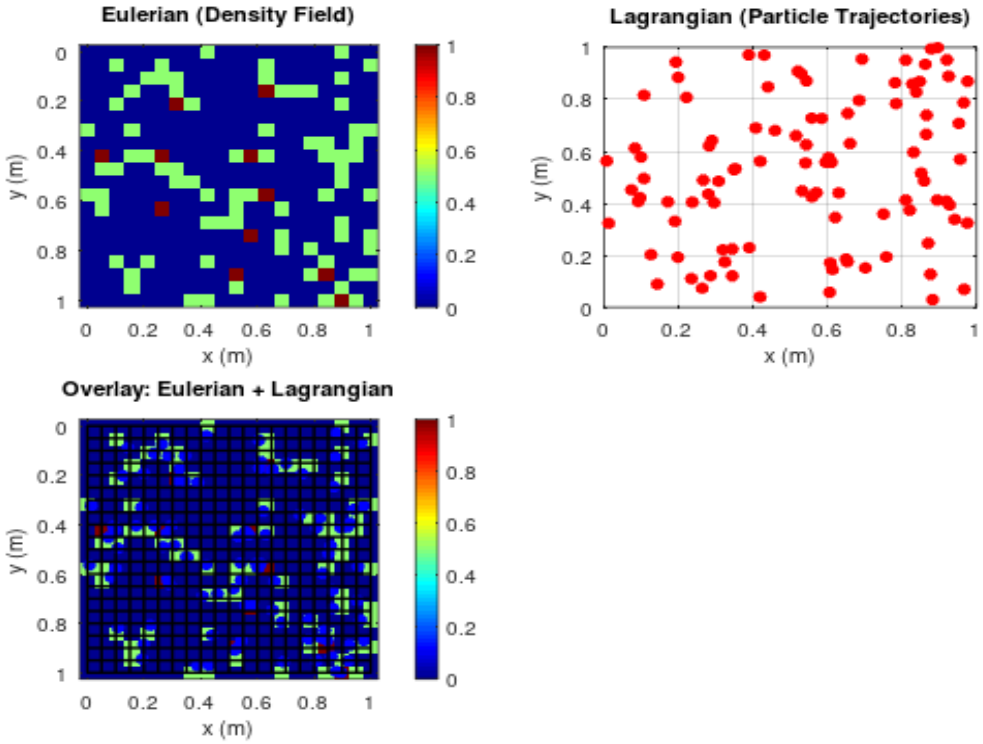


a) Filtration system efficiency of 50 %

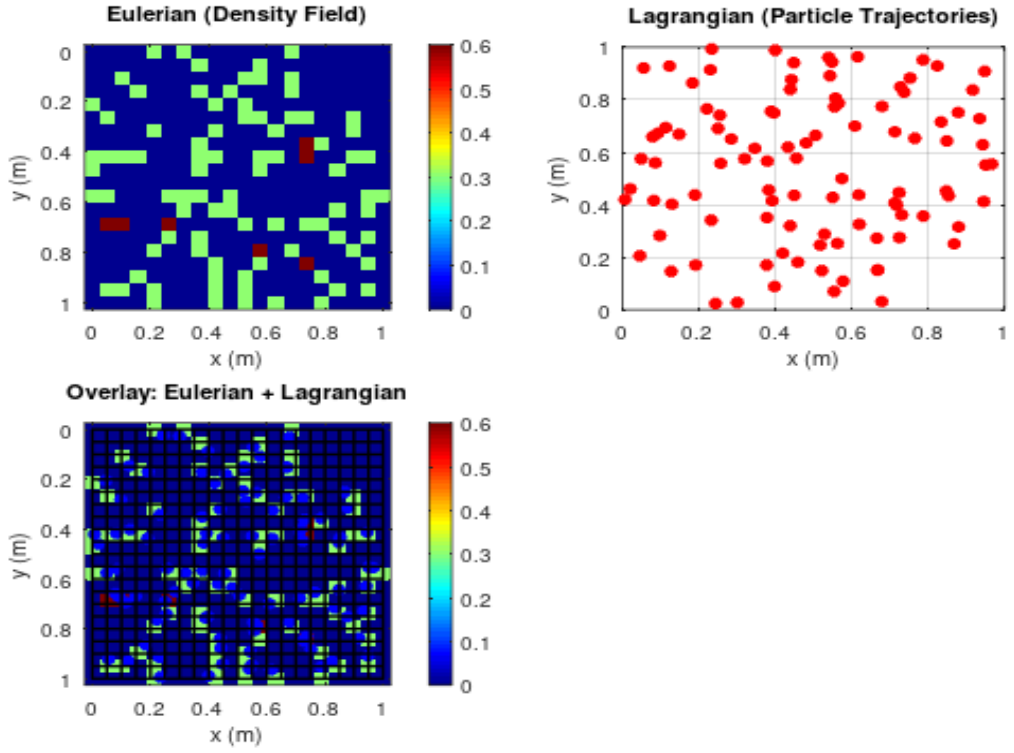


b) Filtration system efficiency of 70 %

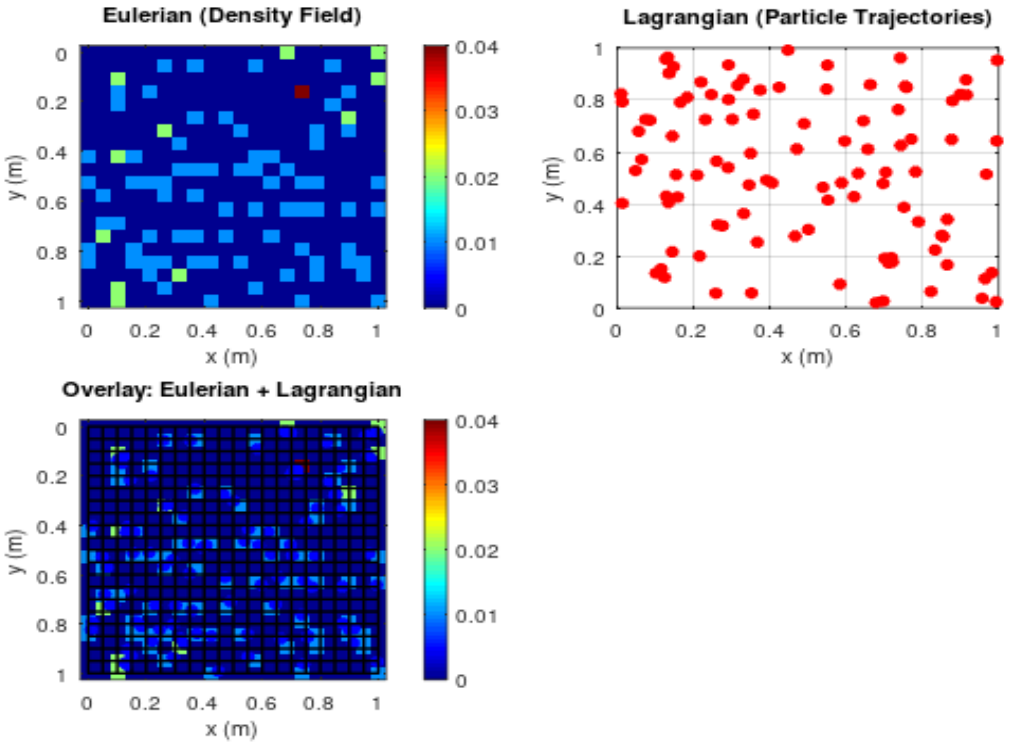


c) Filtration system efficiency of 99 %

**Fig. 7.** The particle contaminant dispersion concentration field and accumulation at the fluid region over time based on hybrid approach with different filtration efficiency values

As shown on the obtained results the concentration of contaminant particles is drastically reduced in the case of analysis corresponding to the high values of the efficiency of the filtration system as observed in figure 7.
The specific diagram for contaminant concentration according with filtration efficiency is presented in figure 8 highlighting the major differences obtained by the analyzed cases with specific values declared.

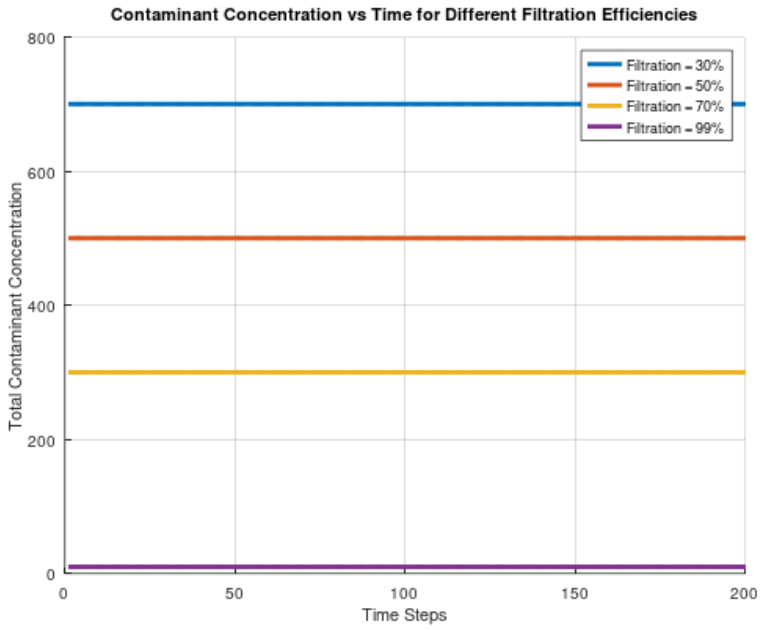


**Fig. 8.** Contaminant concentration versus time steps due to filtration efficiency range

Based on the results obtained from the numerical analysis performed, it can be observed the particular importance of the filtration system action on the cleanliness of the working fluid which must be at an upper limit in order to obtain the best operation results for the hydraulic system. Based on the specific analysis methods, the situations of specific concentrations of contaminant particles were identified and how they can be removed as a result of the action of the filtration system operating at different efficiency values, resulting from this the importance of permanently ensuring a high filtration efficiency, as an essential condition to be applied in order to ensure the optimal operating conditions of the hydrostatic system serving a certain work equipment.

## 5. Conclusions

Fluid contamination in hydraulic systems arises from a variety of sources, both internal and external, during system operation.
Contaminants directly affect the system performance, reduce component lifespan and further increase the maintenance costs.
The present paper presents the modeling approach using the Euler and Lagrange methods widely used in fluid mechanics and for contamination analysis enhancing the contaminants motion, dispersion and interactions with hydraulic fluid systems.
As shown in the paper, each method presents a unique perspective on how particles or contaminants move through the fluid region, each method being suited for different analyzes types in fluid dynamics field, including hydraulic and lubrication systems.
The Euler method focuses on fixed points in space, monitoring the fluid properties like velocity, pressure and contaminant concentration, as they change over time. The main advantages are related by analyzing large-scale contamination behavior, being well-suited for steady-state and continuous-flow scenarios and representing a simpler computationally method for systems with fixed geometries.
The Lagrange method tracks individual particles or fluid elements as they move through the system, following their trajectories over time and provides detailed, particle-level insights, captures localized effects, such as particle deposition and wear, being ideal for transient (time-varying) contamination events.
In practical contamination analysis, Euler and Lagrange methods are often used together, as hybrid models. In this manner the Euler model describe the overall flow field and contaminant concentrations, while the Lagrange model track the specific particles for detailed insights.
It is emphasized the practical importance within the hydraulic systems regarding special design optimization, while through Euler model is optimized the filter placement and flow paths for efficient contaminant removal.
For wear and damage prediction the Lagrange model provide a proper prediction on where the particles will be accumulated and further could cause wear.
As the hydro static system operation requires real-time monitoring, both methods support advanced diagnostic tools, represented by numerical analysis approaches for simulations, in order to predict the contamination risks and improve maintenance schedules.

**Acknowledgments**

The research within this paper was conducted within Fluid Mechanics Laboratory, Engineering Sciences and Management Department, Engineering and Agronomy Faculty of Braila, "Dunarea de Jos" University of Galati and with the support of Machine Mechanics and Technological Equipments MECMET Research Center, "Dunarea de Jos" University of Galati, Engineering and Agronomy Faculty of Braila and received no external funding.

**References**

[1] Axinti, G., and A.S. Axinti. *Hydraulic and pneumatic drives – Components and systems, Functions and features/Acţionări hidraulice şi pneumatice – Componente și sisteme, Funcții și caracteristici*. Vol. 1. Chişinău, Tehnica-Info Publishing House, 2008.
[2] Axinti, S., and F.D. Șcheaua. *Introduction to industrial hydraulics/Introducere în hidraulica industrială*. Galati, Galati University Press, 2015.

[3] Axinti, G., and A.S. Axinti. *Hydraulic and pneumatic drives – Bases of Calculation, Design, Operation, Reliability and Drive Diagrams*/*Acţionări hidraulice şi pneumatice – Baze de Calcul, Proiectare, Exploatare, Fiabilitate şi Scheme de Acționare*. Vol. 3. Chişinău, Tehnica-Info Publishing House, 2009.

[4] Muttenthaler, Lukas, and Bernhard Manhartsgruber. "Euler–Lagrange CFD simulation and experiments on accumulation and resuspension of particles in hydraulic reservoirs*." Journal of the Brazilian Society of Mechanical Sciences and Engineering* 42, no. 4 (2020): 209.

[5] Zhang, Dongxiao, and Shlomo P. Neuman. "Eulerian-Lagrangian analysis of transport conditioned on hydraulic data: 1. Analytical- numerical approach." *Water Resources Research* 31, no. 1 (1995): 39-51.

[6] Borges, Jonatas Emmanuel, Sammy Cristopher Paredes Puelles, Marija Demicoli, and Elie Luis Martínez Padilla. "Application of the Euler–Lagrange Approach and Immersed Boundary Method to Investigate the Behavior of Rigid Particles in a Confined Flow." *Axioms* 12, no. 12 (2023): 1121.

[7] Sruthi, K. V., Heejun Suk, Elango Lakshmanan, Byung-Gon Chae, and Hyun-su Kim. "The Modified Eulerian-Lagrangian Formulation for Cauchy Boundary Condition Under Dispersion Dominated Flow Regimes: A Novel Numerical Approach and its Implication on Radioactive Nuclide Migration or Solute Transport in the Subsurface Environment." *Journal of Soil and Groundwater Environment* 20, no. 2 (2015): 10-21.

[8] Muttenthaler, Lukas, and Bernhard Manhartsgruber. "Prediction of particle resuspension and particle accumulation in hydraulic reservoirs using three-phase CFD simulations." Paper presented at the ASME/BATH 2019 Symposium on Fluid Power and Motion Control, Longboat Key, Florida, USA, October 7–9, 2019.

[9] Croucher, Adrian E., and Michael J. O'Sullivan*. "*Source terms in Eulerian–Lagrangian contaminant transport simulation." *International Journal for Numerical Methods in Engineering* 62, no. 5 (2005): 682-699.

[10] Ziggaf, Moussa. *Study and implementation of an Eulerian-Lagrangian method on 2D/3D unstructured meshes for the numerical simulation of fluid flow models*. Diss. Université Paris-Nord-Paris XIII; Université Mohammed VI Polytechnique (Benguérir, Maroc), 2023.

[11] Han, Kun, Yongfa Diao, Jiawei Zhuang, and Minghao Chu. *"*The effects of imposed swirling flow on the transport and deposition of particulate pollutants in the 90° industrial duct bends: An Eulerian-Lagrangian approach*." Indoor and Built Environment* 33, no. 4 (2024): 707-721.

[12] Lovrec, Darko, and Ignacijo Biluš. "Flow conditions inside a small hydraulic tank at excessive flow rates." Paper presented at the International Conference Fluid Power – FT 2021, Maribor, Slovenia, September 16-17, 2021.

[13] Morel-Seytoux, Hubert J. "Conjunctive operation of a surface reservoir and of groundwater storage through a hydraulically connected stream." Technical report. Colorado State University, 1984.

[14] Emmanouil, V., E.P. Skaperdas, T.D. Karapantsios, and K.A. Matis. *"*Two-phase simulations of an off-nominally operating dissolved-air flotation tank*." International Journal of Environment and Pollution* 30, no. 2 (2007): 213-230.

[15] Feo, Alessandra, Riccardo Pinardi, Emanuele Scanferla, and Fulvio Celico. *"*How to minimize the environmental contamination caused by hydrocarbon releases by onshore pipelines: The key role of a three-dimensional three-phase fluid flow numerical model.*" Water* 15, no. 10 (2023): 1900.

[16] Havryliv, Roman, Iryna Kostiv, and Volodymyr Maystruk. *"*Using the Computational Fluid Dynamic to the Wet Scrubbing Process Modeling*."* Paper presented at the 2021 11th International Conference on Advanced Computer Information Technologies (ACIT), Deggendorf, Germany, September 15-17, 2021.

[17] Azimian, Mehdi, and Hans-Jörg Bart. *"*CFD simulation and experimental analysis of erosion in a slurry tank test rig." Paper presented at the 7th International Conference EFM12 – Experimental Fluid Mechanics, Hradec Králové, Czech Republic, November 20-23, 2012. *EPJ Web of Conferences* 45 (2013): 01009.

# Mechatronic System for Monitoring a Warehouse of Hydraulic and Pneumatic Equipment

PhD. student **Iulian-Alexandru VLĂSCEANU[1,*],** Ph.D.Eng. **Mihai AVRAM[1],**
Ph.D.Eng. **Victor CONSTANTIN[1]**

[1] National University of Science and Technology POLITEHNICA Bucharest

* alexandru_vlk@yahoo.com

***Abstract:*** *The paper presents an original structure for an autonomous system designed to monitor objectives of strategic importance. The system was physically developed, then validated and optimized. In this work, the authors propose a methodology for implementing the designed system for a potential beneficiary***.**

***Keywords:*** *Mechatronic system, monitoring system, drone, mobile robots*

## 1. Introduction

Today, there are numerous applications for robots in both industry and other fields, one of which is their use for monitoring a strategic objective. Used individually or as part of surveillance "teams," mobile robots and drones can compensate for the shortage of personnel in security patrols and, at the same time, help reduce the costs associated with this activity.
In the United States, for example, according to the Bureau of Labor Statistics, approximately one million work hours are needed each night for security guards to perform their duties, at an annual cost of around $47,000 per agent [1]. This immense workload involves mentally monotonous and often exhausting patrols in poorly lit areas, dirty environments, and similar conditions. These harsh conditions significantly increase costs for security companies due to the high employee turnover, necessitating constant recruitment, hiring, and training activities. Additionally, because of the aforementioned conditions, many recruits quit after a short period of time.
Under these circumstances, the issue of security guards requires a new and innovative solution. The use of mobile robots and drones in security and surveillance activities can address the problem outlined above. In this way, the shortage of personnel can be compensated, and costs will be significantly reduced, as expenses related to recruitment, background screening, drug testing, uniforms, and training for security guards will no longer be necessary.
Autonomous mobile robots or drones move freely within the supervised area along dynamic trajectories generated by intelligent software that optimizes movements and assigns the perfect path for each operation [2]. Thanks to the use of state-of-the-art sensors and scanners, they can identify and avoid obstacles, operating safely in the area in collaboration with people and other equipment. However, highly versatile mobile robots and drones must be used, capable of easily integrating with all types of objectives that require surveillance, as no modifications to the existing infrastructure should be necessary. A member of the surveillance team, whether a mobile robot or a drone, must have the following characteristics:

- *be autonomous:* meaning it should move freely, navigate using virtual maps of its operating area, and not be confined to predefined trajectories or closed, perimeter navigation circuits;
- *be intelligent:* their movements should adapt to each task and follow routes generated by integrated navigation software that calculates the most efficient path for each member. Additionally, they must detect and avoid all types of obstacles, whether stationary or moving, and reconfigure their route in real time;
- *it should be flexible:* meaning it should be able to perfectly adapt to the general layout of the monitored objective and not require any structural modifications; its operation should be easy and quick to implement;
- *it should be scalable:* meaning the team structure should be easily expandable by introducing new robots or drones, or reduced by eliminating some members to adapt to the

specific requirements of the monitored objective at different times; there may be operational changes in the company using the objective, such as when seasonal peaks in demand occur;
- *it should be efficient:* a management software for the entire team monitors and ensures the movement of team members and anticipates their trajectories to assign the ideal task to each member;
- *it should be precise:* each member must perform tasks with absolute accuracy, which contributes to a significant reduction in errors and an increase in the efficiency of the surveillance operation;
- it should be safe: team members operate in highly complex environments involving people, goods, layout systems, and other equipment; a series of highly precise anti-collision sensors and scanners provide stability and reliability to all their movements.

To fully harness the potential of these teams in ensuring security, it is essential to follow certain steps and carefully plan the implementation of the solution.

## 2. The structure of the proposed surveillance system

The solution proposed in this paper consists of creating a "team" made up of:
- several mobile robots (their number being determined by the complexity of the objective to be monitored); two design options for mobile robots have been considered, namely: tracked mobile robots (figure 1) and quadruped mobile robots (figure 2);
- a drone; two design solutions have been developed (figure 3);
- a measurement system that provides real-time information about the positions of the monitoring team members to the command unit;
- a series of sensors placed on the robots - proximity sensors, temperature sensors, humidity sensors, cameras, etc.;
- a camera mounted on the drone;
- the command unit of the system.

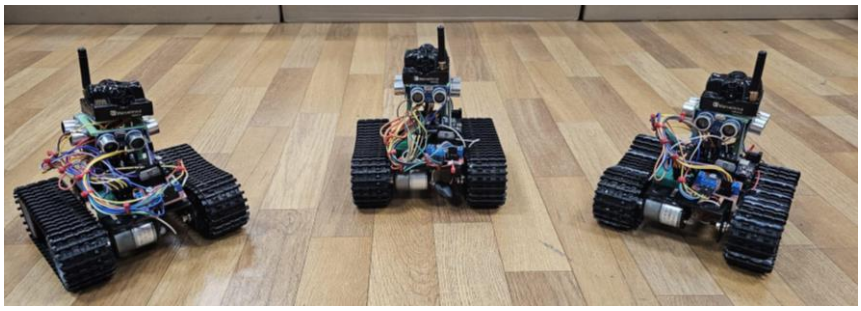

**Fig. 1.** Mobile tracked robots

**Fig. 2.** Quadruped mobile robots

**Fig. 3.** The drone models used

The robots patrol the monitored area; their movement follows predefined routes based on the needs and geometry of the monitored objective. The position of the robots will be tracked by a specially designed measurement system placed within the respective enclosure; any deviation of the robots from the predefined route is corrected in real-time. When an "event" is detected, the system's command unit will be notified. Immediately, the measurement system will transmit the position of the mobile robot near the event to the command unit; at the same time, the command system will deploy a drone to the event area. The drone will gather additional information about the event, primarily images from the event's location. This information will be processed and analyzed in real-time, and based on it, the command unit will decide what actions should be taken.
The measurement system used is manufactured by Marvelmind [3], a company specializing in autonomous robotics, which provides users with a complex architecture designed to combine ultrasonic sensors with an Inertial Measurement Unit (IMU) and post-processing for fast-moving objects. This system uses fixed and mobile ultrasonic beacons to accurately track (± 2 cm) the location of mobile robots and drones. Its setup and operation are managed via a router and a configuration application. The location of a mobile beacon is calculated based on the propagation delay of an ultrasonic signal to a set of stationary ultrasonic beacons using trilateration, a geodetic method based on measuring the sides of the triangles in a network. Trilateration is the foundation of GPS; the method involves determining distances, which are then used to calculate angles. Once calculated, these angles can be used alongside the distances to determine the position of target points.
The proposed system, as a whole, is a mechatronic system because:

- the mobile robots and drones are typical mechatronic products;
- the mobile robots and drones are equipped with a series of sensors that transmit real-time information about the environment in which they operate;
- each "member" autonomously performs its task, only calling on the central unit in situations it cannot resolve alone;
- there is an internal measurement system that tracks the positions of the mobile robots and the drone in real-time;
- the "members" of the team can communicate with each other and with the central unit through special communication interfaces;
- the entire process is controlled by a command unit structured around a PC.

It is therefore a complex mechatronic structure that can be seen as one that aligns with the principles underlying the new industrial revolution – Industry 4.0 [4].
The system was created, for validation purposes, using mostly components available in the Mechatronics and Precision Mechanics Department, with the rest being inexpensive, standardized, and easily accessible components.
The authors aimed to provide users of such systems with an intelligent surveillance solution that could be easily implemented at an acceptable cost.

## 3. The methodology for implementing the developed system for a potential user

In order to implement the developed system for a potential user, such as a warehouse for hydraulic and pneumatic automation equipment, the algorithm presented in figure 4 was developed.

The proposed implementation methodology involves the following steps: evaluating the monitored area, creating a map of this area, identifying the hardware structure of the robots, determining the trajectory of the mobile robots, identifying the events that need to be reported, and activating the system.

Evaluating the monitored area involves measuring the surfaces considered so that the optimal number of robots required for efficient monitoring of the working area can be determined. At this stage, it is also useful to identify the main obstacles that robots may encounter, such as architectural elements, furniture, etc. Interaction with human elements will not be considered at this stage. Additionally, factors that may negatively impact the operation of mobile robots or interfere with drone functionality are considered, such as areas with high or low temperatures, increased humidity, or areas where robots could be exposed to certain corrosive chemical elements, etc..

Indoor mapping involves creating detailed maps of buildings, rooms, and other enclosed environments. It utilizes technologies such as lidar, 3D sensors, cameras, and indoor GPS to determine the dimensions and structure of the monitored space. The technology is evolving rapidly, making mapping more accessible and accurate [5].

Mapping robots are a modern solution, and with their help, the necessary maps can be created quickly and correctly. Today, mapping robots are an indispensable tool in the exploration and optimization of complex interior spaces.

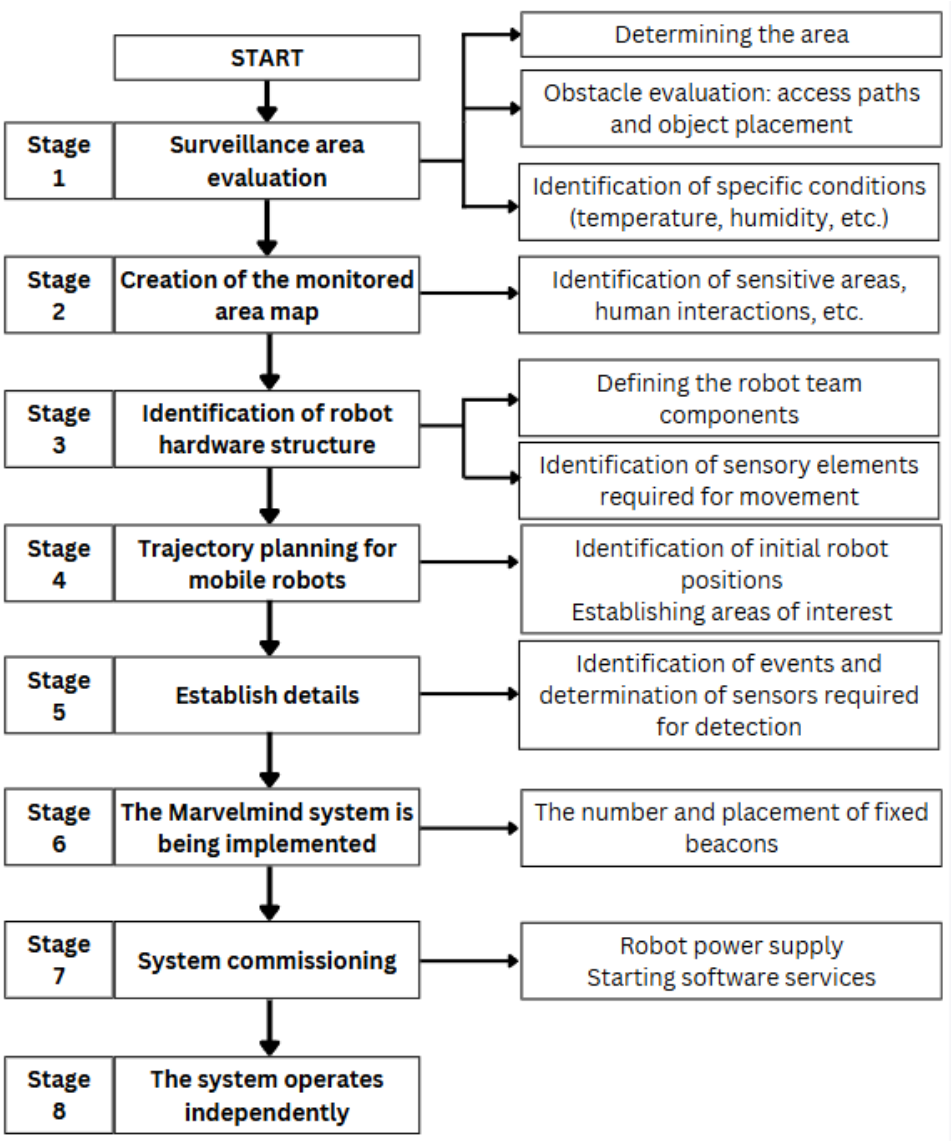


**Fig. 4.** The logical diagram of the implementation algorithm

As already mentioned, mobile robots are equipped with a variety of sensors, enabling precise navigation while simultaneously creating digital maps. Among these, we can mention:

- Lidar (Light Detection and Ranging) sensors, used to measure distances and generate detailed 3D representations of the environment;
- Ultrasonic sensors, often used for obstacle detection;
- RGB and RGB-D cameras, designed for capturing visual images and depth information;
- Inertial Measurement Units (IMUs) - monitor the robot's movement and orientation using accelerometers and gyroscopes, contributing to autonomous navigation;
- IR (infrared) sensors help detect proximity and object contours, being effective in low-light conditions;
- Pressure and contact sensors to prevent collisions.

SLAM (Simultaneous Localization and Mapping) technologies, based on combinations of sensors, allow the robot to localize itself and simultaneously map the space. Recent innovations, such as stereoscopic cameras and sensors with artificial intelligence, significantly increase mapping accuracy, opening up new possibilities for robots working in complex environments.

After the system is set up, it will operate autonomously, and intervention will only occur for maintenance operations. If necessary, any of the previously specified parameters (map, number of robots, etc.) can be modified at any time.

After the system is installed and powered on, it will operate according to the following logic:

- The Marvelmind measurement system reads the position of each member at any given moment in time;
- The location of the event is identified using sensors placed on the mobile robots;
- If an anomaly is detected, the drone moves to the coordinates of the mobile robot that sensed the event;
- The drone positions itself near the critical location and provides additional information about the event to the control systems;

The control system decides on the actions to be taken depending on the nature of the event.

## 4. Conclusions

The continuous development of mobile robots, drones, sensors, and transducers, which enable real-time data acquisition from the system, along with the increased processing power of computing systems, has created the conditions for integrating intelligent solutions for monitoring strategic objectives. In this way, in the initial phase, it is possible to track and record the parameters of interest from the monitored area to identify "events" and then determine the necessary measures.

The proposed system is capable of identifying and avoiding obstacles, operating safely in the monitored area, while also being cost-effective and easy to implement.

### References

[1] Atu Tech. "Robots could make up for the shortage of personnel in security patrols / Robotii ar putea compensa deficitul de personal din patrulele de securitate", July 6, 2016. Accessed December 9, 2024. https://www.supraveghere.org/robotii-ar-putea-compensa-deficitul-de-personal-din-patrulele-de-securitate/

[2] Nitzan, David. "Development of intelligent robots: Achievements and issues." *IEEE Journal on Robotics and Automation* 1, no. 1 (1985): 3-13.

[3] Constantin, V., M. Avram, C. Bucsan, and A. Vlasceanu. "Hardware structure of a surveillance system for strategic objectives." Paper presented at the 9th International Conference on Manufacturing Science and Education – MSE 2019 "Trends in New Industrial Revolution", Sibiu, Romania, June 5-7, 2019. *MATEC Web of Conferences* 290 (2019): 08004.

[4] Sfetcu, Nicolae. "The fourth industrial revolution, Industry 4.0 / A patra revoluție industrială, Industria 4.0". *MultiMedia*, December 2, 2020. Accessed December 9, 2024. https://www.telework.ro/ro/a-patra-revolutie-industriala-industria-4-0/.

[5] Sharma, Nitin, Jitendra Kumar Pandey, and Surajit Mondal. "A review of mobile robots: Applications and future prospect." *International Journal of Precision Engineering and Manufacturing* 24 (2023): 1695-1706.

# Air Quality Monitoring in the Environmental Processes

PhD. Stud. Eng. **Marius-Valentin DUMITRESCU[1],** PhD. Eng. **Fănel-Viorel PANAITESCU[2],** PhD. Eng. **Mariana PANAITESCU[2,*],** PhD. Eng. **Diana-Mariana COCÂRȚA[1]**

[1] Doctoral School of Power Engineering, National University of Science and Technology POLITEHNICA Bucharest

[2] Constanta Maritime University, Marine Engineering Faculty, Engineering Sciences in Mechanics and environment Department

* panaitescumariana1@gmail.com

***Abstract:*** *Classic air quality monitoring technology has reached its technological and cost limits. As spatial monitoring improves, pollution sources, dispersion patterns and health effects can be better addressed while reducing reliance on predictive models. In this context, the work presents a sustainable process of obtaining recycled plastic filament and the environmental conditions and testing of the finished product.*

***Keywords:*** *Plastic recycles, 3D printing process, fused deposition modelling, mechanical recycling*

## 1. Introduction

The sustainability of the environment is dependent on: the number of the population; rapidity materials development; technological processes and industry-specific activities; all these, more or less, are waste generators [1].
Aspects related to environmental sustainability are in the attention of researchers, but also among legislative priorities at European and global level, thus "Directive (EU) 2018/851/EC amending Directive 2008/98/EC on waste" emphasizes the need for improvement and transformation waste management terminology in sustainable materials management to protect, to conserve and improve the quality of the environment, to protect human health, to ensure the prudent, efficient and rational use of natural resources, to promote the principles circular economy, to increase the use of energy from renewable sources, to grow energy efficiency, to reduce the Union's degree of dependence on imported resources, to create new economic opportunities and boost long-term competitiveness [2].
Over time, waste legislation has evolved from the simple management of them to addressing health problems, protecting the environment and even avoiding them waste and the recovery of resources from generated waste [3].
The concern for the field of waste management is topical worldwide, given the fact that in recent years there has been an intensification and diversification of activities in all economic-social sectors, reaching an upward dynamic of the quantity generated [4,5, 6].
In the current context of the development of the sustainable society, there is the problem of reusing waste, especially plastic waste. The activity of selective collection of waste and its transformation into reusable materials is an important concern at the global level [1,2, 5]. One of these materials is Polyethylene terephthalate (PET), which was patented in 1941 by Dickson and Winfield when they combined phthalic acid with glycol-based substances [7].
PET is a common plastic substance used to make water bottles, carbonated drinks, juices and others. It is a semi-crystalline thermoplastic material created by the condensation of terephthalic acid and ethylene glycol. This material can be found like: semi-crystalline PET, amorphous PET and glycol modified PET with higher impact resistance. PET is durable and easy to transport, but can be difficult to degrade in nature. If not recycled, PET can remain in the environment for hundreds of years, polluting the sea and other environmental areas [6].
The purpose of this study is to analyse the method of transforming PET into filament for use in the 3D printing process. "PET 3D printing is the process of creating a three-dimensional part using PET (polyethylene terephthalate) via additive manufacturing. This type of PET is a stiff, strong material used to make products for waterproofing, bottling, and food packaging. It's one of the most

popular materials for Fused Deposition Modelling FDM/FFF-style 3D printing due to its chemical resistance, mechanical properties, and favourable melting temperature of 260°C" [7]. The material for 3D printing is named filament.

## 2. Material and Methods

### 2.1 Information about general characteristics of PET filament

PET is a polyester resulting from the esterification reaction of ethylene glycol in terephthalic acid. As the percentage of aromatic units in the polymer chain increases, so does its hardness and strength.

The properties of PET filament are [7]:

- excellent mechanical, thermal and electrical resistance;
- low absorption features;
- good flow characteristics.

The recycled material for PET filament are used PET bottles (virgin resin vPET, recycled material rPET and commercial material PETG) [6].

Another sources for 3D printing filament are:

- corn starch, tapioca roots or sugar cane, a very easy-to-use material for Polylactic Acid (PLA) (Figure 1) [8];
- glycol (G) + PET (Polyethylene terephthalate) for PETG (Figure 1) [8];
- thermoplastic polymer, ABS (acrylonitrile-20%, butadiene-25%, styrene-55%);

For each of these materials the properties are different (Table 1) [7].


**Fig. 1.** Types of PET filament [8]

**Table 1:** The properties of different types of PET [7]

| Characteristics of polyester | Polyethylene terephthalate (PET) | Polylactic Acid (PLA) | Acrylonitrile Butadiene Styrene (ABS) | PETG |
|---|---|---|---|---|
| Tensile strength (MPa) | 57 | 38 | 44 | 50.4 |
| E-modulus (MPa) | 2300 | 3120 | 1900 | 2020 |
| Elongation at break (%) | 70 | 7 | 10 .... 50 | 130 |
| Flexural Strength (MPa) | 82.5 | 106 | 2400 | 70 |

| Characteristics of polyester | Polyethylene terephthalate (PET) | Polylactic Acid (PLA) | Acrylonitrile Butadiene Styrene (ABS) | PETG |
|---|---|---|---|---|
| Glass transition temperature (°C) | 70 | 56.9 | 105 | 85 |
| Recycled content | 100% | 55% | 65% | 67% |
| Heat deflection temperature (°C) | 71.6-80.0 | 52 | 73 | 71 ... 103 |

The most common materials for 3D printing filament are PLA (in biomedical field, tissue engineering, in packaging industry, in textile industry) and ABS (in high temperature resistant objects).

### 2.2 Method

The purpose of this study is to analyse the method of transforming PET into filament for use in the 3D printing process, FDM - Fused Deposition Modelling. This FDM (Fused Deposition Modelling) rapid prototyping technology is the most widely used additive manufacturing technology and due to its simplicity it is also the most accessible. These characteristics recommend it for use in modelling, prototyping, but also in micro-production applications in low-technology, hard-to-reach areas. This method FDM is a process that includes "layer – by - layer deposition material, via a series of cross sectional slices" [9]. A CAD software is used to print 3D objects (Figure 1, Figure 2) [6].


**Fig. 2.** The design of sample PET filament

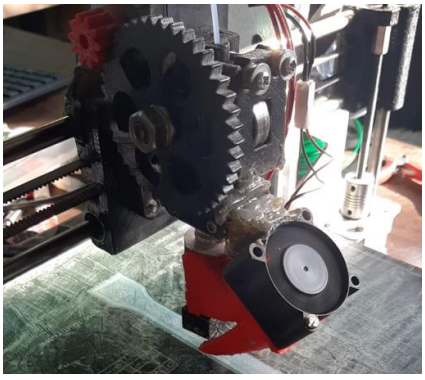

**Fig. 3.** 3D printing process with sample PET filament [6]

The design of the object is introduced in 3D printer (Figure 4) and after this the object is printed layer –by- layer deposition of raw material.

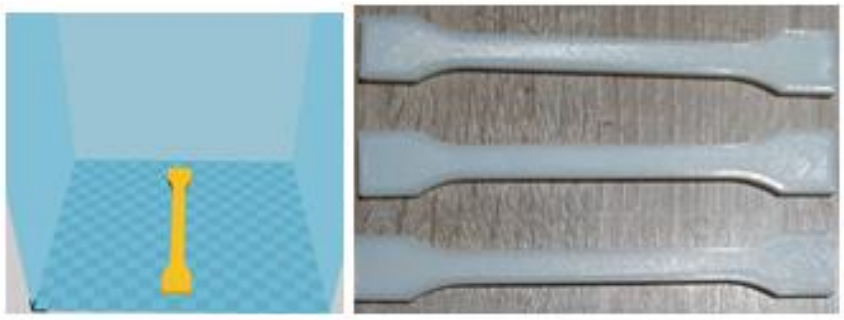

**Fig. 4.** CAD software used to print 3D objects

There are many other methods to design the objects [10, 11, 12].

### 2.3 Mechanical properties of PET filament

After obtaining the 3D printing material, the mechanical properties are analysed. The testing speed is varied from 3.5 to 5 mm/min. The time variation of the extrusion speed has a major influence on the filament thickness (Figure 5, Figure 6).

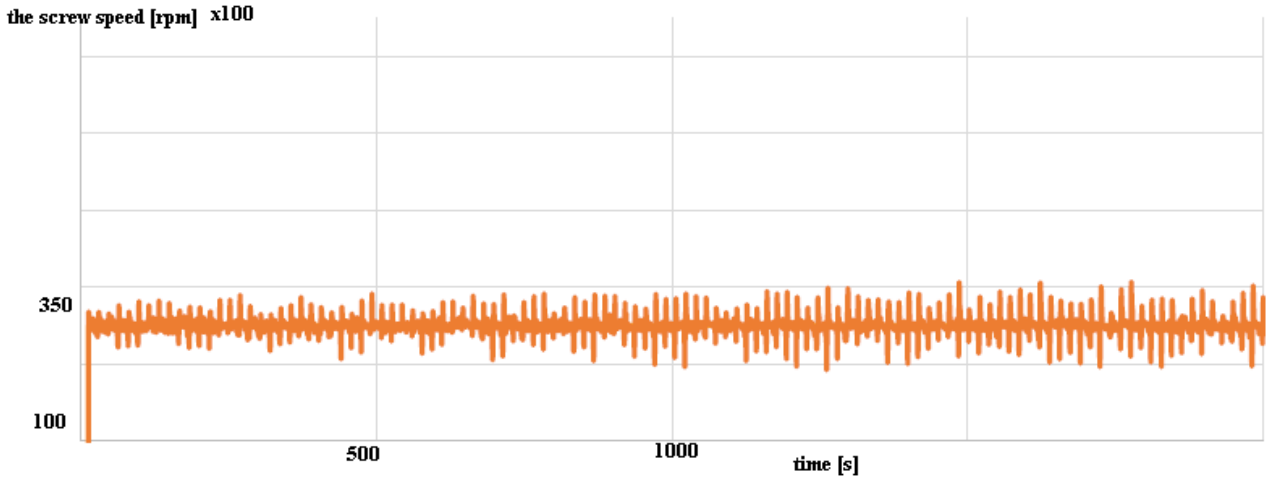


**Fig. 5.** The variation of screw extruder speed

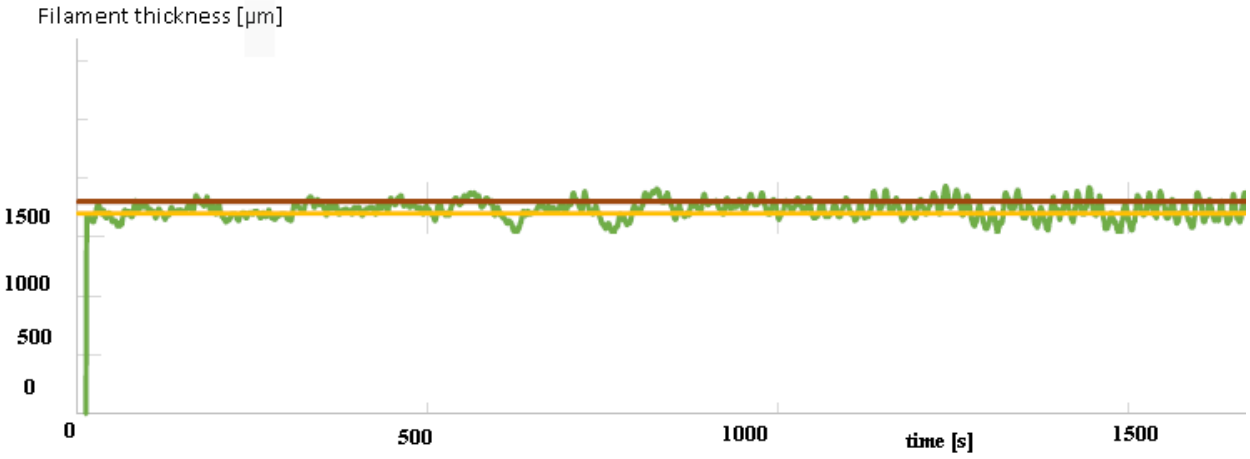


**Fig. 6.** The variation of filament thickness

It is observed that the variable speed changes the thickness of the filament. Therefore, a stable speed crew extruder is recommended (about 350 ... 380 rpm).
3D printing mostly uses plastic filaments which can be of various types and are made by following

the process of heating, extruding and cooling plastic.
Many industries have adapted re-using waste plastic products for the same purpose [9].
In this work the characteristics of PET filament which will be used for 3D printing process are shown in Table 2.

**Table 2:** Characteristics of 3D printing PET filament

| Characteristics | Polyethylene terephthalate (PET) |
|---|---|
| Tensile strength (MPa) | 42 ... 63 |
| E-modulus (MPa) | 3 330 |
| Elongation at break (%) | 69 |
| Flexural Strength (MPa) | 82.4 |
| Glass transition temperature (°C) | 70 |
| Recycled content | 100% |
| Heat deflection temperature (°C) | 70 .... 80 |

After a comparative analysis of the mechanical properties of general PET and PET filament we conclude:

- The minimum value of tensile strength for PET filament is 42 MPa, for industrial PET is 57 MP; the maximum value for PET filament is 63 greater than industrial PET;
- The PET filament has a better elasticity, when heat deflection temperature has a variation in the range 70 ... 800 C;
- During the heating cycles can observed the lamellar thickness distribution of the crystallites (~25% crystallinity);
- some printed objects show structural changes (elongations to tractions, ductile fractures) [13].

### 2.4 Environmental details of location for air quality monitoring

- **Thermal analysis of plastics**

The heat flux curves of waste PET and PLA are given in Fig. 7.

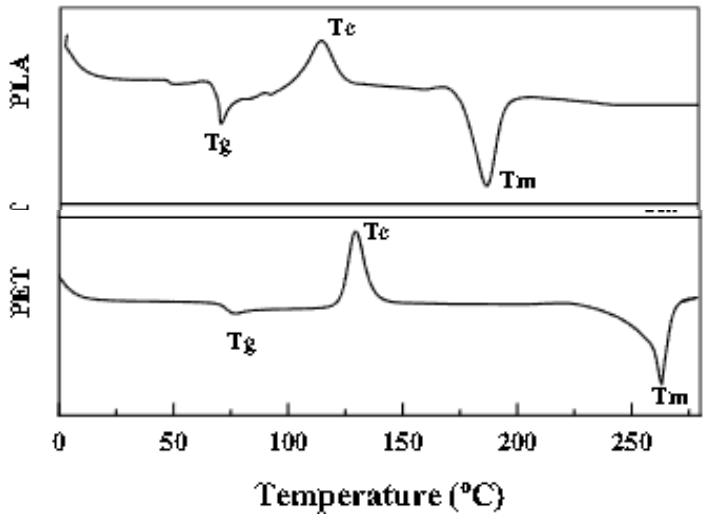


**Fig. 7.** The variation of heat flux

Where Tc (°C) – the crystallization temperature; Tg (°C) (glass tran-sition temperature; Tm (°C)-melting temperature.
We observe that if compare the heat capacity values of pure PET and pure PLA, the heat capacity value of PET is lower than PLA.

- **Environmental data of air monitoring in location**

The location of process is a workspace for which we have collected daily and weekly data (Table 3, Figure 8, Figure 9) to monitoring air quality in closed space.

**Table 3:** Daily and weekly variation on temperature and humidity

| Day/hour | Air temperature ( $^0$C ) | Air humidity (%) |
|---|---|---|
| 5/15/2023 21:21:00 | 22 | 39.1 |
| 5/15/2023 20:01:00 | 22 | 39.1 |
| 5/15/2023 18:51:00 | 22.4 | 38.6 |
| 5/15/2023 18:01:00 | 22.3 | 39.1 |
| 5/15/2023 14:41:00 | 22 | 39 |
| 5/15/2023 13:21:00 | 22 | 39.1 |
| 5/15/2023 12:51:00 | 21.5 | 40.6 |
| 5/15/2023 12:11:00 | 21.9 | 39.6 |
| 5/15/2023 9:21:00 | 21.7 | 40.1 |
| 5/15/2023 3:41:00 | 21.5 | 40.6 |

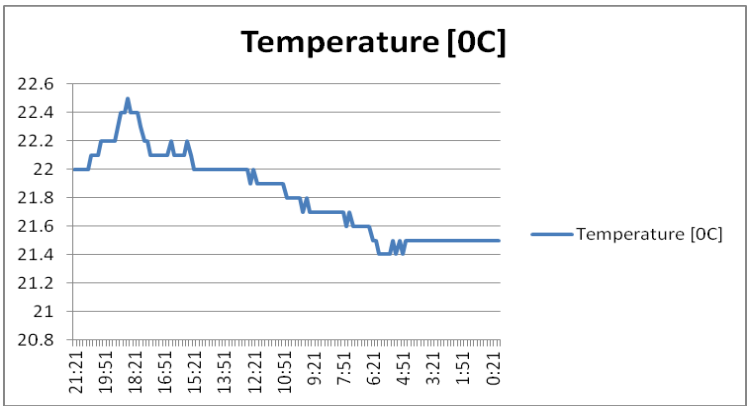


**Fig. 8.** Daily variation of temperature

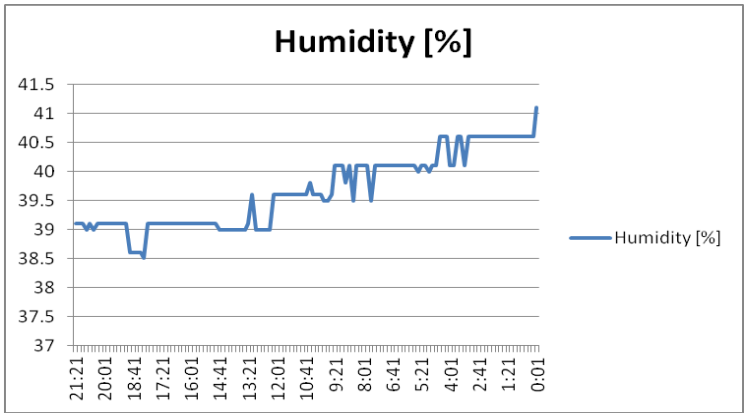


**Fig. 9.** Daily variation of humidity

The location can be provided with a connection to a photovoltaic system, consisting of a solar panel, buck boost inverter and battery (battery), which provides electricity on sunny days, thus contributing to the application of the concept of environmental sustainability.

## 3. Conclusions

According to the test standards for tensile (SR EN ISO 527-4:2000), shear (SR EN ISO 14129:2000), bending (SR EN ISO 14125:2000), impact (SR EN ISO 179-2:2002/ SR EN ISO 180:2001) test standards we can conclude that the samples obtained by 3D printing respect the layering of the fibres, their distribution being symmetrical and balanced, framing belong to the group of thermoplastic materials.
After several experiments, it can be concluded that the variation of the screw extrusion speed can influence the thickness of PET filament and its structural qualities. Also, the temperature variation of the heating cycle of the printing material is very important.

### References

[1] Department for Sustainable Development / Departamentul pentru Dezvoltare Durabilă. *National Strategy for Sustainable Development of Romania 2030 / Strategia Națională pentru dezvoltarea durabilă a României 2030*. 2018. Accessed November 12, 2024. https://dezvoltaredurabila.gov.ro/strategia-nationala-pentru-dezvoltarea-durabila-a-romaniei-2030-i.
[2] European Parliament and the Council of the European Union. *Directive (EU) 2018/851 of the European Parliament and of the Council of 30 May 2018 amending Directive 2008/98/EC on waste / Directiva (UE) 2018/851 a Parlamentului European și a Consiliului din 30 mai 2018 de modificare a Directivei 2008/98/CE privind deșeurile*. Accessed November 12, 2024. https://lege5.ro/Gratuit/gi4dinrwgu2q/directiva-nr-851-2018-de-modificare-a-directivei-2008-98-ce-privind-deseurile-text-cu-relevanta-pentru-see.
[3] Johnson, A. **"**The Development of Waste Management Law". Eastern Metropolitan Regional Council, International Solid Waste Association - ISTWA. Accessed November 12, 2024. https://www.iswa.org/knowledge-base/the-development-of-waste-management-law/?v=f5b15f58caba.
[4] United Nations Climate Change. **"**Kyoto Protocol Reference Manual on Accounting of Emissions and Assigned Amounts". *What is the Kyoto Protocol?* Accessed November 12, 2024. http://unfccc.int/kyoto_protocol.
[5] Bilitewski, B., G. Härdtle, and K. Marek. *Waste Management*. Springer Science & Business Media, 1996.
[6] McClements, Dean. **"**All About PET 3D Printing Filament". *Xometry*, September 19, 2022. Accessed November 14, 2024. https://www.xometry.com/resources/3d-printing/pet-3d-printing-filament/.
[7] Prior, Madeleine. "PLA vs PETG: Which Material Should You Choose?" *3Dnatives*, May 11, 2024. Accessed November 14, 2024. https://www.3dnatives.com/en/pla-vs-petg-which-material-should-you-choose-110520215/#!
[8] Raza, S.M., and D. Singh. *Experimental Investigation on Filament Extrusion using recycled materials.* Master Thesis in Mechanical Engineering, Halmstad University, 2020.
[9] Berman, B. "3-D printing: The new industrial revolution." *Business Horizons* 55, no. 2 (2012): 155-162.
[10] Hull, C.W. *Apparatus for production of three dimensional objects by stereolithography.* U.S. Patent, 4575330, 1986.
[11] Drumright, R.E., P.R. Gruber, and D.E. Henton. "Polylactic Acid Technology." *Advanced Materials* 12, no. 23 (December 2000): 1841-1846.

# A Flood Early Warning System Design and Implementation for the Rio Grande de Morelia Basin, Mexico

Dr. **Rodrigo ROBLERO-HIDALGO**[1], Dr. **Hector BALLINAS-GONZALEZ**[1],
M.I. **Margarita PRECIADO-JIMÉNEZ**[1,*], Dra. **Maritza Liliana ARGANIS-JUÁREZ**[2,3,*]

[1] Instituto Mexicano de Tecnología del Agua, Jiutepec, Mor., México

[2] Universidad Nacional Autónoma de México, Facultad de Ingeniería, México

[3] Universidad Nacional Autónoma de México, Instituto de Ingeniería, México

*preciado@tlaloc.imta.mx, MArganisJ@iingen.unam.mx

***Abstract:*** *This paper addresses flood risk management and the need for preventive measures to minimize flood impacts in the Rio Grande de Morelia basin, Mexico. Due to rapid population growth and limited urban planning, the city of Morelia faces recurring flood threats that cause significant damage to communities, infrastructure, and the environment. This research proposes the development of a Flood Early Warning System (FEWS) that integrates data monitoring across three levels, utilizing a hydrological model calibrated with a 0.77 correlation coefficient. Hydraulic modelling identified 878.87 hectares as high flood-risk areas. The results suggest that this methodology can structure an effective FEWS system for the Rio Grande de Morelia, enhancing flood prediction and mitigation capabilities through continuous system improvement, data expansion, and real-time monitoring.*

***Keywords:*** *Flooding, hazard management, hydrological basin, early warning system, Rio Grande de Morelia*

## 1. Introduction

Flooding occurs when precipitation in a watershed generates runoff that surpasses the capacity of riverbeds to contain it, causing overflow. This excess water can inundate low-lying areas, impacting nearby populations and surroundings. In Mexico, numerous cities have developed along rivers and are frequently affected by floods. Yet, policies and response measures to address flooding are typically reactive, deployed either during or after events, and often fall short of significantly mitigating damage. This reactive approach underscores the need for a shift in disaster management—moving from a passive to a proactive stance that prioritizes risk management and preventive actions. Effective flood prevention and mitigation require understanding the origins and flooding behaviour, along with fostering community awareness and preparedness [1]

Flooding remains a serious issue in the city of Morelia, exacerbated by increasing runoff from rain and a reduced capacity for water evacuation due to narrowing of the Rio Grande-Chiquito River system, including its main drains and tributaries in both urban and agricultural areas. Between 2002 and 2017, 22 neighbourhoods in Morelia, comprising 25,811 residents in 6,212 homes, were designated as flood-prone, alongside 500 hectares of farmland in the Rio Grande floodplain [2]. Mitigating flood damage requires both structural measures (e.g., construction projects) and non-structural measures (institutional and policy-based interventions). For this study, the focus is on non-structural civil protection measures, including planning, organization, coordination, and execution of actions aimed at reducing flood impact [3]

### 1.1 Flood Early Warning Systems Worldwide

A Flood Early Warning System (FEWS) relies on observation networks to collect environmental data, particularly rainfall and flow metrics for flash flood situations. Rainfall data is gathered from in-situ measurement stations, radar systems, satellite estimates, or a combination of these methods. An effective EWS requires computer infrastructure to collect, analysed, and distribute data through alert systems and communication channels. When a preparedness plan is in place and the population is educated on flood risks, early warning alerts can prompt individuals to take protective actions, such as seeking shelter, safeguarding personal items, or securing property.

Examples of EWS implementations include the United States, where hydrometeorological bulletins provide national information, supported by local measurement systems. Italy's Piedmont region employs a multidisciplinary Real-Time Flood Forecasting and ALERT system, while Colombia's Aburrá Valley leverages radar information within its Early Warning System for Natural Hazards. These systems generally operate through four key stages: data input (collected from field sources), data processing (building a forecasting model), alert dissemination (determining and communicating alert indicators), and system feedback for continuous improvement [4].

## 2. Materials and Methods

### 2.1 Study Area

This paper was conducted at RH12Gb-Lake Cuitzeo sub-basin, where the Rio Grande de Morelia flows through into of urban area Morelia, Michoacán, Mexico. The study area spans from the upstream portion from Cointzio Dam to the river's mouth at Cuitzeo, Lake covering a basin area of 1,748 km² [5], as shown in Figure 1.


**Fig. 1.** Location of the RH12Gb-Lake Cuitzeo sub-basin, Michoacán, Mexico [5]

## 3. Methodology

Developing an Early Warning System (FEWS) for the city of Morelia in Michoacán, Mexico, is essential due to the city's vulnerability to floods caused by heavy rains, particularly during the rainy and hurricane seasons. This type of system helps mitigate the risk of human and material losses through early detection and prompt response to potential flooding events. Below is an outline for implementing an effective EWS in Morelia.

A. Hydrometeorological Early Warning System (EWS) Operations:

The EWS operation integrates data from Automatic Meteorological Stations (EMAs), Automatic Hydrometric Stations (EHAs), and a central reception centre. This system consolidates data acquisition, hydrometeorological modelling, result analysis, and the issuance of alerts, as shown in Figure 2.

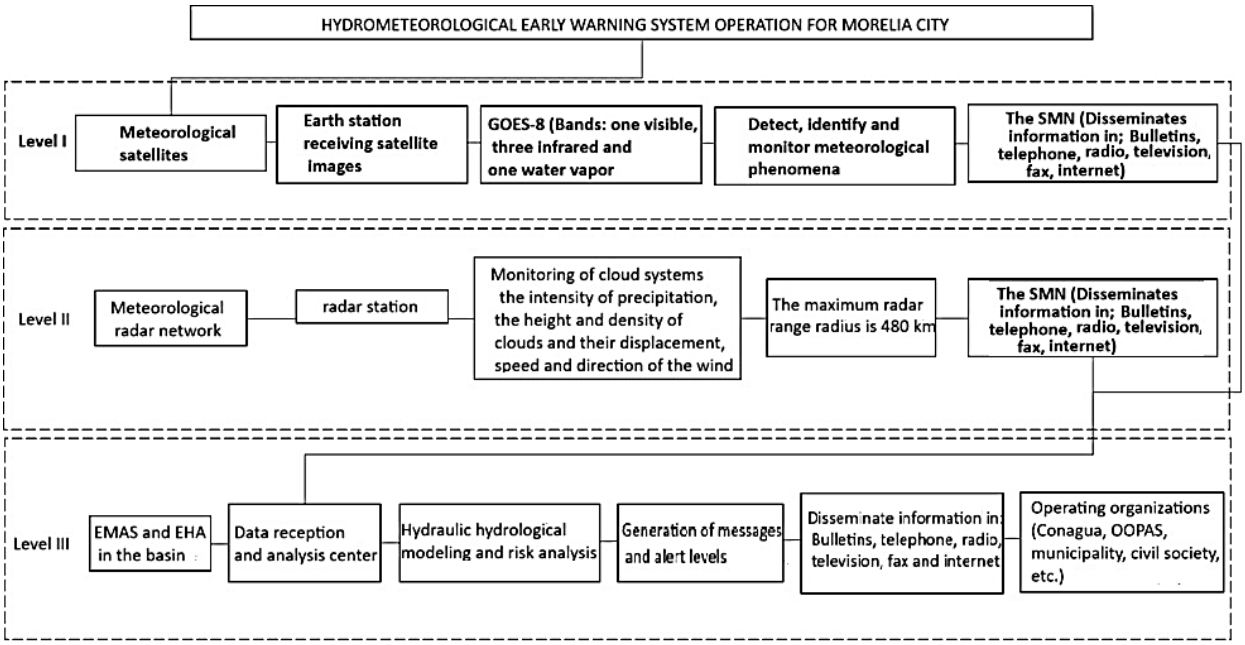


**Fig. 2.** Flood Early Warning System for Morelia. Source: Own design

B. Technical Organization

Key organizations involved in EWS operations and information dissemination include CONAGUA (National Meteorological Service), the Morelia Drinking Water, Sewerage, and Sanitation Agency (OOAPAS), civil protection agencies, media, educational institutions, private entities, and civil society.

C. Hydrometeorological Data Capture

The information reception centre aggregates data from meteorological and hydrometric stations, as well as satellite and radar feeds, to issue alarms for public protection. This centre comprises an interdisciplinary team responsible for informed decision-making.

D. Hydrological and Hydraulic Modelling

Hydrological simulations are initiated using HEC-HMS during critical weather events, utilizing input data from EMAs and EHAs, processed at 10-minute intervals. The output hydrographs are then inputted into the IBER hydraulic model, which generates flood envelope maps based on the water flow at sub-basin outflows.

E. Data Evaluation and Analysis

Following the modelling process, an evaluation phase compares simulation results with field data. This analysis assesses the progression of flood patterns and validates model results, as illustrated in Figure 3.

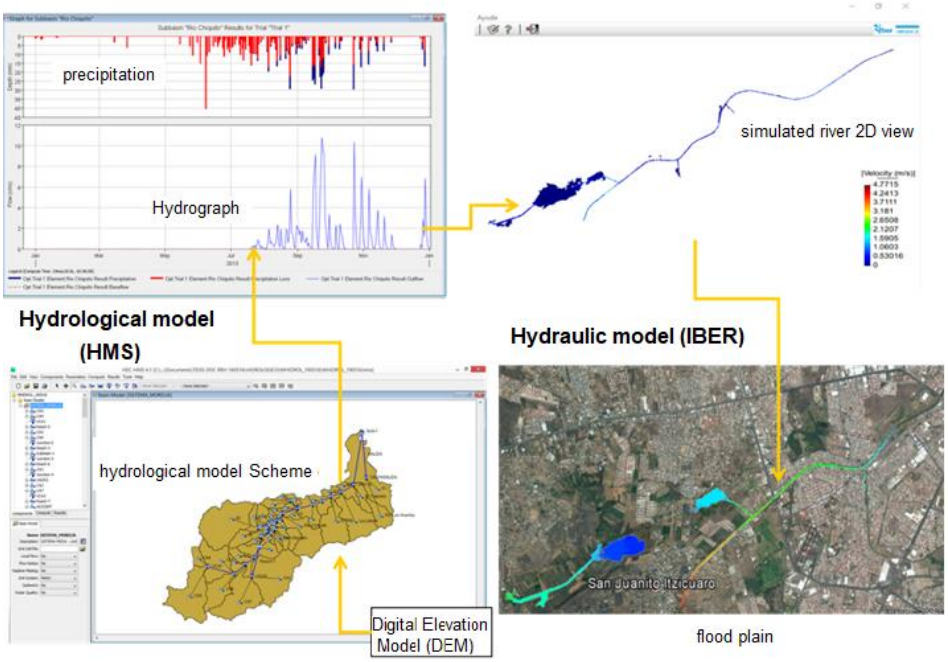


**Fig. 3.** Hydraulic simulation process using hydrological models

F. Issuance of Hydrometeorological Alerts

Flood risk alerts are issued in three levels during the rainy season:

Level I (Yellow): Initiates early warnings based on geostationary satellite (GOES) imagery. Data from visible, infrared, and water vapor channels covering North America are analyzed by the National Meteorological Service (SMN) and disseminated to relevant agencies.

Level II (Orange): Signals an imminent emergency based on continuous monitoring from 13 national radars. These radars provide real-time data on cloud systems, precipitation intensity, and wind conditions. The radar in Querétaro monitors the Morelia area, feeding back into Level I observations for updated alerts.

Level III (Red): Based on EWS data, it indicates an immediate flood threat when a tropical cyclone impacts the study area. This level incorporates information from automatic stations and GOES-based hourly updates to enable timely public warnings.

G. Level III EWS Operations for Morelia

Level III monitoring includes extensive data capture and model calibration to assess hydrometeorological threats. The system integrates hydrological [6] and hydraulic [7] models with topographic, soil, vegetation, meteorological, and hydrometric data, as depicted in the FEWS structural diagram in Figure 4.

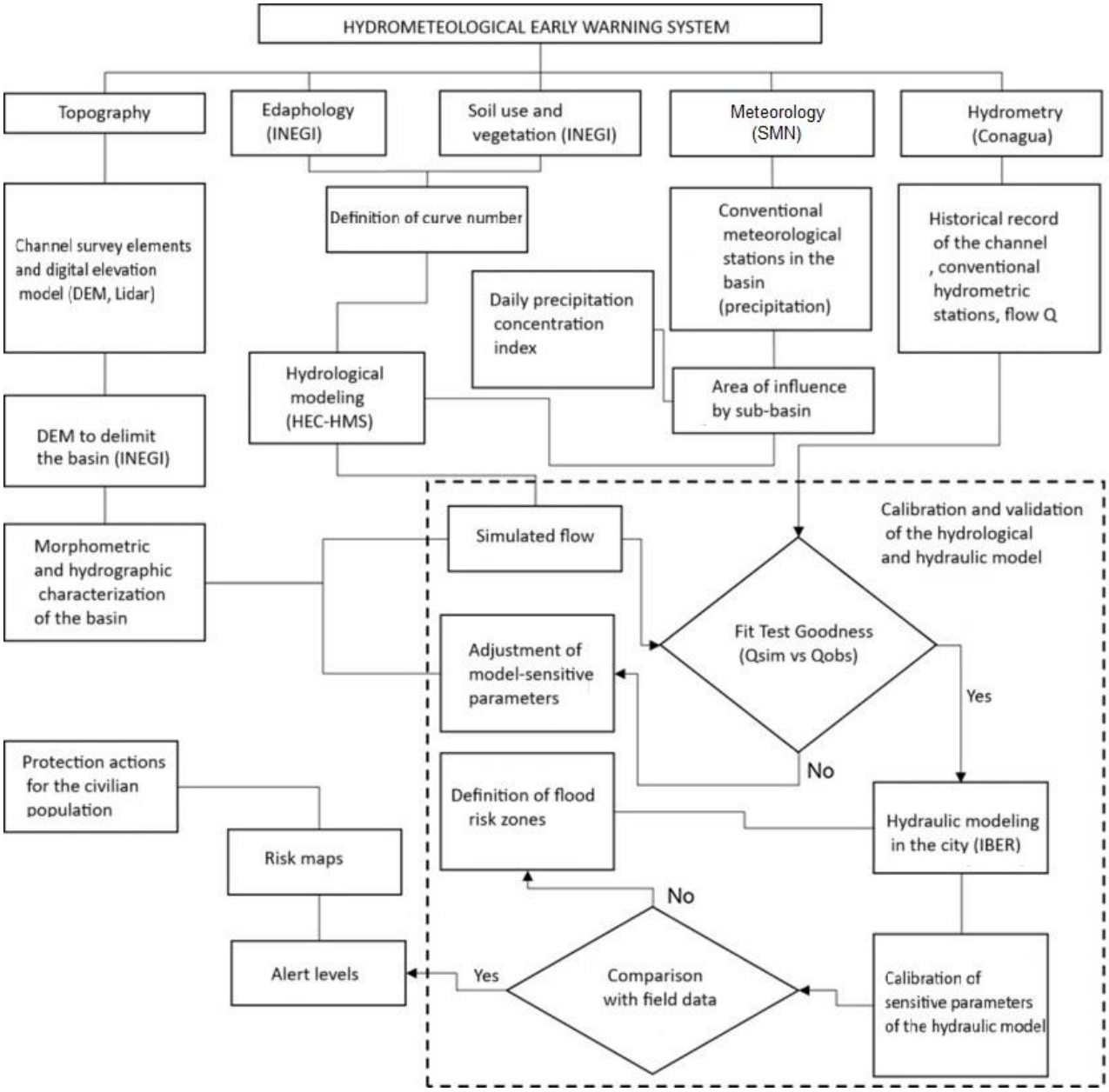


**Fig. 4.** Framework for FEWS implementation in the Rio Grande de Morelia basin. Source: Own design

## 4. Results and Discussion

A. Morphometric and Hydrographic Characterization

The morphometric and hydrographic analysis of the Rio Grande de Morelia basin involved calculating linear, area, and relief parameters. These are summarized in Table 1.

**Table 1:** Linear, area, and relief parameters of the Rio Grande de Morelia basin, as calculated by the authors

| Characteristics | Parameters | Value |
|---|---|---|
| Linear parameters associated with hydrography | channel Slope | 0.24% |
| | main channel Length | 59,275 km |
| | Stream Order | 6th order |
| | Fork ratio | 1.91 |
| | channels length average | 0.710 km |
| | Drainage Density | 1,622 km/km$^2$ |
| | Current Density | 2.03 channel/km$^2$ |
| | surface flow length Average | 0.308 km |
| Linear and area parameters of the basin | Area | 1,646.299 km$^2$ |
| | Form | elongated blade |
| | Perimeter | 284.714 km |
| | Basin length | 80,673 km |
| | Form Factor | 0.248 |
| | Elongation Ratio | 0.56 |
| | Roundness coefficient | 3.161 |
| Parameters associated with relief | basin slope Average | 1.51% |
| | Mean Basin Elevation | 2,176.951 m |

B. Soil Characterization

The basin comprises various soil types, including Fluvisol, Gleysol, Leptosol, Luvisol, Phaeozem, Regosol, Solonchak, Umbrisol, and Vertisol. Luvisol is the predominant soil, covering 32.98% of the basin area (515 km²), followed by Andosol, which spans 20.89% (326 km²).

C. Land Use and Vegetation

Land use in the basin is primarily dedicated to "annual rainfed agriculture," covering 29.76% of the area (486.53 km²). The second-largest coverage is "Pine Forest," occupying 10.61% (173.53 km²). The urbanized areas of the basin account for 9.83% of its area (160.76 km²).

D. Curve Number Generation for Each Sub-Basin

The Curve Number (CN) values were assigned based on the soil and vegetation characteristics in each sub-basin. The highest CN value of 81 was associated with "annual and semi-permanent irrigated agriculture" on type B soil, covering 9.4 km². The second largest CN area was "secondary shrubby vegetation of low deciduous forest" on type C soil, occupying 9.35 km² with a CN value of 78. These values were then used to calculate the weighted CN for each sub-basin, which served as input for the hydrological model.

E. Hydrological Model Calibration

The model calibration involved adjusting parameters, particularly the Curve Number (CN), to ensure alignment between simulated and observed flow data. This was achieved by fine-tuning model parameters until simulated flow closely matched observed flows within the calibration period, reducing discrepancies between the two [8]). Figure 5 presents a comparison between the simulated and measured hydrographs at The Plan hydrometric station, employing statistical tools like Calibration Coefficient (r), Schultz Criterion (D), Nash-Sutcliffe Efficiency (NSE), Mass Balance Error (m), and Root Mean Square Error (RMSE).

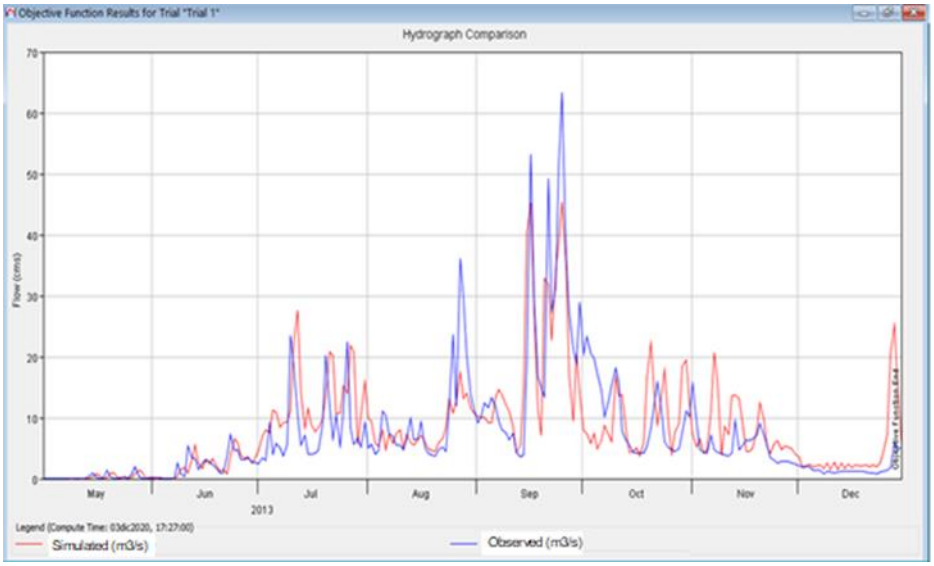


**Fig. 5.** Calibration hydrograph: Observed vs. Simulated flow at The Plan hydrometric station

Based on Figure 5, the difference between observed and simulated flows is 5.35 m³/s, which is considered acceptable for analysing the Rio Grande de Morelia.

F. Analysis and Identification of Vulnerable Areas from Hydraulic Modelling

The hydraulic modelling conducted for Morelia identified 878.87 hectares as high-risk flood zones (Figure 6). These areas include neighborhoods such as Fraccionamiento San Lorenzo Itzícuaro, Ampliación del Club Campestre La Huerta, Molino de Parras, Profesor Jesús Romero Flores, and the Cuauhtémoc sports unit, which align with findings reported [9]. These zones are especially susceptible to flood damage, highlighting the urgency for targeted mitigation measures and early warning capabilities.

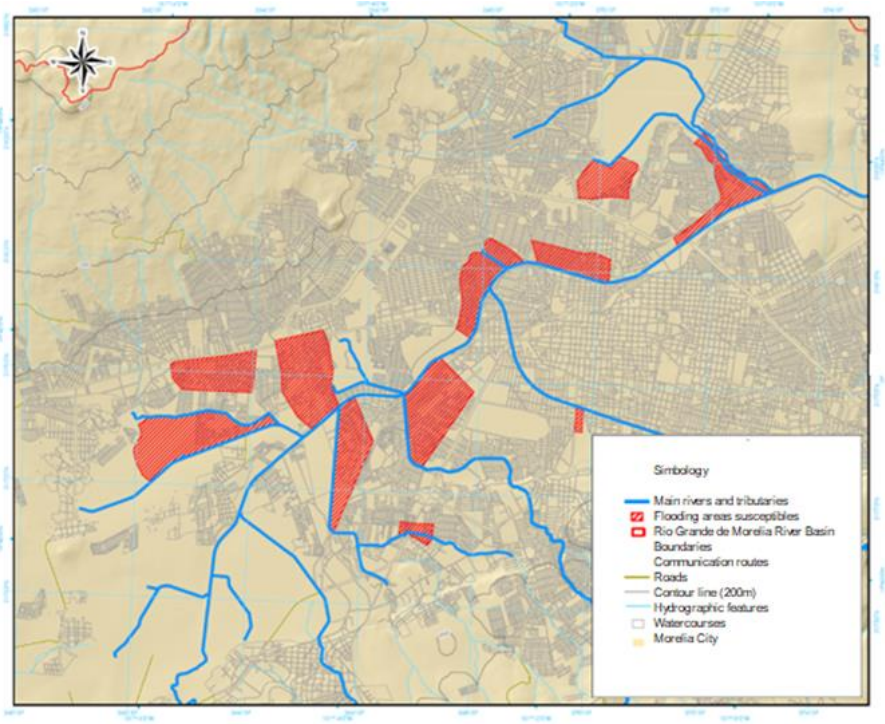


**Fig. 6.** Flood areas in Morelia

## 5. Conclusions

The implementation of a Flood Early Warning System (FEWS) in the Río Grande de Morelia basin represents a transformative advancement in proactive flood management for the area. Historically, Morelia's response to flooding has been largely reactive, proving insufficient given the rising frequency and intensity of flood events driven by rapid urbanization and limited infrastructure planning. FEWS leverages data-driven, real-time monitoring combined with hydrological modelling to provide a structured approach for anticipating flood risks and enabling timely interventions. This approach holds the potential to save lives, protect critical infrastructure, and contribute to regional economic stability. This paper underscores the importance of high-quality, extensive precipitation and flow data and the establishment of an automated hydrometric monitoring network to enhance predictive accuracy and responsiveness. The integration of these elements within FEWS encourages collaboration among government agencies, academic institutions, private entities, and local communities, elevating flood risk management to a priority level in Morelia's urban planning agenda.

As FEWS continues to evolve, it could become a model for flood management systems in other flood-prone regions. Ongoing improvements in data acquisition, model calibration, and community engagement can drive significant advances in flood mitigation throughout Mexico, fostering a shift toward prevention, resilience, and adaptive capacity in the face of climate variability. This system not only redefines flood preparedness but also highlights the need for a cohesive, multi-stakeholder approach to environmental resilience.

### References

[1] National Center for Disaster Prevention / Centro Nacional de Prevención de Desastres (CENAPRED). 2001. *Hazard Diagnosis and Disaster Risk Identification in Mexico*. Accessed October 21, 2024. http://www.cenapred.unam.mx.

[2] National Water Commission / Comisión Nacional del Agua (CONAGUA). 2015. *Update of the Study for Flood Control in the Río Grande-Río Chiquito System from the Cointzio Dam to Its Mouth to Lake Cuitzeo*. Michoacán Local Address. pp. 1–244.

[3] Salas, M. A. *Flood Protection Works*. National Center for Disaster Prevention, 1999.

[4] National Oceanic and Atmospheric Administration (NOAA). *Reference Guide for Flash Flood Early Warning Systems*, 2012. http://www.meted.ucar.edu/communities/hazwarnsys/ffewsrg_es/FFG_completa_es.pdf.

[5] SIATL. 2024. *River Basin Water Flow Simulator* / *Simulador de Flujos de Agua de Cuencas Hidrográficas*. Accessed October 22, 2024. https://antares.inegi.org.mx/analisis/red_hidro/siatl/.

[6] Feldman, A. D. *Hydrologic Modeling System HEC*-HMS.*Technical* Reference Manual, 2000.

[7] IBER. 2024.*Two-Dimensional Free-Sheet Flow Modelling in Shallow Water - Hydraulic Reference Manual*. p. 59. CEDEX, FLUMEN, GEAMA, CIMNE.

[8] Cabrera, J. *Calibration of Hydrological Models* / *Calibración de Modelos Hidrológicos*. Vol. 1. Universidad Nacional de Ingeniería, 2009. Accessed October 21, 2024. http://www.imefen.uni.edu.pe/Temas_interes/modhidro_2.pdf.

[9] Alarcón Neva, Anastasia, Jesús Chávez Morales, Óscar Luis Palacios Vélez, and Laura Alicia Ibáñez Castillo. "Estimating Areas Vulnerable to Flooding in Urban Zones: Morelia, Michoacán, Mexico." *Tecnología y Ciencias del Agua* 11, no. 3 (2020): 1–26.

# 3/2-Way Pneumatic Solenoid Valves: An Overview

Dr. eng. **Tiberiu AXINTE[1,*],** Dr. eng. **Mihăiță CAZACU[2],** Dr. math. **Elena Gabriela CURCĂ[1],**
Eng. **Lidia CALANCEA[1],** Eng. **Mihai DIACONU[1],** Drd. eng. **Alexandru SAVASTRE[1]**

[1] Research and Innovation Center for Navy, Romania

[2] Ovidius University of Constanta, Romania

*tibi_axinte@yahoo.com

***Abstract:*** *The paper presents importance of the 3/2-way solenoid valve in the electro-pneumatic circuit. Besides, in this article we present three electro-pneumatic circuits endowed with 3/2-way solenoid valve. Thus, the first electro-pneumatic circuit is composed of the following devices: compressed air supply, 3/2-way solenoid valve, throttle valve, single acting cylinder (SAC 1) and valve solenoid. The second electro-pneumatic circuit is composed of the following parts: compressed air supply, 3/2-way solenoid valve, throttle check valve, single acting cylinder (SAC 2), relay, valve solenoid and lamp. The last electro-pneumatic system is made of the following components: compressed air supply, 3/2-way solenoid valve, single acting cylinder (SAC 3), valve solenoid and logic module.*

***Keywords:*** *Circuit, solenoid, valve, symbol*

## 1. Introduction

Electro-pneumatic circuits that have 3/2-way solenoid valves are widely used in many areas of industrial automation.
In electro-pneumatic fields, pneumatic components (ex. single-acting cylinders) are controlled by using electrical and electronic circuits with 3/2-way solenoid valves, [1].
In direct-operated valves, the spool or poppet is moved directly by the 3/2-way solenoid valves.
These valve opens or closes by moving the spool or poppet. Various device (3/2-way solenoid valves) types include: push button, solenoid (coil), lever or foot pedal.
Based on stability, the pneumatic actuator can have:

- Monostable valves – return to their default position using spring force.
- Bistable valves – have a coil at each position are pulse-operated.

A 3/2-way solenoid valve is an electromechanically operated valve. However, the 3/2-way solenoid valves depend on: the characteristics of the electric current they use, the strength of the magnetic field they generate and the mechanism they use to regulate the air.
In the specialized papers, the valves have the symbol below, Fig. 1.

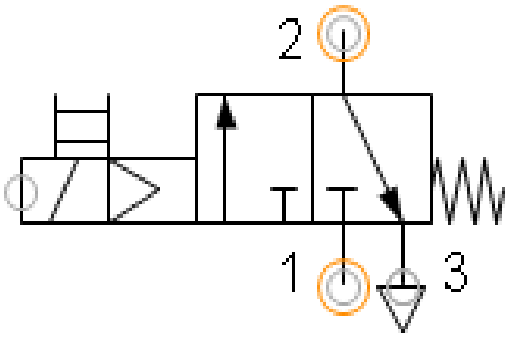


**Fig. 1.** Symbol of 3/2-way solenoid valve

Any 3/2 way valve has three ports and two positions that can be operated: pneumatically, mechanically, manually or electrically through a valve.
Some 3/2-way solenoid valves are equipped with a return spring, [2].
In these manuscript we use only MFH-3-1/4 pneumatic solenoid valve from Festo. These valves have one in an electro-pneumatic circuits, Fig. 2.


**Fig. 2.** 3/2-way solenoid valve type MFH-3-1/4

Technical characteristics of a 3/2-way solenoid valve are shown in Table 1.

**Table 1:** Technical characteristics

| Feature | Value |
|---|---|
| Construction width | 0.3 m |
| Standard nominal flow rate (DIN 1343) | 0.013 $m^3/s$ |
| Pneumatic working port | G1/4 |
| Operating pressure | $15 \cdot 10^3$ Pa...$80 \cdot 10^3$ Pa |
| Nominal size | $7 \cdot 10^{-3}$ m |
| Grid dimension | $32 \cdot 10^{-3}$ m |
| Storage temperature | 253.15 K … 333.15 K |
| Media temperature | 263.15 K … 333.15 K |
| Ambient temperature | 268.15 K … 313.15 K |
| Product weight | 0.350 kg |

## 2. Study of 3/2-way valve solenoid

Hydraulics involves the use of air (in our case) to perform quality mechanical work. In fact, the mechanical work is necessary to perform movements and generate forces in the electro-hydraulics circuits. All electro-hydraulic circuits are electro-controlled by an electrical source. The electro-hydraulic circuits are the voltage supply and then the signals are generated by 24V and sent to the 3/2-way solenoid valves for the directional control of the hydraulic fluid. Moreover furthermore, the function of hydraulic drives (e.g. single acting cylinder) is to convert stored energy into moving hydraulic fluid, [3].

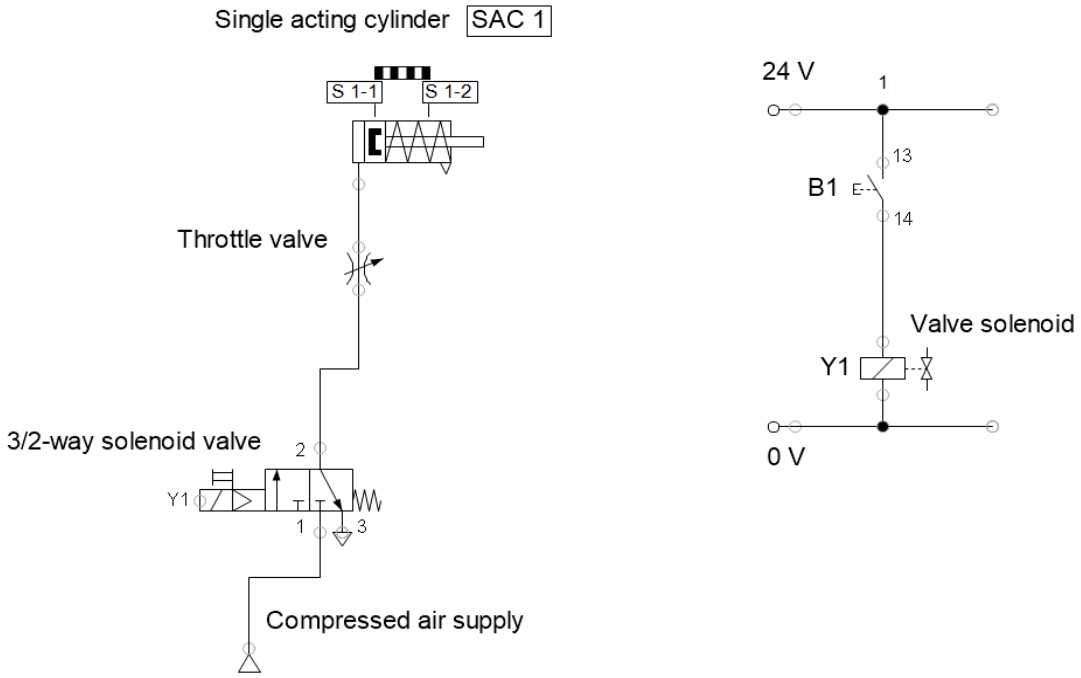


**Fig. 3.** First electro-pneumatic circuit with 3/2-way solenoid valve

First electro-pneumatic circuit made in this paper is designed as a simple scheme use only a single acting cylinder (SAC 1). Hence, 3/2-way solenoid valve from first electro-pneumatic control system has a spring-returned, Fig. 3.
In the table below there are given five devices used in the first electro-pneumatic scheme with 3/2-way solenoid valve.

**Table 2:** Devices of first electro-pneumatic scheme

| Description | Number of components |
|---|---|
| Compressed air supply | 1 |
| 3/2-way solenoid valve | 1 |
| Throttle valve | 1 |
| Single acting cylinder (SAC 1) | 1 |
| Valve solenoid | 1 |

The 3/2 – way solenoid valve with spring makes the connection between compressed air supply and throttle valve, [4].
If the operator presses B1 button, the piston rod moves from point S 1-1 to point S 1-2. After that, those both piston rods returns from point S1-2 to point S1-1, because the 3/2-way solenoid valve has a spring, Fig. 4.

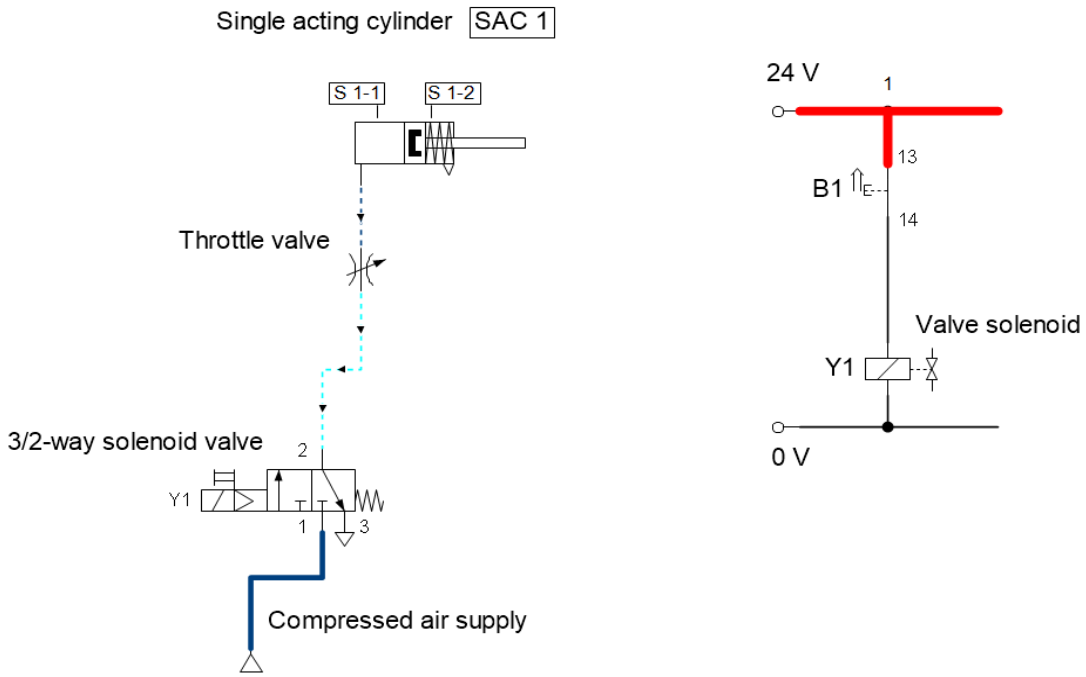


**Fig. 4.** First electro-pneumatic circuit with 3/2-way solenoid valve. Simulation

The usual parameters of single acting cylinder (SAC 1) are: position (x), velocity (v) and acceleration, Fig. 5.

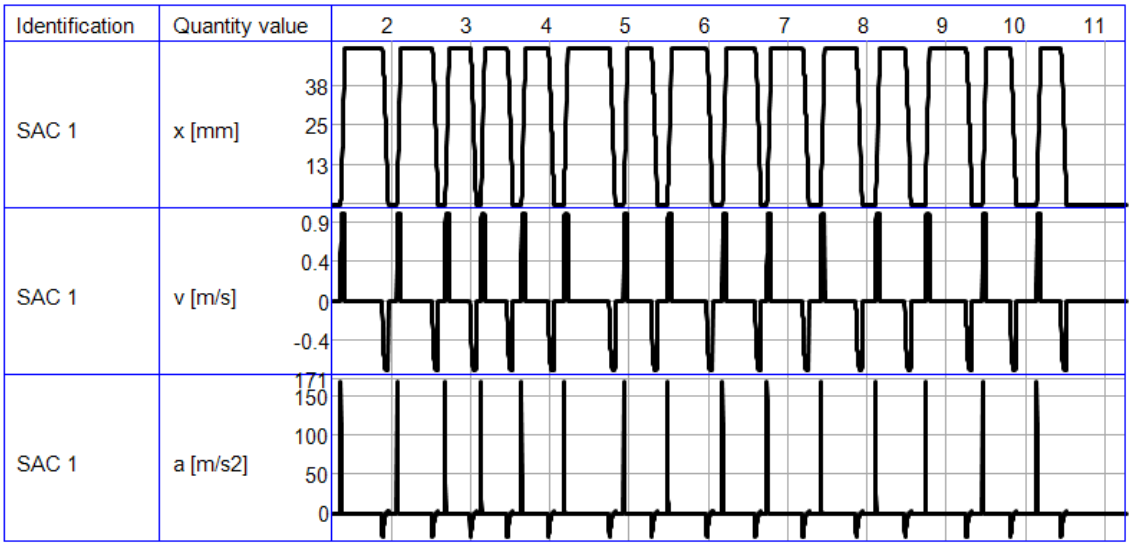


**Fig. 5.** Diagrams of parameters

The second electro-pneumatic installation has a single acting cylinder (SAC 2), Fig. 6.

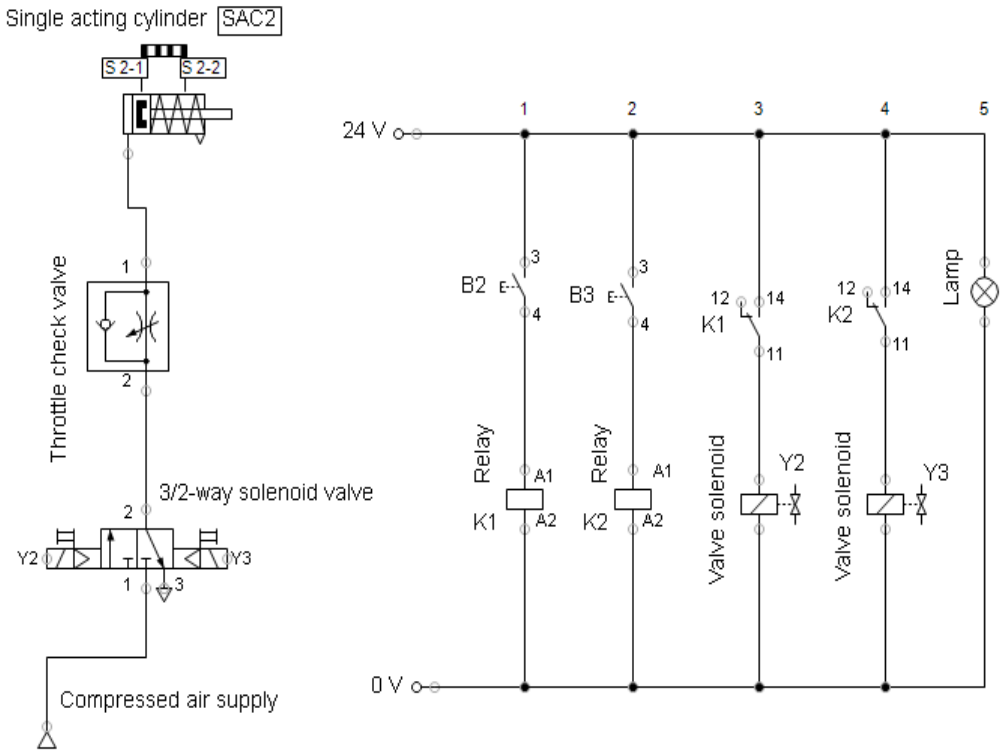


**Fig. 6.** Second electro-pneumatic circuit with 3/2-way solenoid valve

The simple electro-pneumatic system with 3/2-way solenoid valve have the following nine devices listed in the table below, [5].

**Table 3:** Devices of second electro-pneumatic scheme

| Description | Number of components |
|---|---|
| Compressed air supply | 1 |
| 3/2-way solenoid valve | 1 |
| Throttle check valve | 1 |
| Single acting cylinder (SAC 2) | 1 |
| Relay | 2 |
| Valve solenoid | 2 |
| Lamp | 1 |

The second electro-pneumatic circuit with single acting cylinder (SAC 2) opens if the operator presses B2 button from 3/2-way solenoid valve and lamp shows green signal, Fig. 7.

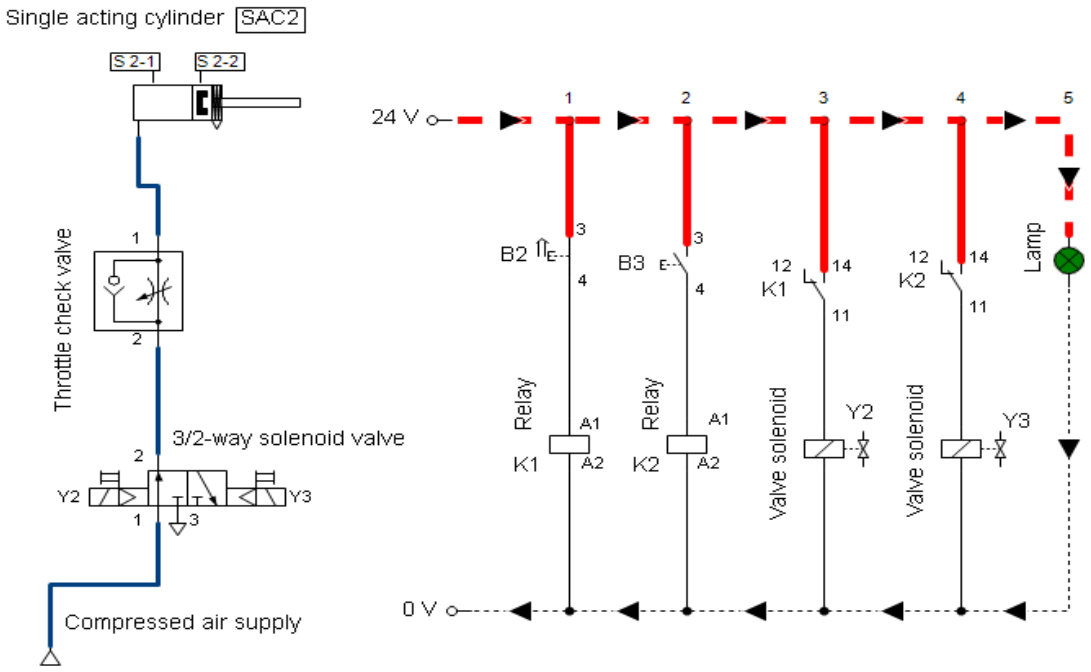


**Fig. 7.** Second electro-pneumatic circuit with 3/2-way solenoid valve. Simulation I

If the operator presses B3 button, the piston rod of the single acting cylinder (SAC 2) moves from point S 2-2 to point S 2-1.

And the same time the lamp shows green signal, Fig. 8.

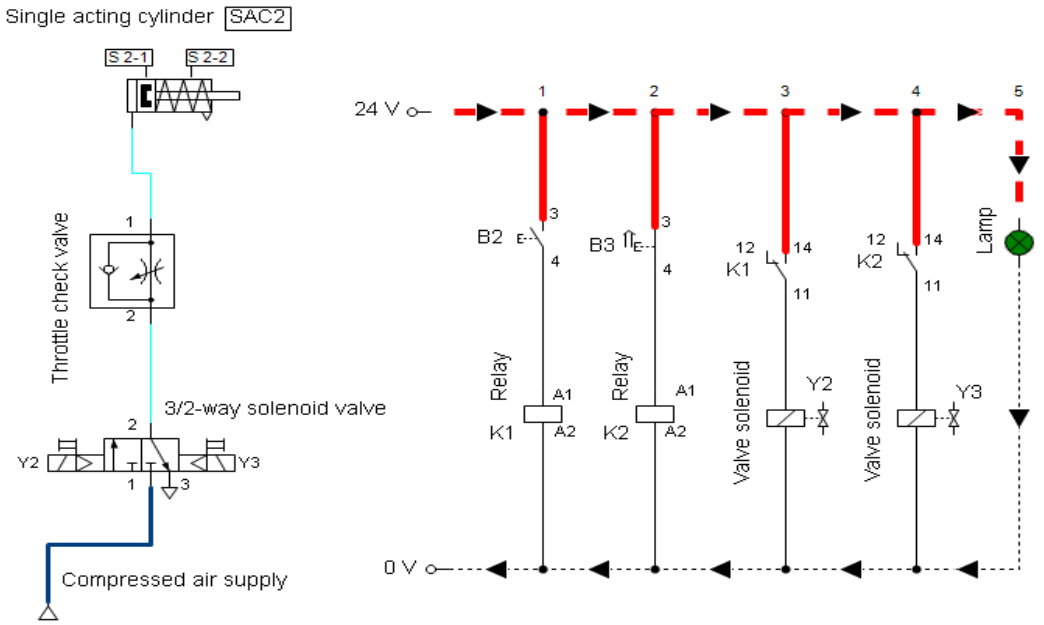


**Fig. 8.** Second electro-pneumatic circuit with 3/2-way solenoid valve. Simulation II

In addition, an electro-pneumatic circuit with a 3/2-way solenoid valve is studied together with a logic module, Fig. 9.

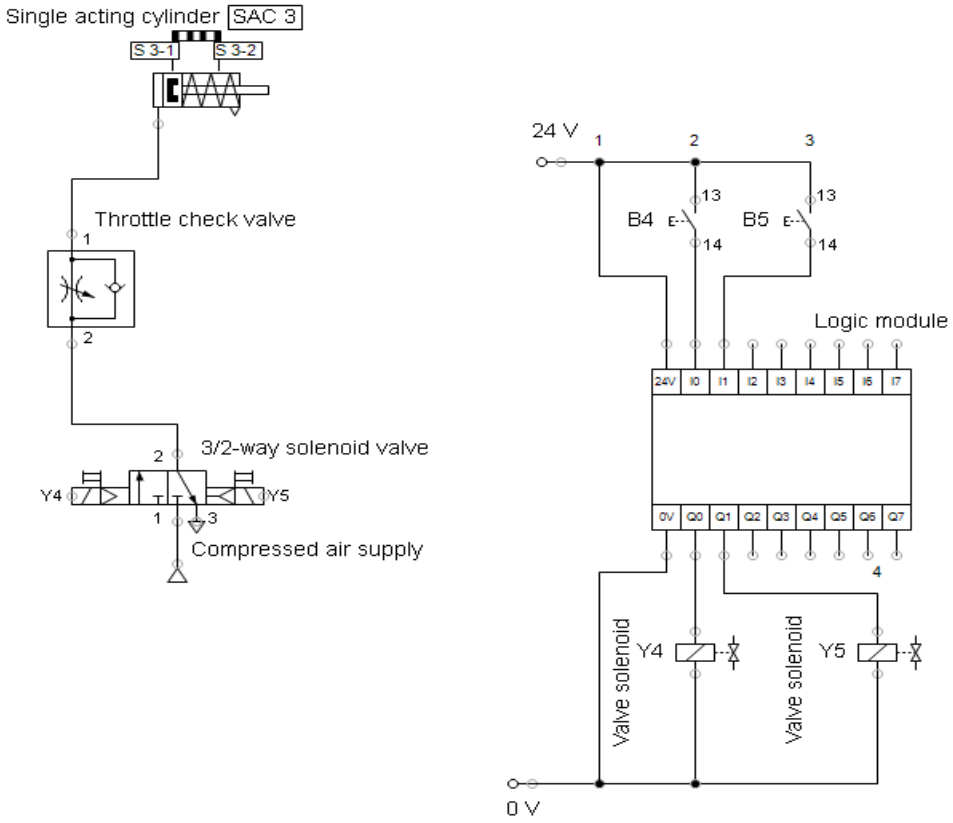


**Fig. 9.** Third electro-pneumatic circuit with single acting cylinder

The last of electro-pneumatic system with 3/2-way solenoid valve have the following seven devices listed in the table below, [5].

**Table 4:** Devices of second electro-pneumatic scheme

| Description | Number of components |
|---|---|
| Compressed air supply | 1 |
| 3/2-way solenoid valve | 1 |
| Throttle check valve | 1 |
| Single acting cylinder (SAC 3) | 1 |
| Valve solenoid | 2 |
| Logic module | 1 |

Finally, if operator presses B4 button, the piston rod of the multi-position cylinder (2) moves from point S 3-1 to point S 3-2. After that, this piston rod returns from point S 3-2 to point S 3-1. Because of the single acting cylinder (SAC 3) has a spring, Fig. 10.

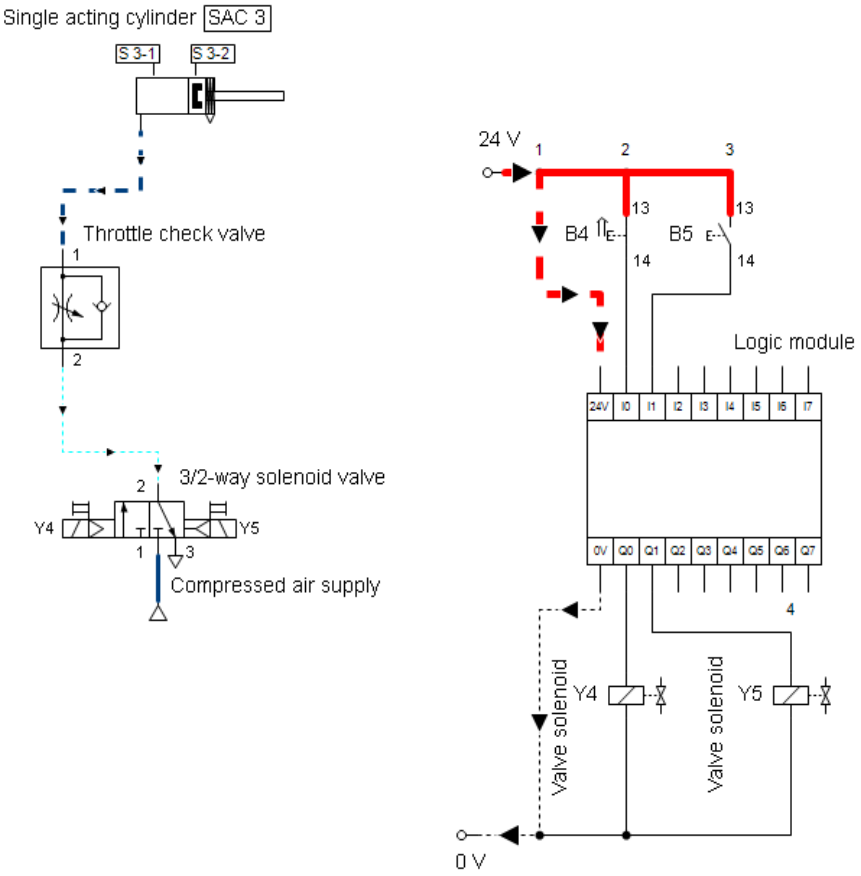


**Fig. 10.** Third electro-pneumatic circuit with single acting cylinder. Simulation.

## 3. Conclusions

Electro-pneumatic circuits with 3/2-way solenoid valves is an integration of electrical and mechanical components with compressed air source.
On the other hand, the 3/2-way solenoid valves are control units that, when electrically energized or disconnected, either close or allow air to flow.
Electro-pneumatic circuit with 3/2-way solenoid valves to have a bright future in technology, especially in the design and simulation of pneumatic suits.
Below are some advantages of electro-pneumatic circuits with 3/2-way solenoid valves:

- Greater reliability.
- Less moving parts subjected to wear compared to mechanical control systems.
- Reduced installation complexity.
- Less components and hoses, leads to less effort in planning and commissioning especially with large and complex systems.
- The control system can be easily modified and adapted.
- It is easier to change wiring and modify programs rather than changing mechanical components and hose networks.
- Easy handling.
- Less complexity
- Secure mounting.
- Environmentally-friendly coupling system.

In the future, we want to perform simulations of electro-pneumatic circuits with 3/2-way solenoid valves to perform various complex activities.

**References**

[1] Radoi, R., M. Blejan, I. Dutu, G. Sovaiala, and I. Pavel. “Determining the step response for a pneumatic cylinder positioning system.” *Hidraulica Magazine*, no. 2 (June 2014): 25-31.

[2] Pereyras, J. “Development of a Basic Electro-Pneumatic Control trainer.” *Asian Journal of Multidisciplinary Studies* 2, no. 2 (2019).

[3] Rojas Suárez, J. P., J.A. Pabón León, and M.S. Orjuela Abril. “Development of an electro-pneumatic system for the practical training of pneumatic process in the university environment.” Paper presented at the 1st STEAM Education Congress (1st STEAMEC), San José de Cúcuta, Colombia, June 10-11, 2021. *Journal of Physics: Conference Series* 2073 (2021): 012016.

[4] Tripathy, S., A. Das, B. Sahu, and D.K. Srivastava. “Electro-pneumatic variable valve actuation system for camels engine: Part I – development and characterization.” *Energy* 193 (February 2020): 116740.

[5] Selvam, C. “Design & Fabrication of Electro-Pneumatic Gantry Type Sorting Robot.” *International Research Journal of Engineering and Technology (IRJET)* 9, no. 12 (2022): 787-794.

# Experimental Evaluation of a Digital Hydraulic Pumping System

Dipl. Eng. **Bogdan Alexandru TUDOR-ROTILĂ[1,*],** PhD. Eng. **Radu-Iulian RĂDOI[1],**
Dipl. Eng. **Ștefan-Mihai ȘEFU[1],** PhD. Stud. Eng. **Robert BLEJAN[1]**

[1] National Institute of Research & Development for Optoelectronics/INOE 2000, Subsidiary Hydraulics and Pneumatics Research Institute/IHP, Romania

* btudor.ihp@fluidas.ro

***Abstract:*** *The field of digital hydraulics is in full expansion and a lot of research teams contribute to its development, in order to be competitive with classic hydraulic systems, and reduce the energy loses from the hydraulic systems. This article presents the experimental results for a Digital Hydraulic Pumping System (DHPS), with 4 pumps with fix displacement connected in parallel and the capacities of each pump is in the binary progression. The experimental results show that such a system can achieve 15 discrete values of flow, without hydraulic fluid throttling to achieve flowrates regulation. The system is tested using an application that can do an automatic test of the system using a excel file defined by the operator, and the results are showed live on the app screen as numeric values or as a chart.*

***Keywords:*** *Digital hydraulics, hydraulic system, pumping system, programable logic controller*

## 1. Introduction

Hydraulic systems are vital for some fields like mining, construction, and manufacturing, but have a lot of energy loses due to hydraulic fluid throttling made by different hydraulic components in order to achieve good control and rapid response from the system. The energy loses due to hydraulic fluid throttling are a big disadvantage for the hydraulic systems and a big throwback for the worldwide direction to reduce the pollution and control the climate changes and global warming. Hydraulic systems lined up with the trend of pollution reduction by introducing equipment such as load sensing pumps but those are quite expensive and the investment is not worth it if the system does not require a multitude of fluid variations.
In recent years, the researchers from the hydraulic field have developed a new field that can align to the worldwide trend to reduce energy consumption and pollution, called digital hydraulics. The field of digital hydraulics is defined as a system that has discrete components and can actively control the output of the system [1].
Many of the digital hydraulic systems use on/off directional valves and they have various advantages, such as [2]:

- More simple and cheaper directional valves;
- Simpler electronics;
- Decreased energy consumption;
- Increased life span of the directional valves;
- Higher flexibility;
- Easy connection with a Programable Logic Controller (PLC);
- Less sensitive to fluid contamination;
- Do not need a feedback for the spool position, like proportional or servo-valves do.

The digital hydraulic pumping systems concept is split between digital hydraulic systems in parallel, and high frequency digital hydraulic systems [3].
The first one uses codding methods such as Pulse Number Modulated (PNM), which uses the series 1, 1, 1, 1 … etc., and the Pulse Coded Modulated method, which uses the binary series ($2^n$, where $n$ is the number of components, such as pumps or directional valves), and the Fibonacci series (this one is rarely used in systems presented in literature). The output flowrate for a parallel digital hydraulic system is the sum of the directional valves that are open.
The second one uses a single directional valve that has the capacities of high frequency switching of the spool between the open and close position, and uses control signal named Pulse Width

Modulated (PWM). The output flowrate of the high frequency digital hydraulic system is obtained by the open and close ratio periods made by the directional valve spool.

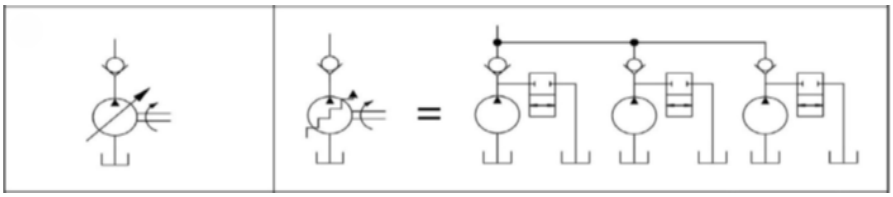

a) b)

**Fig. 1.** A) Analog pumping system; b) Digital hydraulic pumping system in parallel [4]

Figure 1 illustrates a comparison between the symbol of analogue pumping system with variable capacity and the symbol of a digital hydraulic pumping system.
Generally, in digital hydraulic parallel systems, the PNM coding method is not as used as the PCM coding method, because the first one needs a lot more components in its structure to achieve a decent flow variation. For example, a digital hydraulic system coded using the PNM method with 10 directional valves can achieve 10 discrete flow variations; instead a digital hydraulic system coded with the PCM method with 4 directional valves can achieve 16 discrete flow variations; so, it is more convenient to use the PCM coding method for space reasons.
In [5] authors have simulated, using Amesim software, the function of a digital hydraulic system with 4 parallel connected fix displacement pumps, having the capacities in binary progression, and this paper is a sequel of that paper and it comes with the experimental data for the simulated system.

## 2. Material and Methods

The Digital Hydraulic Pumping System (DHPS) investigated in this paper is designed to adjust the non-resistive fluid flow by independently enabling and disabling each pump to direct flow in the system or to the oil tank with the help of 4 directional valves and 4 check valves.
The DHPS hydraulic diagram is presented in figure 2 and is composed of:

- 4 fix displacement pumps with the capacities in binary progression (2, 4, 8, 16 cc/rev) marked as P1, P2, P3, P4;
- biaxial three phase electric motor, with a nominal power of 11 kW, marked as M;
- 4 ON/OFF directional hydraulic valves, cartridge type, marked as DV1, DV2, DV3, DV4, used to control the output of each pump;
- 4 check valves, marked as CV1, CV2, CV3, CV4, used to stop the hydraulic oil to flow back in the output of the pumps when 1, 2 or 3 pumps are used.
- 1 relief valve for the system safety, marked as RV, used to protect the system when pressure limit is exceeded by the load;
- 1 pressure transducer mounted on the system output branch, marked as PT, used to measure the system pressure generated by the load;
- 2 flow meters marked as FM1, FM2; FM2 is used to measure the system output, and FM1 is used to monitor the return flow when the valves DV (1…4) are used, and measure the flow that pass through the relief valve when all the pumps are sending the flow to the load, and pressure from the system is exceeding the relief valve adjusted limit;
- 1 temperature meter marked as TM, used to measure system temperature;
- 1 throttle valve marked as TR, used to generate load in the system;
- 1 return filter marked as RF, used to filter the return oil from the pumps;
- Oil tank marked as T;
- Electric enclosure, which contains all the electric components necessary for the system to work, perform data acquisition, and control the system by using a Programable Logic Controller (PLC);
- Energy meter, used to show the power absorbed from the grid by the electric engine.

The transducers values for pressure (PT), flowrate for the system output (FM2), energy meter (EM), and the electric engine speed are displayed live on the app screen as numeric values or charts. The transducers values for return flow (FM1), and temperature (TM) are showed locally on the system test bench by using 2 display units, and these are not displayed on the result charts.

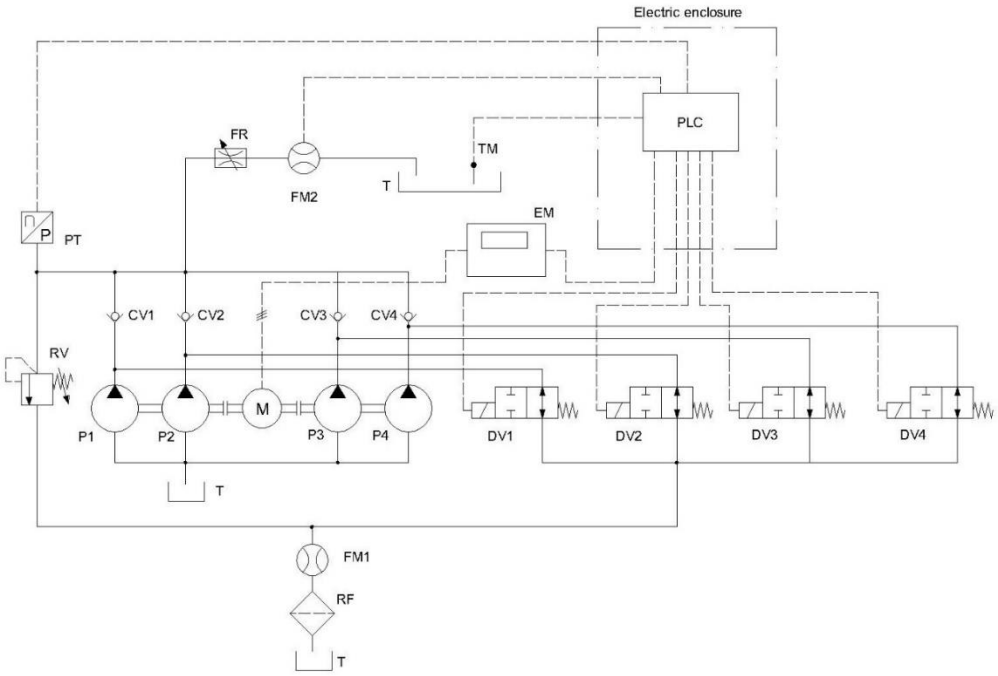


**Fig. 2.** Hydraulic diagram of the DHPS

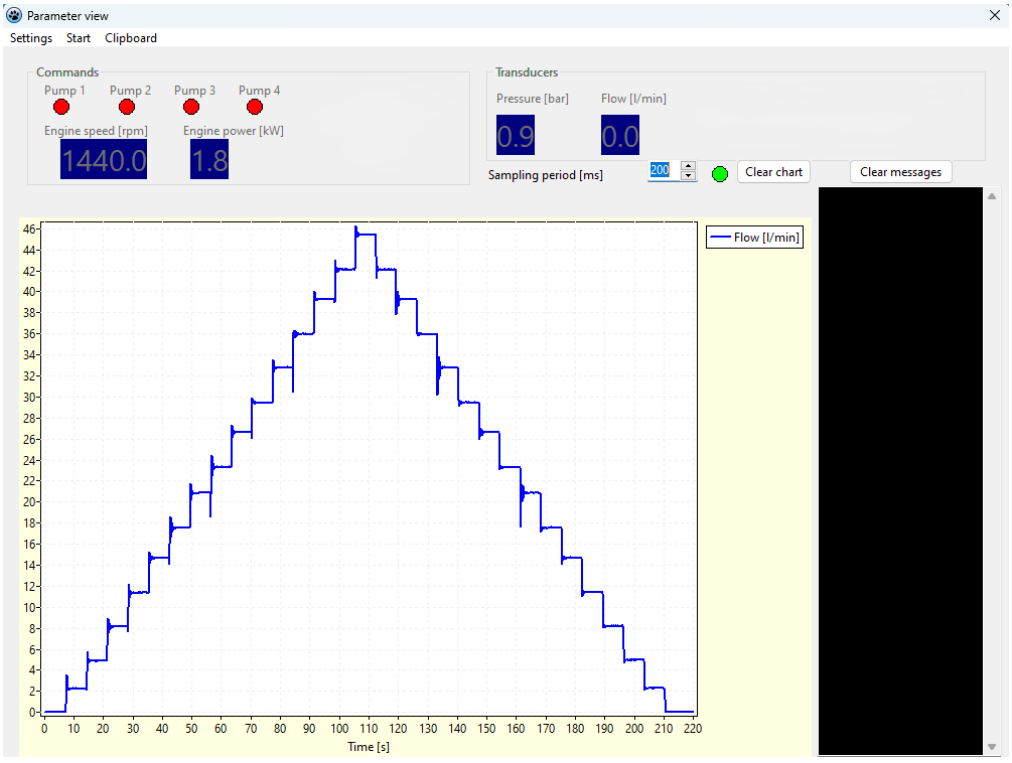


**Fig. 3.** Application for the digital hydraulic pumping system

**Fig. 4.** The DHPS test stand

Figure 4 illustrates the DHPS test bench, assembled based on the hydraulic diagram from figure 2. The system was designed to achieve different flowrates in 15 points with the step of the flow generated by the small pump P1. The number of flowrates that the system can achieve was calculate using the formula: $2^n$-1, where *n* is the number of parallel connected pumps; so, $2^4$-1 = 15 maximum flowrates.

To enable system operation, we programmed the Programable Logic Controller (PLC) form the electric enclosure, and developed a software application (figure 3) installed on a computer that can control the system function, view numeric value of parameters in real time and build charts also in real time.

The software application is built to do an automatic test on the system using a excel file that commands each of the pumps outputs by sending command signals to the directional valves, in order to obtain each of the 15 points of flowrates that the system can achieve.

The excel file needed by the application to do the automatic test is basically a table with 5 columns and minimum 18 rows (according with the experiment type), defined earlier by the operator.

The experiment was made with the following parameters:

- the time interval for each step was set to 7 seconds, time required for the system to became stable;
- the electric engine rotation speed was set to 1440 rev/min;
- the test was conducted from zero flowrate to maximum flowrate and back to zero flowrate;
- for this test, no load was created at the output of the system;
- the excel table that the application requires to run the test in automatic mode was a table with 5 columns and 34 rows, shown in figure 5.

| Time [s] | Pump 1 | Pump 2 | Pump 3 | Pump 4 | Engine speed [rpm] |
|---|---|---|---|---|---|
| 0 | 0 | 0 | 0 | 0 | 1440 |
| 7 | 1 | 0 | 0 | 0 | 1440 |
| 14 | 0 | 1 | 0 | 0 | 1440 |
| 21 | 1 | 1 | 0 | 0 | 1440 |
| 28 | 0 | 0 | 1 | 0 | 1440 |
| 35 | 1 | 0 | 1 | 0 | 1440 |
| 42 | 0 | 1 | 1 | 0 | 1440 |
| 49 | 1 | 1 | 1 | 0 | 1440 |
| 56 | 0 | 0 | 0 | 1 | 1440 |
| 63 | 1 | 0 | 0 | 1 | 1440 |
| 70 | 0 | 1 | 0 | 1 | 1440 |
| 77 | 1 | 1 | 0 | 1 | 1440 |
| 84 | 0 | 0 | 1 | 1 | 1440 |
| 91 | 1 | 0 | 1 | 1 | 1440 |
| 98 | 0 | 1 | 1 | 1 | 1440 |
| 105 | 1 | 1 | 1 | 1 | 1440 |
| 112 | 0 | 1 | 1 | 1 | 1440 |
| 119 | 1 | 0 | 1 | 1 | 1440 |
| 126 | 0 | 0 | 1 | 1 | 1440 |
| 133 | 1 | 1 | 0 | 1 | 1440 |
| 140 | 0 | 1 | 0 | 1 | 1440 |
| 147 | 1 | 0 | 0 | 1 | 1440 |
| 154 | 0 | 0 | 0 | 1 | 1440 |
| 161 | 1 | 1 | 1 | 0 | 1440 |
| 168 | 0 | 1 | 1 | 0 | 1440 |
| 175 | 1 | 0 | 1 | 0 | 1440 |
| 182 | 0 | 0 | 1 | 0 | 1440 |
| 189 | 1 | 1 | 0 | 0 | 1440 |
| 196 | 0 | 1 | 0 | 0 | 1440 |
| 203 | 1 | 0 | 0 | 0 | 1440 |
| 210 | 0 | 0 | 0 | 0 | 1440 |
| 217 | 0 | 0 | 0 | 0 | 1440 |
| 224 | 0 | 0 | 0 | 0 | 1440 |

**Fig. 5.** The table for the automated experiment

## 3. Results and Discussion

Figure 6 illustrates a capture from the control app screen where one can see a chart with four curves which describes the system parameters, such as Electric engine speed (in rpm, with color orange), Pressure (in bar, with color red), Flowrate (in l/min, with color blue), and Active power (in kW, with color olive), absorbed from the grid by the electric engine during the experiment.
As displayed in figure 6, one can see that the system output achieves a number of 15 flowrates on the ascendent and the same number on the descendent part of the flowrate trace. The reason that the experiment was made from minimum flowrate to maximum flowrate and back again to minimum flowrate was to prove that the system repeatability is very good and it achieves the same values of flowrates on each part of the chart. In the same figure one can see that the maximum flowrate that the system can achieve is approximatively 44 l/min and the minimum flowrate is approximatively 2 l/min, while the step for each flowrate between minim to maxim is approximatively 2 l/min.

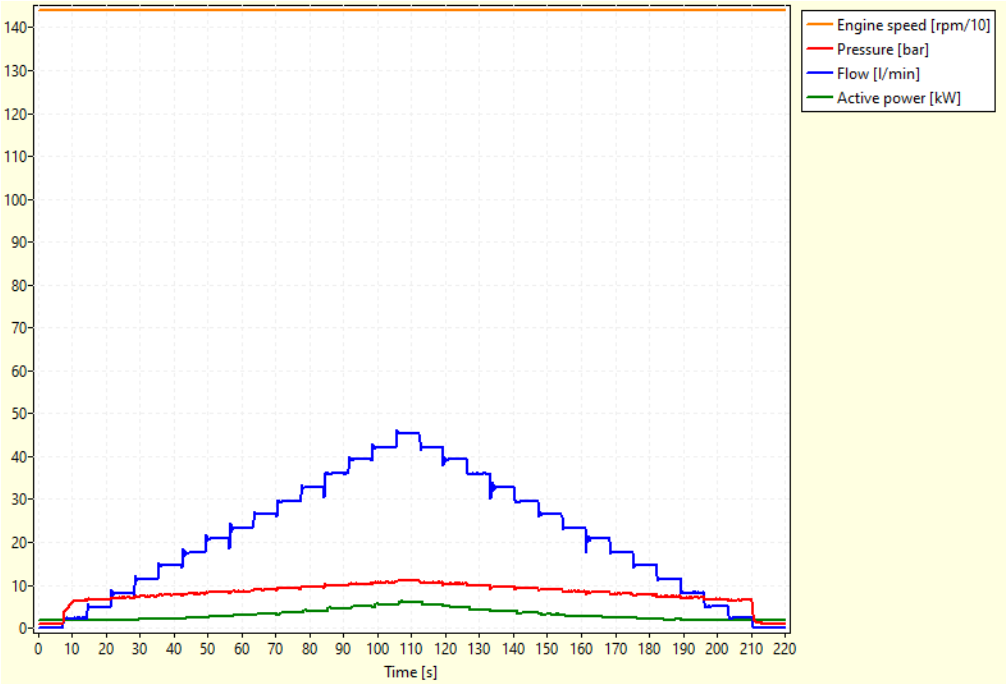


**Fig. 6.** Experimental results showing traces for engine speed, pressure, flowrate, and active power on the same chart

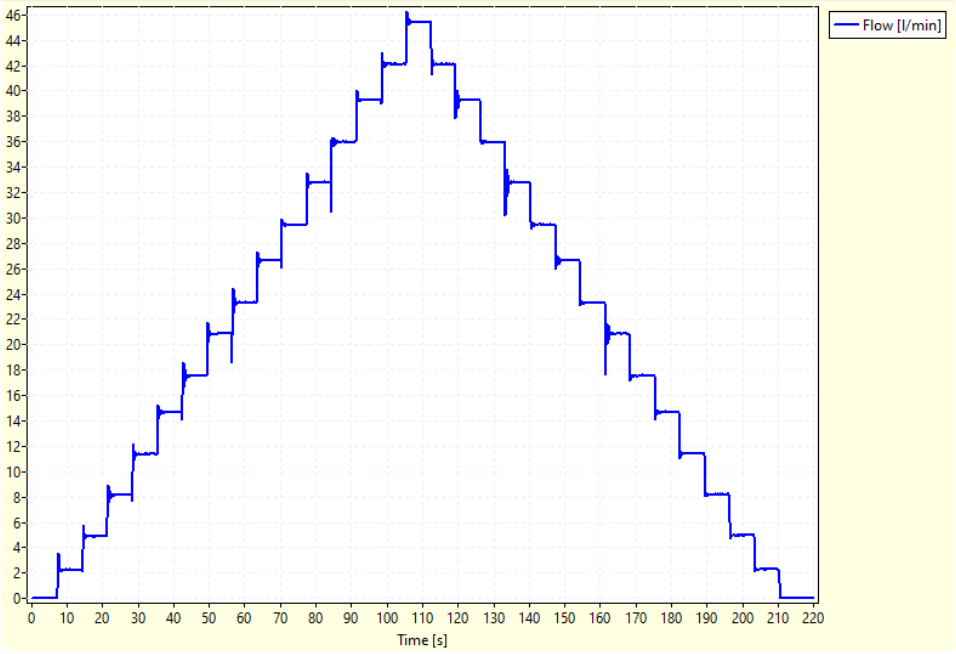


**Fig. 7.** Experimental result showing only the flowrate trace on the chart

Figure 7 displays a chart with only one trace that shows the value for flowrate. The reason that we suppressed the other 3 traces from figure 6 is to properly view the flowrate steps and see that when the system is moving on to another step, some peaks are appearing on the chart. Those peaks of flowrates are appearing due to the fluid inertia, and, as one can see in figure 8, those peaks appear also on the pressure trace.

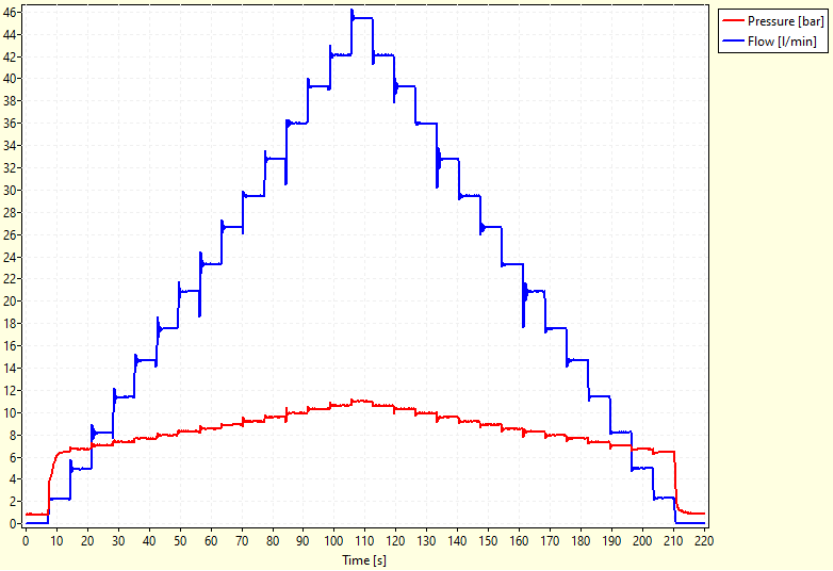


**Fig. 8.** Experimental results showing the flowrate and pressure traces

Figure 8 illustrates the flowrate and the pressure traces of the experiment, and one can see that both pressure and flowrate have the same number of steps.

## 4. Conclusions

The system presented in this paper proves that a flowrate variation can be successfully achieved with simple components and can be used in hydraulic systems that don't need many flowrate variations such as the ones provided by proportional and servo systems.
As one can see from figures in the result section, the system has a good repeatability, proven by obtaining the same values for the evaluated parameters for each step on the ascendent and descendent part of the traces.
Based on the results presented above, the digital hydraulic pumping system needs to be optimised to reduce flow and pressure peaks that system have, but this is the subject of another work that will be done in future.
This paper shows that the field of digital hydraulics is expanding rapidly and it is worth to be developed further so that components become more reliable, cheaper, more efficient, and have smaller dimensions than they currently have.

### Acknowledgement

This work was carried out through the Core Program within the National Research Development and Innovation Plan 2022-2027, carried out with the support of the Romanian Ministry of Research, Innovation and Digitalization (MCID), project no. PN 23 05.

### References

[1] Linjama, Matti, Arto Laamanen, and Matti Vilenius. "Is it time for digital hydraulics?" Paper presented at The Eighth Scandinavian International Conference on Fluid Power, SICFP'03, Tampere, Finland, May 7-9, 2003.
[2] Sciatti, Francesco, Paolo Tamburrano, Elia Distaso, and Riccardo Amirante. "Digital hydraulic valves: Advancements in research." *Heliyon* 10, no. 5 (2024): e27264. 10.1016/j.heliyon.2024.e27264.
[3] Zhang, Qiwei, Xiangdong Kong, Bin Yu, Kaixian Ba, Zhengguo Jin, and Yan Kang. "Review and Development Trend of Digital Hydraulic Technology." *Applied Sciences* 10, no. 2 (2020): 579. https://doi.org/10.3390/app10020579.
[4] Mäkelä, Jani. *Energy efficiency of a digital hydraulic multi-pressure actuator for use in load-lifting applications*. Master's thesis. Aalto University School of Engineering, 2020.
[5] Hristea, Mihai Alexandru, Bogdan Tudor, Radu Radoi, and Stefan Mihai Sefu. "Digital pumping unit with gear pumps use to provide the flow required for mobile equipment with high energy efficiency." *INMATEH - Agricultural Engineering* 64, no. 2 (2021): 289-296.

# Numerical Aspects of Fluid Peristaltic Circulation Model

Associate professor **Fănel Dorel ȘCHEAUA**[1,*]

[1] Dunarea de Jos University of Galati, MECMET Research Center

* fanel.scheaua@ugal.ro

***Abstract:*** *The peristaltic model of flow describes the movement of fluids through channels or tubes, highlighting the natural process of peristalsis observed in biological systems, such as the gastrointestinal tract, blood vessels and lymphatic systems. Peristalsis is characterized by rhythmic, wave-like contractions of muscle layers that propel fluids forward. In the human body, this mechanism is crucial for the transport of various substances, of interest being the mechanisms by which this process occurs. In this paper, a description of the fluid movement typology with a mathematical model and a numerical analysis are presented in order to highlight the main parameters involved and their effects in the flow. The results obtained highlight the main possibilities of intervention and the changes that occur in the flow phenomenon in case when certain involved parameters values are modified.*

***Keywords:*** *Fluid flow, peristaltic flow, fluid type, vessel elasticity, mathematical model, numerical analysis*

## 1. Introduction

The peristaltic flow typology represents a fundamental mechanism of fluid transport in nature, being found in various biological systems such as the digestive system, urethras, or lymphatic vessels, being taken up and used further even in industrial field for applications involving peristaltic pumps for the circulation and transport of liquids. The movement is characterized by undulating movements of a flexible channel or tube walls within which the flow takes place, which ultimately has the ability to create a directed flow without requiring internal mechanical components.
Peristaltic fluid flow is driven by cyclic contractions and relaxations of the channel walls, which generate peristaltic waves. These waves create a pressure difference that causes the fluid to move in a specific direction, usually in the longitudinal direction of the channel in which the flow occurs.
The main characteristics of peristaltic flow are given by the periodicity with which the movement of the channel walls occurs, since the channel walls move in a repetitive manner, often described by a sinusoidal function.
The flow also occurs in a non-mixing flow because the fluid is pushed forward without significant mixing, which is essential for the transport of sensitive fluids such as blood.
This ensures a flow that is not dependent on valves because this mechanism does not require valves to prevent reflux, the movement of peristaltic waves ensuring directionality.
The flexibility of the channel walls is a main characteristic in that peristaltic tubes can transport fluids of various viscosities, including suspensions and non-Newtonian fluids.
The peristaltic flow type is characteristic mainly of biological systems represented by the digestive system by transporting food through the oesophagus, stomach and intestines which is accomplished by peristaltic contractions, the urinary system where the urethras use peristaltic waves to conduct urine from the kidneys and also the circulatory system where peristaltic movements help transport blood and lymph, in the body necessary to transport nutrients, oxygen, carbon dioxide, especially in small lymphatic vessels.
The advantages of this type of movement are presented in biology and technology by preventing contamination within peristaltic pumps, where the fluid remains isolated within the tube, thus preventing contact with the pump components, and regarding transport safety elements, peristalsis has a delicate action on fluids and implicitly does not intervene to affect the chemical composition, offering increased adaptability because it works for fluid typologies with different specific values of viscosity and composition.
Practical applications of the peristaltic flow typology involve the use of peristaltic pumps used in laboratories and medicine for performing infusions or transporting sterile liquids, various

simulations in biomedical engineering for design activities of various implants or medical devices, as well as for irrigation systems and fluid transport in industrial processes.
The limitations related to the type of peristaltic flow are related to the fact that it presents decreases in efficiency at high speed values or at high pressures.
For the case of very viscous fluids, to ensure continuity of flow, waves with higher amplitudes are needed in order to maintain the flow, as well as possible wear of the channel walls or flexible tubes, especially in mechanical applications.

## 2. Physical and mathematical model of peristaltic flow

The physical and mathematical model of peristaltic flow considers the occurrence of a generated peristaltic wave, which can be described by means of sinusoidal equations considering a circular channel of radius *(r)*, an emitted contraction of amplitude *(a)*, a wavelength $(\lambda)$ and an angular wave frequency $(\omega)$:

$$r(x,t) = r_0 + a\sin\left(2\pi\frac{x}{\lambda} - \omega t\right) \tag{2.1}$$

The flow regime within peristaltic flow can be in the laminar or turbulent range, depending on the Reynolds Number (Re), which describes the ratio between inertial and viscous forces.
Regarding the viscosity values of the fluid, it should be highlighted that Newtonian fluids such as water and non-Newtonian fluids such as blood exhibit different behaviours.
The fluid pressure and flow rate are directly dependent on the frequency of the peristaltic waves *(f)*, the amplitude of the contractions *(a)*, as well as the resistance of the channel with reference to the dependence on the viscosity of the fluid.
Fluid flow is described by the Navier-Stokes equations and the continuity equation [1].
The continuity equation ensures the conservation of mass, where the velocity components *(u, v)* are considered in two main axial *(x)* and radial *(r)* directions:

$$\frac{\partial u}{\partial x} + \frac{1}{r}\frac{\partial(rv)}{\partial r} = 0 \tag{2.2}$$

The Navier-Stokes equation in cylindrical coordinates describes the conservation of momentum for a viscous fluid, highlighting the values of pressure *(p)*, dynamic viscosity *(μ)* and density of the fluid *(ρ)* [1]:

$$\rho\left(\frac{\partial u}{\partial t} + u\frac{\partial u}{\partial x} + v\frac{\partial u}{\partial r}\right) = -\frac{\partial p}{\partial x} + \mu\left[\frac{\partial^2 u}{\partial x^2} + \frac{1}{r}\frac{\partial}{\partial r}\left(r\frac{\partial u}{\partial r}\right)\right] \tag{2.3}$$

The introduction of approximations to simplify the calculation must be taken into account, defining initially a laminar fluid flow, with dominant viscous stresses, while inertial forces are negligible (Re≪1), maintaining a small value for the wave amplitude $(a << r_0)$, which allows the linear approximation of the wave, as well as a periodic oscillating flow where it is assumed that the velocity and pressure exhibit periodic variations.
In order to obtain an approximate solution for the fluid velocity, it is assumed that the axial velocity *(u)* depends only on the radius *(r)* and time *(t)*, making it possible to calculate the velocity using a relationship similar to Poiseuille's law [1-5]:

$$u(x,r,t) = \frac{1}{4\mu}\left(\frac{\partial p}{\partial x}\right)\left(r_{xt}^2 - r^2\right) \tag{2.4}$$

Where $(r_{xt})$ is the radius of the channel at position *(x)* and time *(t).*

The volumetric flow rate $Q(x,t)$ circulating through the channel is obtained by integrating the velocity over the cross section [1-7]:

$$Q(x,t)=\int_0^r 2\pi r u(x,r,t)dr \tag{2.5}$$

Performing the velocity substitution, we obtain:

$$Q(x,t)=-\frac{\pi}{8\mu}\frac{\partial p}{\partial x}r_{x,t}^4 \tag{2.6}$$

The pressure required to maintain the flow is determined based on the pressure gradient:

$$\Delta p=\frac{8}{\pi}\frac{\mu l_c Q}{r^4} \tag{2.7}$$

where $(l_c)$ represents the length of the channel segment considered [8-10].
The main effects of the parameters on the flow typology are represented by direct actions of the wave amplitude (a), since high values of the amplitude have the possibility of increasing the volumetric flow circulated, but can generate increased hydrodynamic resistances.
Higher frequencies lead to faster transport, but can increase the energy required to perform the pumping process, while dynamic viscosity (μ) has an influence related to the need to generate a higher pressure to maintain a constant circulation flow, valid for fluids with higher dynamic viscosity.
For turbulent regime, peristaltic flow presents a higher complexity degree compared to the laminar domain, by involving nonlinear interactions between inertial and viscous forces, as well as the formation of turbulent structures (vortices). In this case, the model must take into account the characteristics of turbulence, such as random velocity fluctuations and large pressure gradients. The information of peristaltic flow in turbulent regime is related to the Reynolds Number that exceeds the critical value characteristic of the laminar regime. The flow becomes turbulent when the Reynolds Number (Re) exceeds the critical value (Re>2000, approximately, for cylindrical channels) [5-11]:

$$\mathrm{Re}=\frac{1}{\mu}(\rho\cdot\bar{u}\cdot r) \tag{2.8}$$

where $(\bar{u})$ represents the average flow velocity and $(\mu)$ dynamic viscosity.

Within the structure of turbulent flow, eddies (vortices) are formed in the flow, which leads to a loss of energy through dissipation, having a direct impact on the propagation of the peristaltic wave, in the sense that it introduces additional instabilities in the flow, amplifying turbulent fluctuations. For the turbulent flow regime, the wave contribution to the net flow depends on the frequency (f), amplitude (a) and the degree of dissipation.

Turbulent flow is described by the time-averaged Navier-Stokes equations (RANS – Reynolds-Averaged Navier-Stokes) combined with a turbulence model:

$$\rho\left(\frac{\partial\bar{u}}{\partial t}+\bar{u}\frac{\partial\bar{u}}{\partial x}+\bar{v}\frac{\partial\bar{u}}{\partial r}\right)=-\frac{\partial\bar{p}}{\partial x}+\mu\left[\frac{\partial^2\bar{u}}{\partial x^2}+\frac{1}{r}\frac{\partial}{\partial r}\left(r\frac{\partial\bar{u}}{\partial r}\right)\right]-\frac{\partial\tau_{xx}}{\partial x}-\frac{\partial\tau_{xr}}{\partial r} \tag{2.9}$$

where $(\bar{u})$ is average velocity in the *(x)* direction, $(\tau_{xx})$ is Reynolds stress in the *(x)* direction (velocity fluctuations) and $(\tau_{xr})$ is Reynolds stress in the *(x)* and *(r)* directions, [1, 6-12].

For Reynolds stress modelling, turbulence models are used to close the system of equations, such as the $(k-\varepsilon)$ model containing the turbulent energy model *(k)* and the turbulent energy dissipation rate $(\varepsilon)$:

$$\begin{aligned}(k):\ &\frac{\partial k}{\partial t}+\bar{u}\frac{\partial k}{\partial x}=\tau_{ij}\frac{\partial \bar{u}_i}{\partial x_j}-\varepsilon+\nu_t\nabla^2 k\\ (\varepsilon):\ &\frac{\partial \varepsilon}{\partial t}+\bar{u}\frac{\partial \varepsilon}{\partial x}=C_1\frac{\varepsilon}{k}\tau_{ij}\frac{\partial \bar{u}_i}{\partial x_j}-C_2\frac{\varepsilon^2}{k}+\nu_t\nabla^2\varepsilon\end{aligned} \tag{2.10}$$

Another approach is given by the $(k-\omega)$ model which considers the use of specific vortices $\left(\omega=\frac{\varepsilon}{k}\right)$ instead of the dissipation rate.

The model for peristalsis in the turbulent regime takes into account the displacement of the walls, and the equations are solved with dynamic boundary conditions, which primarily consider the displacement of the channel wall, thus periodically modifying the channel radius according to the peristaltic wave function:

$$r(x,t)=r_0+a\sin(kx-\omega t) \tag{2.11}$$

The boundary conditions must be established primarily at the walls, where the radial velocity of the fluid must coincide with the wall velocity:

$$v(r,t)=v(r=r(x,t),t)=\frac{\partial r(x,t)}{\partial t} \tag{2.12}$$

as well as at the flow channel axis level through the radial derivative of the axial velocity which is zero (symmetry):

$$\left.\frac{\partial u}{\partial r}\right|_{r=0}=0 \tag{2.13}$$

The turbulent regime volumetric flow as averaged volumetric flow rate $(\bar{Q})$ is directly dependent on the turbulent velocity and the peristaltic shape of the channel:

$$\bar{Q}=\int_0^{r(x,t)}2\pi r\bar{u}(x,r,t)dr \tag{2.14}$$

In turbulent regime, the axial velocity $(\bar{u})$ shows a flatter distribution than that in the laminar regime, precisely due to the achievement of turbulent mixing within the fluid [13-15].

### 3. Numerical analysis for peristaltic fluid flow

For numerical simulation of peristaltic flow in turbulent regime, usually CFD (Computational Fluid Dynamics) methods are used, which enable RANS solution iterations with software such as OpenFOAM, ANSYS Fluent or COMSOL Multiphysics.
The problem of peristaltic flow is described by the Navier-Stokes equations for an incompressible fluid, in the context of a time-varying flow domain with a sinusoidal wall or other type of periodic motion.
Usually, the channel wall is assumed to follow a sinusoidal motion, and the fluid is subjected to a non-Newtonian model.
To solve this problem numerically, methods such as finite difference, finite volume, or finite element can be used. A finite difference approach will be used to solve the partial equations in space and time.

To simulate the deformation of a vessel wall under the influence of peristaltic fluid flow, a numerical approach is considered that calculates the interaction between the fluid pressure and the shear forces acting on the channel wall.
The pressure action is introduced as sinusoidal variable in time and axially, while the elasticity properties of channel wall are considered, completing a basic model used to identify solutions related to the pressure distribution and channel wall deformation where the fluid flow takes place (figure 1).

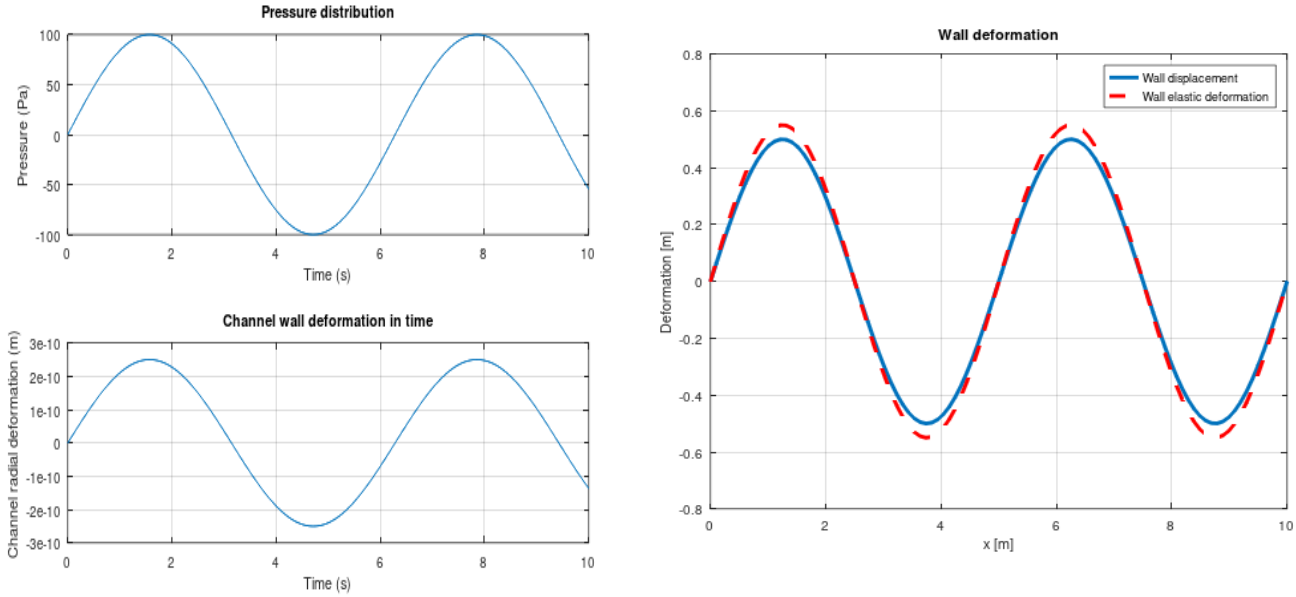


**Fig. 1.** The pressure distribution and channel wall time and space deformation

The numerical analysis is highlighting the proper deformation values of the channel walls depending on the change in the viscosity values of the fluid.
It must be taken into account that the channel in which the peristaltic flow takes place undergo elastic deformations under the action of the internal pressure generated by the flow.
The channel in which the flow takes place is of circular cross-section, aiming to establish the flow rate as a function of viscosity and to determine the pressure value necessary to maintain the flow.
As the viscosity of the fluid increases, the pressure required to maintain flow will increase and this will cause greater channel deformation, an effect that is visualized by a change in the channel radius.
The internal pressure is calculated as a function of viscosity and further the channel deformation limit will be established as a function of this pressure. The basic parameters of the numerical model are presented in Table 1.

**Table 1.** Numerical parameters

| Crt. No. | Parameter | Value |
|---|---|---|
| 1. | Channel radius | 5.00 (mm) |
| 2. | Channel length | 1 (m) |
| 3. | Volumetric flow rate | 5 ml/s |
| 4. | Elasticity modulus of the channel | 1e7 (Pa) |
| 5. | Fluid viscosity range | 0.001-0.003 mPa.s |

The channel deformation is calculated assuming that the channel in which the flow occurs behaves as an elastic material, involving the modulus of elasticity.
The results obtained are presented in the form of diagrams representing the evolution of viscosity as a function of the shear rate, then the pressure values as a function of viscosity, as well as the deformation of the vessel radius as a function of viscosity, highlighting how the increase in viscosity determines a greater deformation of the channel.
It can be seen that as the viscosity increases, the required pressure necessary to maintain a constant flow rate will be higher in value.

The deformation of the channel will increase as the internal pressure rises, which reflects the fact that increased viscosity (especially at low shear) will lead to a higher pressure and, implicitly, to a more significant deformation of the channel.
This basic model demonstrates how an increase in fluid viscosity values can lead to higher internal pressure and implicitly, to a deformation of the channel wall, with results presented in figure 2.

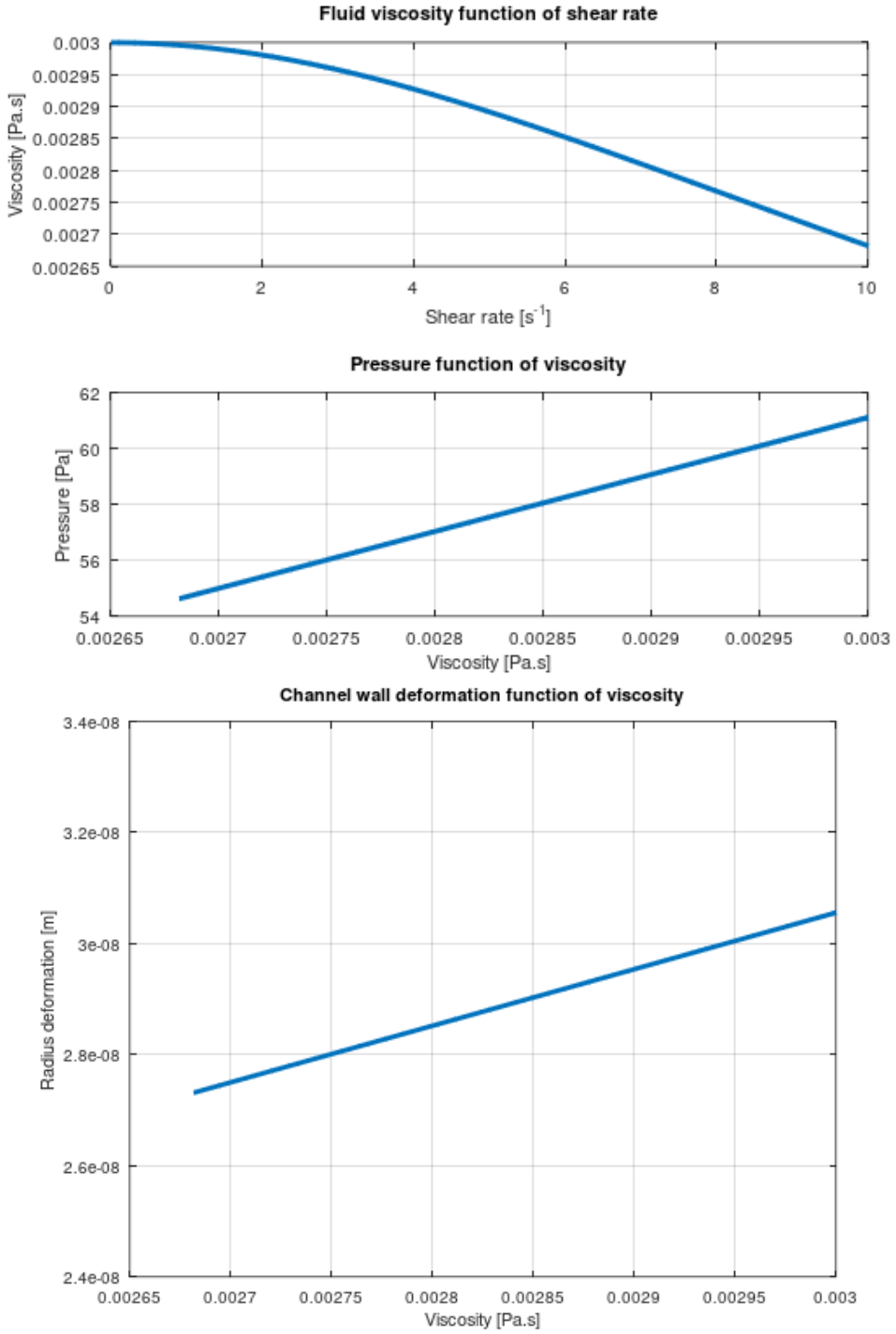


**Fig. 2.** The channel wall elastic deformation function on viscosity and pressure effects

In reality, blood vessels exhibit a more complex behaviour, being subjected to compression and tension effects that require more advanced numerical models, but this model can provide a basic understanding of the fluid viscosity effects on circulation.
Also, the modelling process for peristaltic flow in turbulent regime requires a combination of Navier-Stokes equations, turbulence models and numerical methods, essential for understanding complex

phenomena in biology (e.g. turbulent flow in large blood vessels) and technology (industrial peristaltic pumps).

## 4. Conclusions

Numerical modeling of peristaltic flow is a powerful method to understand the behavior of complex fluids, such as blood circulation in biological systems and further in the engineering field.
Specific approaches have been used over time and the conclusions and perspectives are based on theoretical, practical and numerical aspects.
The method of modeling peristaltic flow based on fluid viscosity, shear rate and channel wall deformation provides a realistic perspective on fluid transport in biological systems, such as blood circulation.
The influence of viscosity and rheological behavior of the fluid is highlighted by non-Newtonian models, which capture well the variation of viscosity as a function of shear rate.
In regions with a high velocity gradient (near the walls), the apparent viscosity decreases, which improves transport, while in the center of the vessel, where the shear rate is low, the increase in viscosity leads to stagnant zones.
Blood, as a non-Newtonian fluid, exhibits shear-thinning behavior (decrease in viscosity at high shear rates), which optimizes transport in large arteries and numerical models that include shear-dependent viscosity better predict the real fluid dynamics.
The shear stress distribution shows that the maximum shear stress occurs at the channel walls and significantly influences their deformation.
In the central regions of the vessel, the stress is low, which creates slow-flowing zones, favorable for the sedimentation of particles (e.g., blood cells).
High shear rate prevents flow stagnation and optimizes the exchange of substances, while low shear rate can favor the formation of thrombi or the sedimentation of particles in slow-flow regions.
The impact of vessel wall deformation shows the fluid-structure interaction mode. The flexible vessel walls play a crucial role in generating peristaltic flow, being responsible for inducing pressure waves and the wall deformation introduces complex phenomena such as the propagation of elastic waves and the variation of the cross-section with time.
The amplitude and frequency of the waves determine the velocity and volume of the transported fluid flow. Stiffer walls reduce the transport efficiency, while very flexible walls can induce flow instabilities.
In channels with deformable walls, the flow is significantly influenced by the interaction between the shear stress and the elastic properties of the walls. Large deformations create separation or reflux zones, reducing the transport efficiency.
Numerical results show that peristaltic flow models integrate shear rate-dependent viscosity, shear stress, wall deformation and provide a realistic description of fluid flow.
Practical applications of flow modeling are particularly important in the medical field, where models can be used to analyze the efficiency of peristaltic pumps in medical devices or to understand thrombus formation in blood vessels and further in the engineering field, where complex fluid transport systems in industrial environments benefit from such models for flow optimization.
The numerical model of peristaltic flow based on viscosity, shear rate and wall deformation provides an advanced understanding of complex fluid transport. This reveals critical interactions between fluid properties, wall mechanics and flow conditions.
The applications of these models are vast, ranging from understanding biological processes to optimizing technological fluid transport systems.

**Acknowledgments**

The research within this paper was conducted within Fluid Mechanics Laboratory, Engineering Sciences and Management Department, Engineering and Agronomy Faculty of Braila, "Dunarea de Jos" University of Galati and with the support of Machine Mechanics and Technological Equipments - MECMET Research Center, "Dunarea de Jos" University of Galati, Engineering and Agronomy Faculty of Braila and received no external funding.

**References**

[1] Scheaua, F*. Fluid mechanics and hydraulic equipment/Mecanica fluidelor şi echipamente hidraulice*. Galati, Galati University Press, 2022.
[2] Axinti, G., and A.S. Axinti. *Hydraulic and pneumatic drives – Components and systems, Functions and features/Acţionări hidraulice şi pneumatice – Componente și sisteme, Funcții și caracteristici*. Vol. 1. Chişinău, Tehnica-Info Publishing House, 2008.
[3] Axinti, S., and F.D. Șcheaua. *Introduction to industrial hydraulics/Introducere în hidraulica industrială*. Galati, Galati University Press, 2015.
[4] Axinti, G., and A.S. Axinti. *Hydraulic and pneumatic drives – Bases of Calculation, Design, Operation, Reliability and Drive Diagrams*/*Acţionări hidraulice şi pneumatice – Baze de Calcul, Proiectare, Exploatare, Fiabilitate și Scheme de Acționare*. Vol. 3. Chişinău, Tehnica-Info Publishing House, 2009.
[5] Formato, Gaetano, Raffaele Romano, Andrea Formato, Joonas Sorvari, Tuomas Koiranen, Arcangelo Pellegrino, and Francesco Villecco. "Fluid–structure interaction modeling applied to peristaltic pump flow simulations." *Machines* 7, no. 3 (2019): 50.
[6] Hostettler, Marco, Raphael Grüter, Simon Stingelin, Flavio De Lorenzi, Rudolf M. Fuechslin, Cyrill Jacomet, Stephan Koll, Dirk Wilhelm, and Gernot K. Boiger. "Modelling of Peristaltic Pumps with Respect to Viscoelastic Tube Material Properties and Fatigue Effects." *Fluids* 8, no. 9 (2023): 254.
[7] Khan, Muhammad Ijaz, Maha M. A. Lashin, Nidhal Ben Khedher, Bilal Ahmed, Sami Ullah Khan, Mowffaq Oreijah, Kamel Guedri, El Sayed Mohamed Tag-ElDin, and Ahmed M. Galal. "Peristaltic phenomenon in an asymmetric channel subject to inclined magnetic force and porous space." *Bioengineering* 9, no. 10 (2022): 588.
[8] Yasmin, Humaira, Naveed Iqbal, and Anum Tanveer. "Engineering applications of peristaltic fluid flow with hall current, thermal deposition and convective conditions." *Mathematics* 8, no. 10 (2020): 1710.
[9] Moulinos, Iosif C., Christos Manopoulos, and Sokrates Tsangaris. "Multivariate Peristalsis in a Straight Rectangular Duct for Carreau Fluids." *Computation* 12, no. 3 (2024): 62.
[10] Guadagni, Simone, Liviu Iulian Palade, Lorenzo Fusi, and Angiolo Farina. "On a Casson fluid motion: Nonuniform width symmetric channel and peristaltic flows." *Fluids* 6, no. 10 (2021): 356.
[11] Tang, Tao-Qian, Muhammad Rooman, Narcisa Vrinceanu, Zahir Shah, and Ahmed Alshehri. "Blood flow of Au-nanofluid using Sisko model in stenotic artery with porous walls and viscous dissipation effect." *Micromachines* 13, no. 8 (2022): 1303.
[12] Magdy, Muhammad, Ramzy Abumandour, Islam Eldesoky, and Hammad Alotaibi. "Synergistic Exploration of Heat Transfer for Integration Magneto hydro dynamics of Nanofluids Peristaltic Transport within Annular Tubes." *Mathematics* 12, no. 13 (2024): 2024.
[13] Polanczyk, Andrzej, Aleksandra Piechota-Polanczyk, Agnieszka W. Piastowska-Ciesielska, Ihor Huk, Christoph Neumayer, Julia Balcer, and Michal Strzelecki. "Reconstruction of the Physiological Behavior of Real and Synthetic Vessels in Controlled Conditions." *Applied Sciences* 14, no. 6 (2024): 2600.
[14] Tinsley, Beth, Sergio Caponi, Lucy McAteer, Gleb Nebesnyy, Dean Sammanthan, Ella Sonia Keza, and Parvez Alam. "Peristaltic Motion Enabled by Pneumatic Artificial Muscles (PAMs) as Structural “Soft–Stiff” Actuators in a Modular Worm-Inspired Robot." *Biomimetics* 9, no. 8 (2024): 447.
[15] Yu, Tai-Ho, Chun-Hung Lai, and Yuan-Hsin Chen. "Design of a Simple Valveless Micropump Using Piezoelectric Actuators." *Journal of Fluids Engineering* 146, no. 8 (2024): 081203.

# Dispersion Curves of Water Quality Parameters in the Fuerte River and Huites Dam, Mexico: Assessment of Aquatic Fauna Survival

Dra. **Maritza ARGANIS[1,*],** M.Eng. **Margarita PRECIADO[2,*],** M.Eng. **Cecilia GONZALEZ[2],** M.I.D. **Helena RIVAS-LÓPEZ[2]**

[1] National Autonomous University of Mexico UNAM, Institute of Engineering, Av. Universidad 3000. Ciudad Universitaria, Coyoacán, CDMX, C.P. 0451

[2] Mexican Institute of Water Technology IMTA, Paseo Cuauhnáhuac 8232 Progreso, Morelos, C.P. 62550

* MArganisJ@iingen.unam.mx; preciado@tlaloc.imta.mx

***Abstract:*** *The water quality parameters profile of a river and a reservoir in the Fuerte River, Sinaloa, Mexico, was analyzed to identify the survival conditions of the Tilapia fish species inhabiting this area. Dissolved Oxygen (DO) was identified as the most critical parameter affecting their survival. Field data reported in publicly accessible databases was used; genetic programming was applied to approximate the model of the average DO concentration profile against the length, resulting in a logarithmic model used for forecasting in a section near the last sampling point. The model also indicated dissolved oxygen conditions below 5 mg/l, implying a survival risk for Tilapia. A heat map (risk) of DO concentration behavior over time and across different sampling sections was obtained, which helped identify dates with higher survival risks for Tilapia. The application of differential equations to hydraulics and environmental engineering topics was evidenced in this practical case.*

***Keywords:*** *Diffusion equation, Concentration, Dissolved Oxygen, Río Fuerte, Huites Dam, Tilapia*

## 1. Introduction

Surface freshwater found on Earth (rivers, lagoons, lakes, human-made reservoirs) supports the development and life of diverse aquatic species (flora and fauna). Anthropogenic activities cause changes in water quality parameters since often, discharges into receiving bodies are made without prior treatment as established by a country's current regulations. Sampling of water parameters helps infer the survival scenarios of organisms [1]. In Mexico, many rivers suffer from a lack of thorough monitoring of water quality parameter concentrations [2]; although efforts have been made to carry out these identifications [3], it is important to have models that not only diagnose but also forecast the behavior of these quality parameters along the river's course, to better document their self-purification capacities.

Mexico's great diversity of environments and species is largely due to its territory being included between two biogeographic regions, the Nearctic and the Neotropical. It is estimated that 57% (289) of the 507 freshwater species living in Mexico are endemic, highlighting the importance of species exclusivity by basin. The basins and regions with the highest percentages of endemic species are: Lerma-Santiago River 66%, Usumacinta-Grijalva 36%, Pánuco 40%, Balsas 35%, Ameca 32%, Papaloapan 21%, Coatzacoalcos 13%, Conchos 21%, Tunal 62%, Cuatro Ciénegas pools 50%, Chichancanab lagoon 85%, and the Media Luna lagoon 65% [4].

Genetic programming [5-8] was applied to approximate the model of the average DO concentration profile against the length. Minimum, maximum, and optimal survival conditions for the Tilapia fish species (Oreochromis niloticus), characteristic of the studied area, were added to the previous data to draw conclusions regarding its survival based on the considered parameters. Additionally, the diffusion equation was numerically solved to determine the temporal and spatial behavior of DO concentration in various sections of the river and the analyzed reservoir. This allowed for the identification of sections and time periods posing risks to the survival of aquatic fauna. The study area for this paper is located in the El Fuerte River basin.

CONAGUA, through the National Water Quality Measurement Network (RENAMECA) [3], conducts systematic and permanent water quality monitoring of the main water bodies in the country. Water quality measurement includes the analysis of physicochemical and microbiological

parameters, established according to the type of water body being characterized. The water quality monitoring stations from RENAMECA were selected, as shown in Figure 1.

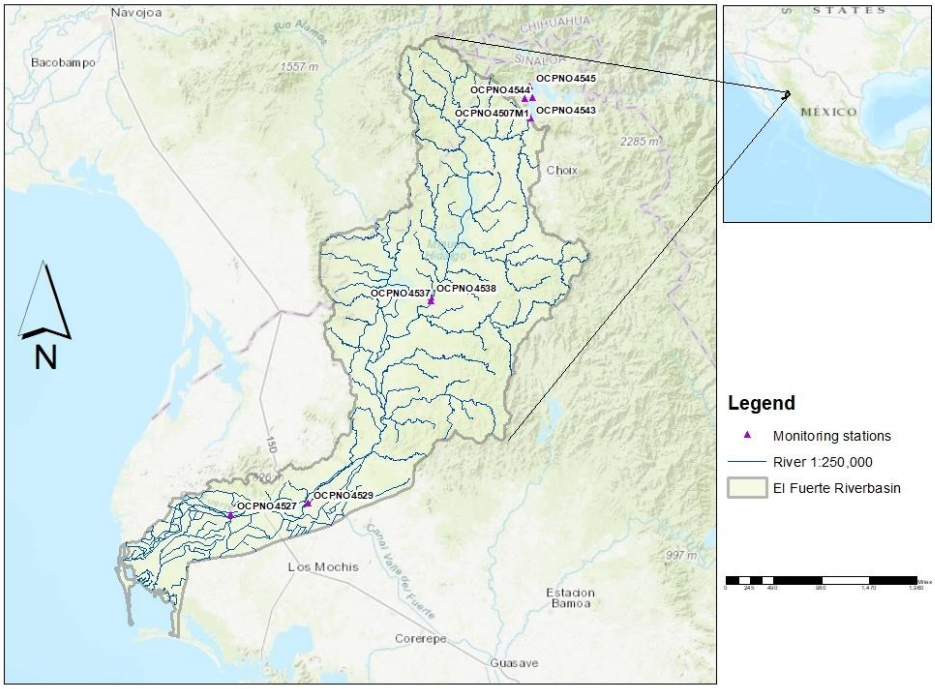


**Fig. 1.** Monitoring stations. Fuerte River, Sin., Mexico

## 2. Methodology

### 2.1 Genetic Programming (GP)

Genetic Programming (GP) [5] is revolutionary in many fields, owing to its ability to evolve programs that solve complex problems. It mirrors natural evolution by using concepts like mutation, crossover, and selection to find solutions that traditional methods may miss. GP can address a wide range of problems in engineering, bioinformatics, economics, and more. It automates solution creation, saving time and reducing the need for extensive human intervention. GP often discovers novel solutions that human designers might not consider, leading to significant breakthroughs. GP is used for predictive modeling and data mining, aiding in the understanding of vast data sets. In engineering, it helps optimize design and operations, enhancing efficiency and performance. GP is crucial in the evolution of AI and machine learning models, pushing the boundaries of what's possible.

Genetic programming harnesses the power of evolution to solve some of the toughest problems out there. Furthermore, GP originated from the need to design computer programs, modifying simple genetic algorithms. Individuals in GP are operators or branches with operators that reproduce, exchange, or mutate to create new operations, resulting in mathematical models or actual code. The traditional Genetic Programming block diagram is shown in Figure 2 [5].

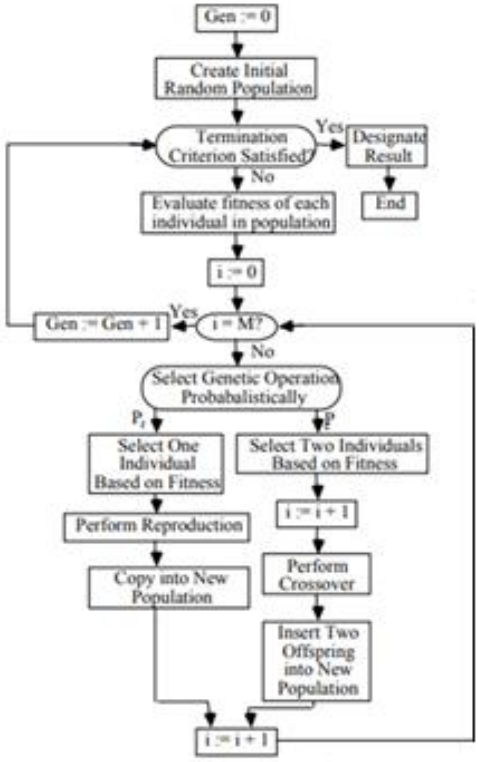


**Fig. 2.** Genetic programming flowchart Source:[5]

In this paper, arithmetic and transcendent operators (+, -, *, /, ln, sin, cos), constant terms and an independent variable (distance d) and a dependent variable the concentration of the analyzed parameter were considered. The parameters used by GP are shown in Table 1.

**Table 1:** GP parameters considered

| Parameter | Value |
|---|---|
| population size | 200, |
| generations | 1000, |
| tournament size | 20, |
| stopping criteria | 0.01, |
| const_range | (-1.0,1.0), |
| p_crossover | 0.7, |
| p_subtree_mutation | 0.1, |
| p_hoist_mutation | 0.05, |
| p_point_mutation | 0.1, |
| max_samples | 0.9, |
| verbose | 1, |
| parsimony_coefficient | 0.01, |
| random_state | 42, |

The objective function considered to obtain the mathematical model to approximate the mean concentration of a water quality parameter as a function of distance x was the minimization of the mean square error. A Python code program generated with the support of an AI [9] and executed in Anaconda's Jupyter notebook [10] was used.

## 2.2 Data set

Dissolved Oxygen (DO), Water Temperature (Tw) and Hydrogen Potential (PH) data recorded on various dates between 2012 and 2022 were considered (Figure 3 shows the distance of each section from section 0).

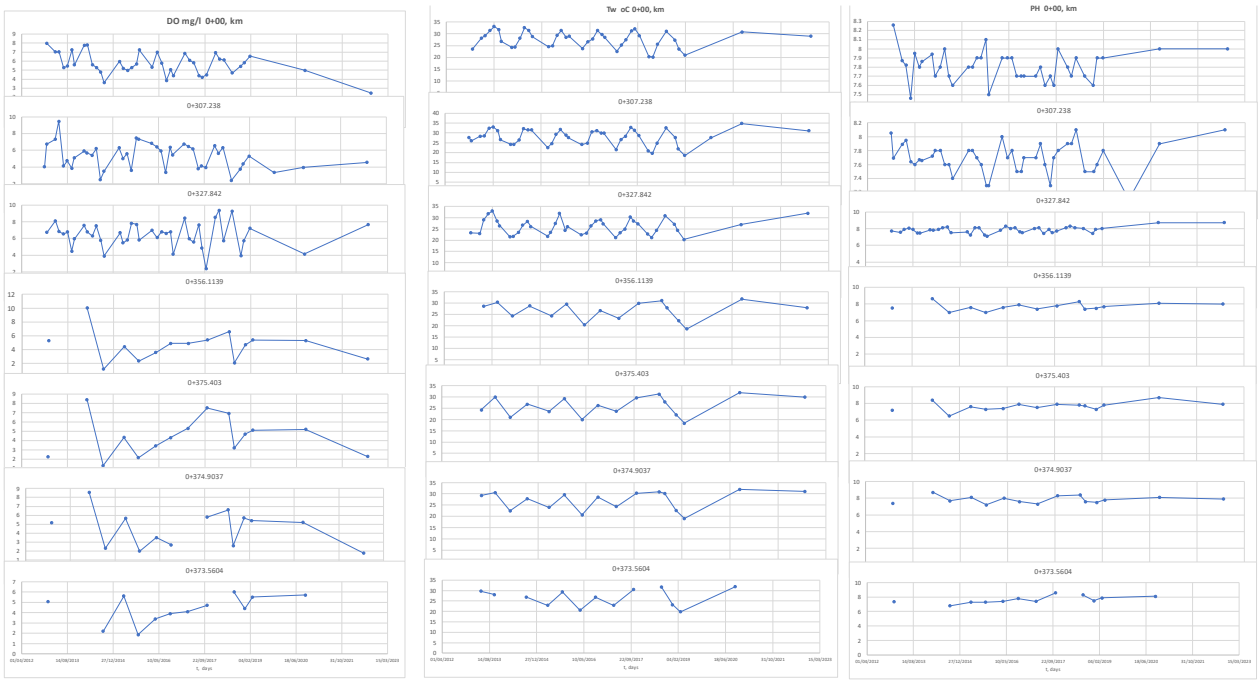


**Fig. 3.** DO, Ta, PH Measured data in different sections of the Fuerte River and Huites Dam, Sin.,Mexico

## 2.2 Average Concentration Profile

Statistical measures including the mean, standard deviation, and skewness coefficient were obtained for each parameter and section analyzed. The mean value was used to construct the concentration profile along the river and the reservoir. Additionally, survival conditions for typical fish species found in Mexico were included [11, 12], along with the minimum values and optimal survival ranges for Tilapia inhabiting the surface waters of the study area.

## 2.3 Diffusion Equation for Heat Map (Risk)

The diffusion equation of the concentration (C) in mg/l of a substance, considering the independent variables time (t) in s, and distance (x) in cm, with diffusion coefficient D in $cm^2/s$, can be expressed as follows [13]:

$$\frac{\partial C}{\partial t} = D\frac{\partial^2 C}{\partial x^2} \tag{1}$$

Selecting derivation schemes of Newtonian advance polynomials of the first and second degree, pivot in xi [14]:

$$\frac{C_i^{n+1} - C_i^n}{\Delta t} = D\frac{C_{i+1}^n - 2C_i^n + C_{i-1}^n}{(\Delta x)^2} \tag{2}$$

Clearing $C_i^{n+1}$: yields an explicit finite difference scheme:

$$C_i^{n+1} = C_i^n + \frac{D\Delta t}{(\Delta x)^2}(C_{i+1}^n - 2C_i^n + C_{i-1}^n) \tag{3}$$

To ensure the stability of the scheme, the Courant-Friedrichs-Lewy (CFL) stability condition [15] is satisfied:

$$\frac{D\Delta t}{(\Delta x)^2} \leq 0.5 \quad (4)$$

To give an example of the case of DO:

Considering a typical value of the diffusion coefficient D for the DO:

$D=2.1\times10^{-5}cm^2/s$

The following values of the increments in time and length are proposed and the stability condition is verified: Δt=7,776,000 s (3 months)

Δx=2,493,333.333 cm (24.93 km)

$$\frac{2.1 \times 10^{-5} \times 7{,}776{,}000}{(2{,}493{,}333.333)^2} \leq 0.5$$

$2.626 \times 10^{-8} \leq 0.5$, cumple estabilidad

Substituting data:

$$C_i^{n+1} = C_i^n + 2.626 \times 10^{-8}(C_{i+1}^n - 2C_i^n + C_{i-1}^n) \quad (5)$$

Finally, the explicit finite difference scheme results:

$$C_i^{n+1} = C_i^n(1 - 5.252 \times 10^{-8}) + 2.626 \times 10^{-8}C_{i+1}^n + 2.626 \times 10^{-8}C_{i-1}^n \quad (6)$$

For the calculation, the DO data were linearly interpolated for quarterly values of time in the initial (0+00 km) and final (0+374 km) sections taken as boundary conditions; the DO data were interpolated in the different sections, to take into account initial conditions at t0=0; the scheme was applied in finite differences and a color scale was used, assigning a green color to the data with the highest DO value and a red color to the data with the lowest DO value, thus building a heat map (risk).

## 3. Results

### 3.1 Average concentration value profiles

Average profiles values of DO, Tw and Ph are shown in Figures 4 to 6.

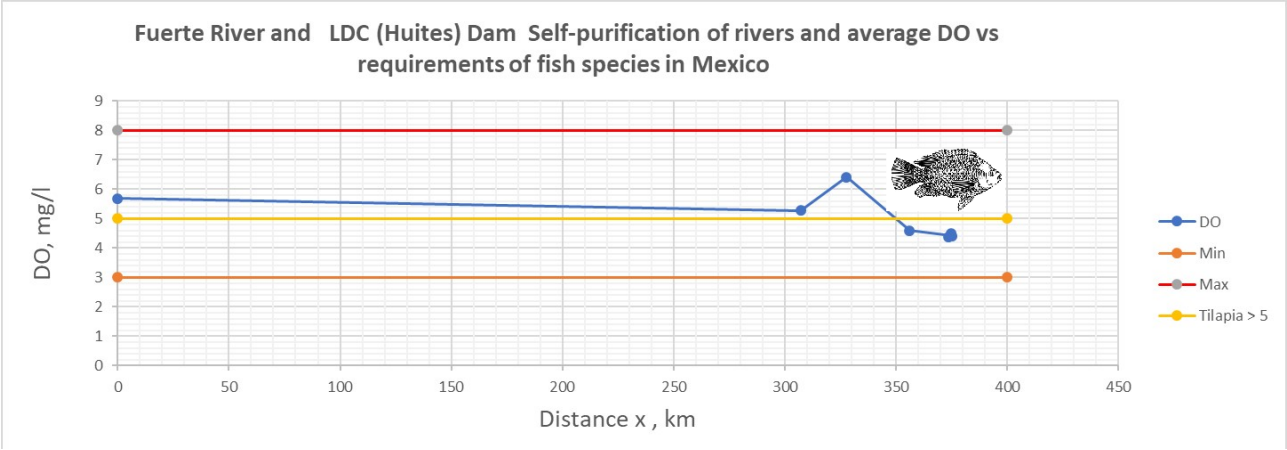


**Fig. 4.** Average value profile for concentration of DO and survival values of Tilapia fish

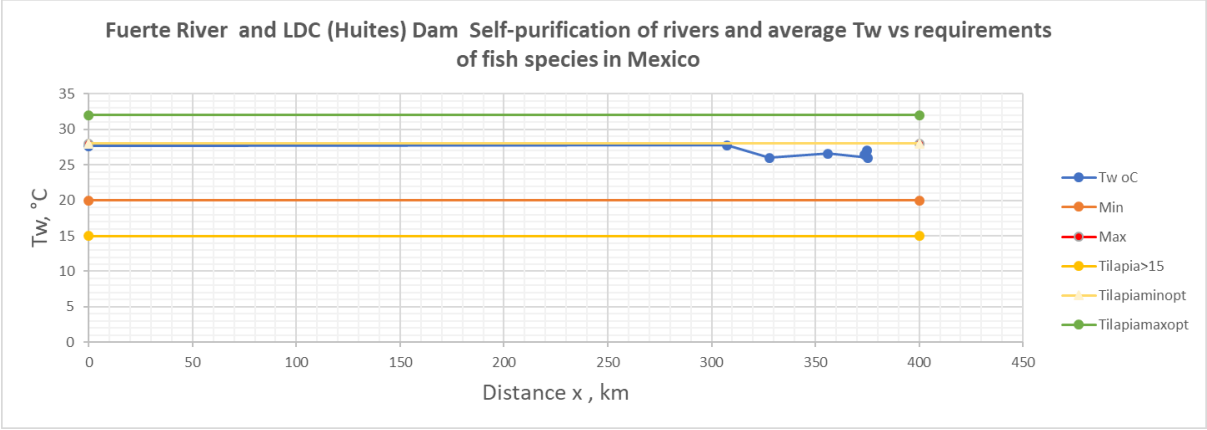


**Fig. 5.** Average value profile for concentration and survival values Tilapia fish

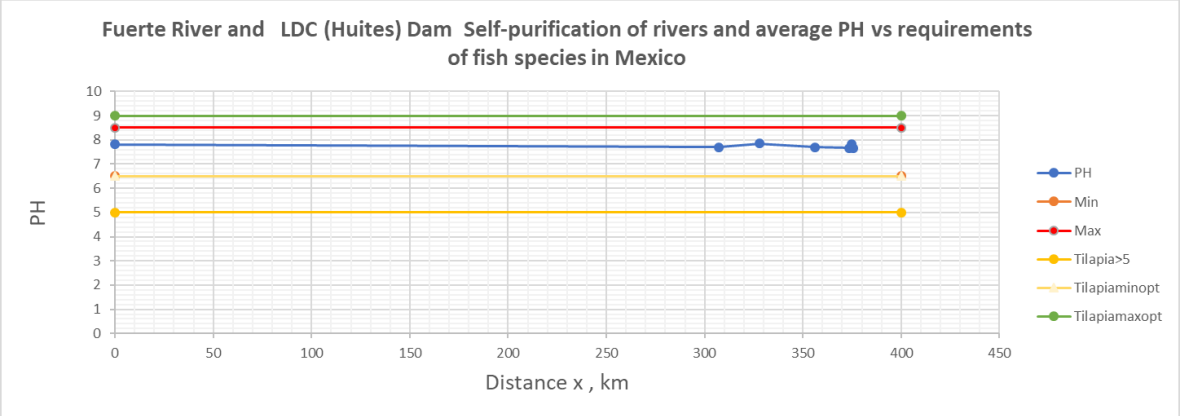


**Fig. 6.** Average value profile for PH concentration and survival values of Tilapia fish

From figures 3 and 4, it can be seen that the parameter with the highest risk of survival of Tilapia is the DO, since the average values in some sections fall to values below 5 mg/l, already in the sections within the reservoir.

### 3.2 GP Model

With GP, 75% of the measured data of the DO was used to obtain a mathematical model and validation was done with 25% of them; The mean square errors (MSE) and the coefficients of determination $R^2$ obtained in the measured and validated data obtained by the Python program developed by an AI reports the following results: MSE (training): 0.8616, $R^2$ (training): -0.4134, MSE (test): 16.6448, $R^2$ (test): -408.48823527524695. Figure 7 shows the comparison of the measured data vs. the calculated data of the mean concentration profile of the DO and with respect to an identity function.

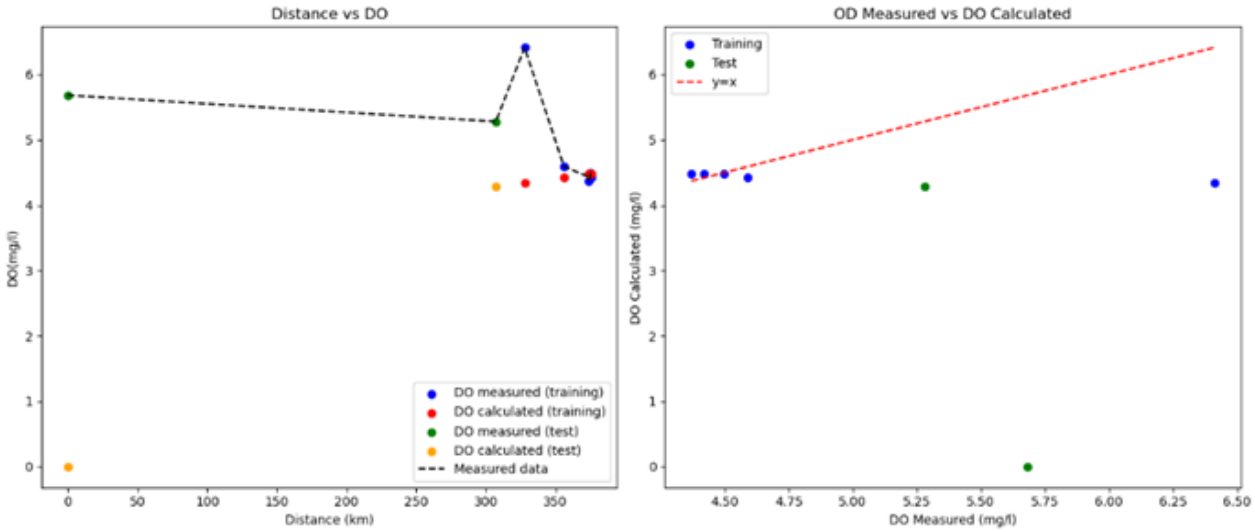


**Fig. 7.** PG algorithm behavior during training and validation, as well as with respect to measured and computed data vs. an identity function

The equation obtained with GP of the average concentration of DO in mg/l vs distance x in km took the form (the negative sign in the natural logarithm that GP originally reported is not considered):

$$DO = ln\,(0.235x) \tag{7}$$

To investigate the survival condition of the Tilapia fish beyond the last section considered, for example, at x= 400 km the dissolved oxygen reported by the model is: 4,543 mg/l, i.e. the model would predict survival risk even at 400 km

### 3.3 Heat Map (risk)

To account for the variation in the critical DO parameter over time and across different sections, it was proposed to numerically solve the diffusion differential equation, resulting in the tabular function of dissolved oxygen. By assigning a color scale where green represents the highest DO value and red the lowest, information appears highlighted with a bold border on dates with the highest risks to the survival of aquatic species (Figure 8). For instance, Tilapia survives with suggested DO values greater than 5 mg/l; below these values, their survival is at risk.

| t día/ d km | 0 | 24.93 | 49.87 | 74.80 | 99.73 | 124.67 | 149.60 | 174.53 | 199.47 | 224.40 | 249.33 | 274.27 | 299.20 | 324.13 | 349.07 | 374 |
|---|---|---|---|---|---|---|---|---|---|---|---|---|---|---|---|---|
| | | | | | | OD mg/l | | | | | | | | | | |
| 30/12/2012 | 7.99 | 7.89 | 7.79 | 7.69 | 7.58 | 7.48 | 7.38 | 7.28 | 7.18 | 7.08 | 6.98 | 6.87 | 6.77 | 6.73 | 5.65 | 5.07 |
| 30/03/2013 | 7.07 | 7.89 | 7.79 | 7.69 | 7.58 | 7.48 | 7.38 | 7.28 | 7.18 | 7.08 | 6.98 | 6.87 | 6.77 | 6.73 | 5.65 | 4.64 |
| 28/06/2013 | 5.45 | 7.89 | 7.79 | 7.69 | 7.58 | 7.48 | 7.38 | 7.28 | 7.18 | 7.08 | 6.98 | 6.87 | 6.77 | 6.73 | 5.65 | 4.21 |
| 26/09/2013 | 7.05 | 7.89 | 7.79 | 7.69 | 7.58 | 7.48 | 7.38 | 7.28 | 7.18 | 7.08 | 6.98 | 6.87 | 6.77 | 6.73 | 5.65 | 3.78 |
| 25/12/2013 | 6.74 | 7.89 | 7.79 | 7.69 | 7.58 | 7.48 | 7.38 | 7.28 | 7.18 | 7.08 | 6.98 | 6.87 | 6.77 | 6.73 | 5.65 | 3.35 |
| 25/03/2014 | 7.56 | 7.89 | 7.79 | 7.69 | 7.58 | 7.48 | 7.38 | 7.28 | 7.18 | 7.08 | 6.98 | 6.87 | 6.77 | 6.73 | 5.65 | 2.92 |
| 23/06/2014 | 5.33 | 7.89 | 7.79 | 7.69 | 7.58 | 7.48 | 7.38 | 7.28 | 7.18 | 7.08 | 6.98 | 6.87 | 6.77 | 6.73 | 5.65 | 2.49 |
| 21/09/2014 | 3.64 | 7.89 | 7.79 | 7.69 | 7.58 | 7.48 | 7.38 | 7.28 | 7.18 | 7.08 | 6.98 | 6.87 | 6.77 | 6.73 | 5.65 | 2.64 |
| 20/12/2014 | 4.9 | 7.89 | 7.79 | 7.69 | 7.58 | 7.48 | 7.38 | 7.28 | 7.18 | 7.08 | 6.98 | 6.87 | 6.77 | 6.73 | 5.65 | 3.99 |
| 20/03/2015 | 5.7 | 7.89 | 7.79 | 7.69 | 7.58 | 7.48 | 7.38 | 7.28 | 7.18 | 7.08 | 6.98 | 6.87 | 6.77 | 6.73 | 5.65 | 5.34 |
| 18/06/2015 | 5.08 | 7.89 | 7.79 | 7.69 | 7.58 | 7.48 | 7.38 | 7.28 | 7.18 | 7.08 | 6.98 | 6.87 | 6.77 | 6.73 | 5.65 | 3.89 |
| 16/09/2015 | 6.15 | 7.89 | 7.79 | 7.69 | 7.58 | 7.48 | 7.38 | 7.28 | 7.18 | 7.08 | 6.98 | 6.87 | 6.77 | 6.73 | 5.65 | 1.9 |
| 15/12/2015 | 6.31 | 7.89 | 7.79 | 7.69 | 7.58 | 7.48 | 7.38 | 7.28 | 7.18 | 7.08 | 6.98 | 6.87 | 6.77 | 6.73 | 5.65 | 2.64 |
| 14/03/2016 | 5.89 | 7.89 | 7.79 | 7.69 | 7.58 | 7.48 | 7.38 | 7.28 | 7.18 | 7.08 | 6.98 | 6.87 | 6.77 | 6.73 | 5.65 | 3.38 |
| 12/06/2016 | 5.66 | 7.89 | 7.79 | 7.69 | 7.58 | 7.48 | 7.38 | 7.28 | 7.18 | 7.08 | 6.98 | 6.87 | 6.77 | 6.73 | 5.65 | 3.67 |
| 10/09/2016 | 4.94 | 7.89 | 7.79 | 7.69 | 7.58 | 7.48 | 7.38 | 7.28 | 7.18 | 7.08 | 6.98 | 6.87 | 6.77 | 6.73 | 5.65 | 3.91 |
| 09/12/2016 | 5.49 | 7.89 | 7.79 | 7.69 | 7.58 | 7.48 | 7.38 | 7.28 | 7.18 | 7.08 | 6.98 | 6.87 | 6.77 | 6.73 | 5.65 | 4.01 |
| 09/03/2017 | 6.56 | 7.89 | 7.79 | 7.69 | 7.58 | 7.48 | 7.38 | 7.28 | 7.18 | 7.08 | 6.98 | 6.87 | 6.77 | 6.73 | 5.65 | 4.11 |
| 07/06/2017 | 5.48 | 7.89 | 7.79 | 7.69 | 7.58 | 7.48 | 7.38 | 7.28 | 7.18 | 7.08 | 6.98 | 6.87 | 6.77 | 6.73 | 5.65 | 4.37 |
| 05/09/2017 | 4.27 | 7.89 | 7.79 | 7.69 | 7.58 | 7.48 | 7.38 | 7.28 | 7.18 | 7.08 | 6.98 | 6.87 | 6.77 | 6.73 | 5.65 | 4.62 |
| 04/12/2017 | 5.83 | 7.89 | 7.79 | 7.69 | 7.58 | 7.48 | 7.38 | 7.28 | 7.18 | 7.08 | 6.98 | 6.87 | 6.77 | 6.73 | 5.65 | 4.98 |
| 04/03/2018 | 6.23 | 7.89 | 7.79 | 7.69 | 7.58 | 7.48 | 7.38 | 7.28 | 7.18 | 7.08 | 6.98 | 6.87 | 6.77 | 6.73 | 5.65 | 5.37 |
| 02/06/2018 | 5.43 | 7.89 | 7.79 | 7.69 | 7.58 | 7.48 | 7.38 | 7.28 | 7.18 | 7.08 | 6.98 | 6.87 | 6.77 | 6.73 | 5.65 | 5.77 |
| 31/08/2018 | 5.03 | 7.89 | 7.79 | 7.69 | 7.58 | 7.48 | 7.38 | 7.28 | 7.18 | 7.08 | 6.98 | 6.87 | 6.77 | 6.73 | 5.65 | 5.49 |
| 29/11/2018 | 5.84 | 7.89 | 7.79 | 7.69 | 7.58 | 7.48 | 7.38 | 7.28 | 7.18 | 7.08 | 6.98 | 6.87 | 6.77 | 6.73 | 5.65 | 4.52 |
| 27/02/2019 | 6.46 | 7.89 | 7.79 | 7.69 | 7.58 | 7.48 | 7.38 | 7.28 | 7.18 | 7.08 | 6.98 | 6.87 | 6.77 | 6.73 | 5.65 | 5.51 |
| 28/05/2019 | 6.23 | 7.89 | 7.79 | 7.69 | 7.58 | 7.48 | 7.38 | 7.28 | 7.18 | 7.08 | 6.98 | 6.87 | 6.77 | 6.73 | 5.65 | 5.54 |
| 26/08/2019 | 5.99 | 7.89 | 7.79 | 7.69 | 7.58 | 7.48 | 7.38 | 7.28 | 7.18 | 7.08 | 6.98 | 6.87 | 6.77 | 6.73 | 5.65 | 5.57 |
| 24/11/2019 | 5.76 | 7.89 | 7.79 | 7.69 | 7.58 | 7.48 | 7.38 | 7.28 | 7.18 | 7.08 | 6.98 | 6.87 | 6.77 | 6.73 | 5.65 | 5.6 |
| 22/02/2020 | 5.53 | 7.89 | 7.79 | 7.69 | 7.58 | 7.48 | 7.38 | 7.28 | 7.18 | 7.08 | 6.98 | 6.87 | 6.77 | 6.73 | 5.65 | 5.63 |
| 22/05/2020 | 5.29 | 7.89 | 7.79 | 7.69 | 7.58 | 7.48 | 7.38 | 7.28 | 7.18 | 7.08 | 6.98 | 6.87 | 6.77 | 6.73 | 5.65 | 5.66 |
| 20/08/2020 | 5.06 | 7.89 | 7.79 | 7.69 | 7.58 | 7.48 | 7.38 | 7.28 | 7.18 | 7.08 | 6.98 | 6.87 | 6.77 | 6.73 | 5.65 | 5.69 |
| 18/11/2020 | 4.77 | 7.89 | 7.79 | 7.69 | 7.58 | 7.48 | 7.38 | 7.28 | 7.18 | 7.08 | 6.98 | 6.87 | 6.77 | 6.73 | 5.65 | 5.72 |
| 16/02/2021 | 4.46 | 7.89 | 7.79 | 7.69 | 7.58 | 7.48 | 7.38 | 7.28 | 7.18 | 7.08 | 6.98 | 6.87 | 6.77 | 6.73 | 5.65 | 5.75 |
| 17/05/2021 | 4.14 | 7.89 | 7.79 | 7.69 | 7.58 | 7.48 | 7.38 | 7.28 | 7.18 | 7.08 | 6.98 | 6.87 | 6.77 | 6.73 | 5.65 | 5.79 |
| 15/08/2021 | 3.83 | 7.89 | 7.79 | 7.69 | 7.58 | 7.48 | 7.38 | 7.28 | 7.18 | 7.08 | 6.98 | 6.87 | 6.77 | 6.73 | 5.65 | 5.82 |
| 13/11/2021 | 3.51 | 7.89 | 7.79 | 7.69 | 7.58 | 7.48 | 7.38 | 7.28 | 7.18 | 7.08 | 6.98 | 6.87 | 6.77 | 6.73 | 5.65 | 5.85 |
| 11/02/2022 | 3.2 | 7.89 | 7.79 | 7.69 | 7.58 | 7.48 | 7.38 | 7.28 | 7.18 | 7.08 | 6.98 | 6.87 | 6.77 | 6.73 | 5.65 | 5.88 |
| 12/05/2022 | 2.88 | 7.89 | 7.79 | 7.69 | 7.58 | 7.48 | 7.38 | 7.28 | 7.18 | 7.08 | 6.98 | 6.87 | 6.77 | 6.73 | 5.65 | 5.91 |
| 10/08/2022 | 2.57 | 7.89 | 7.79 | 7.69 | 7.58 | 7.48 | 7.38 | 7.28 | 7.18 | 7.08 | 6.98 | 6.87 | 6.77 | 6.73 | 5.65 | 5.94 |

**Fig. 8.** Dissolved oxygen DO (mg/l) behavior as a function of time t (months) and length d (km) and critical values for the survival of Tilapia (historical conditions)

## 4. Conclusions

The water quality parameters study on the Fuerte River and Huites Dam demonstrates a critical need for continuous monitoring to ensure the survival of aquatic species like Tilapia. Dissolved Oxygen (DO) emerged as the most influential factor affecting aquatic life, with values consistently below the threshold of 5 mg/l in several sections, posing a high risk to fish survival. The implementation of genetic programming and the diffusion equation provided valuable tools for the behaviour modelling of DO and predicting areas of risk. This study also provides a forward-looking perspective on improving water management in Mexico. This analysis underscores the importance of integrated water resource management, where continuous monitoring, innovative modelling techniques, and the application of advanced technologies such as artificial intelligence can optimize the prediction and mitigation of environmental risks. As Mexico grapples with increasing challenges in water quality due to anthropogenic activities, strengthening regulatory frameworks and expanding the scope of research and development in water treatment and distribution systems is essential.

Key recommendations include an enhanced Monitoring by expanding the coverage of the National Water Quality Measurement Network (RENAMECA) to include more detailed, real-time data collection; also a technological Integration, with an invest in AI-driven models for predictive analysis and risk assessment of water quality, ensuring timely interventions in high-risk areas. Finally to promote the adoption of environmentally sustainable practices in agriculture and industry to reduce contamination of water bodies.

In conclusion, addressing the challenges of water quality in the Fuerte River and other Mexican water bodies requires a multidisciplinary approach, combining scientific research, technological innovation, and robust policy-making to protect aquatic ecosystems and ensure water resource sustainability for future generations.

### References

[1] Official Journal of the Federation / Diario Oficial de la Federación (DOF). *NORMA Oficial Mexicana NOM-001-SEMARNAT-2021*. Accessed October 17, 2024.

https://www.dof.gob.mx/nota_detalle.php?codigo=5645374&fecha=11/03/2022#gsc.tab=01.
[2] Agua. *Pollution in Mexico / Contaminación en México*. Accessed 2024. https://agua.org.mx/agua-contaminacion-en-mexico/.
[3] National Network for Water Quality Measurement / Red Nacional de Medición de Calidad del Agua (RENAMECA). Accessed 2024. https://www.gob.mx/conagua/articulos/resultados-de-la-red-nacional-de-medicion-de-calidad-del-agua-renameca?idiom=es.
[4] Espinoza Pérez, Héctor. “Biodiversidad de peces en México (Fish Biodiversity in Mexico).” *Revista Mexicana de Biodiversidad*, Supl. 85 (2014): S450-S459. https://doi.org/10.7550/rmb.32264.
[5] Koza, J.R. *Genetic Programming: On the Programming of Computers by Means of Natural Selection*. Cambridge, The MIT Press, 1992.
[6] Medupe, Medupe, and Moatlhodi Wise Letshwenyo. “Investigation of Self-Purification and Water Quality Index During Dry and Rainy Seasons in the Khurumela Stream (Botswana).” *Journal of Ecohydraulics*, (June 2024): 1-18. https://doi.org/10.1080/24705357.2024.2363755.
[7] Bozorg-Haddad, Omid, Shima Soleimani, and Hugo A. Loáiciga. “Modeling Water-Quality Parameters Using Genetic Algorithm–Least Squares Support Vector Regression and Genetic Programming.” *Journal of Environmental Engineering* 143, no. 9 (2017): 04017061.
[8] Elsayed, Ahmed, Maysara Ghaith, Ahmed Yosri, Zhong Li, and Wael El-Dakhakhni. “Genetic Programming Expressions for Effluent Quality Prediction: Towards AI-Driven Monitoring and Management of Wastewater Treatment Plants.” *Journal of Environmental Management* 356 (2024): 120510. https://doi.org/10.1016/j.jenvman.2024.120510.
[9] Copilot. Accessed 2024. https://copilot.cloud.microsoft/?fromcode=cmc&redirectid=C0E05F6C48714F4EAC209E64FE37D0F3&auth=2.
[10] Anaconda. Accessed 2024. https://anaconda.org/.
[11] Proain. “Producción de peces (Pisciculture) en México / Fish Production in Mexico”, October 8, 2020. Accessed October, 22, 2024. https://proain.com/blogs/notas-tecnicas/produccion-de-peces-piscicultura-en-mexico?srsltid=AfmBOooiAujXCLhJAGkZXot7inGQSEMGrsXlUYvGOld0ZBe8hZ8A6VHI.
[12] Hendrickson, Dean A., and Alejandro Varela Romero. “Fishes of the Río Fuerte Drainage.” In Libro Jubilar en Honor al Dr. Salvador Contreras Balderas, edited by Ma. de Lourdes Lozano-Vilano, 171-195. Monterrey, Universidad Autónoma de Nuevo León, 2002.
[13] Millán, J. “Simulación numérica. Ecuación de difusión / Numerical Simulation. Diffusion Equation).” *Revista Internacional de Métodos Numéricos para Cálculo y Diseño en Ingeniería* 15, no. 2 (2011): 29-38.
[14] Gerald, Curtis F. *Numerical Analysis / Análisis numérico*. 2nd ed. Alfaomega, 1997.
[15] Laney, Culbert B. *Computational Gasdynamics*. Cambridge, Cambridge University Press, 1998.

# Considerations about Vibratory Processes of Hydrostatic Systems with Rotary Engines

Professor Dr. Eng. **Carmen Nicoleta DEBELEAC**[1,*]

[1] "Dunarea de Jos" University of Galati, Engineering and Agronomy Faculty in Braila,
Research Center for Mechanics of Machines and Technological Equipments, Braila, Romania

* carmen.debeleac@ugal.ro

***Abstract:*** *This paper examines transient regimes in mobile technological equipment that initiate oscillatory processes within hydrostatic systems driven by rotary engines. It provides a detailed analysis of the excitation sources responsible for these dynamic behaviors, particularly within hydraulic circuits that operate the working tool. The study highlights the dynamic characteristics of these systems, including pressure resonance observed during rapid acceleration (when the pump shaft's angular velocity approaches the system's natural frequency), command instability, and the resulting effects on the motion precision of the working tool. Additionally, the conditions for the occurrence of magnitude and phase resonances in the driving pressure are evaluated.*

***Keywords:*** *Hydrostatic system, working regime, vibrations, rotary engine, analysis*

## 1. Introduction

As known, the dynamic instability phenomenon in hydrostatically driven equipment manifests through sudden variations in hydraulic pressure without an obvious cause. This instability often occurs in new equipment when the hydrostatic drive system has not been thoroughly analyzed for dynamic behavior. The instant pressure variations are linked to sudden load increases on the work components, which may suggest the presence of dynamic phenomena like mechanical resonances [1,2]. In this context, the volumetric pump of the hydraulic system acts as a source of harmonic perturbations. The pulsations in the pump's output flow can lead to pressure fluctuations, which resemble resonance phenomena seen in mechanical systems with harmonic excitations. Some studies [3,4] have identified similarities between the behavior of rotating mechanical systems with viscous damping and hydraulic systems with rotary motors.
In the field of hydraulic oscillation research, Wylie [5,6] made significant contributions by advancing the impedance method for determining hydraulic resonance within systems. In 1970, Chaudhry [7] introduced an alternative approach to predict the frequency response of hydraulic systems, while also working to refine and organize oscillatory flow equations using the transfer matrix method. Suo and Wylie [8] further explored hydraulic oscillations in pressurized systems, offering additional improvements to hydraulic resonance analysis. To address transient events in complex piping systems, Kim [9] applied the impedance matrix method, incorporating initial conditions and time-history data.
In this paper the author aims to highlight the conditions under which such resonance phenomena in hydrostatic systems arise. When resonance phenomenon occurs, it results in a pressure increase beyond the system's stable state, often accompanied by an increase in noise, unintended activation of hydraulic safety valves, and dynamic stress on system components, potentially affecting their durability and performance.

## 2. Theoretical background

Let's proposed a hydrostatic drive system that consists of rotative motor, which acts the working tool of a technological equipment, like vibratory roller (Figure 1). Thus, during the startup process of a vibratory roller, fluid flow in the pipelines becomes obstructed, causing an impact on the hydraulic vibration system. The load applied to the motor creates resistance to the hydraulic oil flow, resulting in a reduction in motor speed. According to fluid dynamics theory, a decrease in fluid flow rate inevitably leads to an increase in system pressure. The greater the drop-in flow rate, the

higher the resulting pressure rise. As the total energy of the fluid is converted into pressure energy, the hydraulic system experiences rapid pressure fluctuations, leading to the occurrence of instantaneous high pressure and hydraulic shocks.

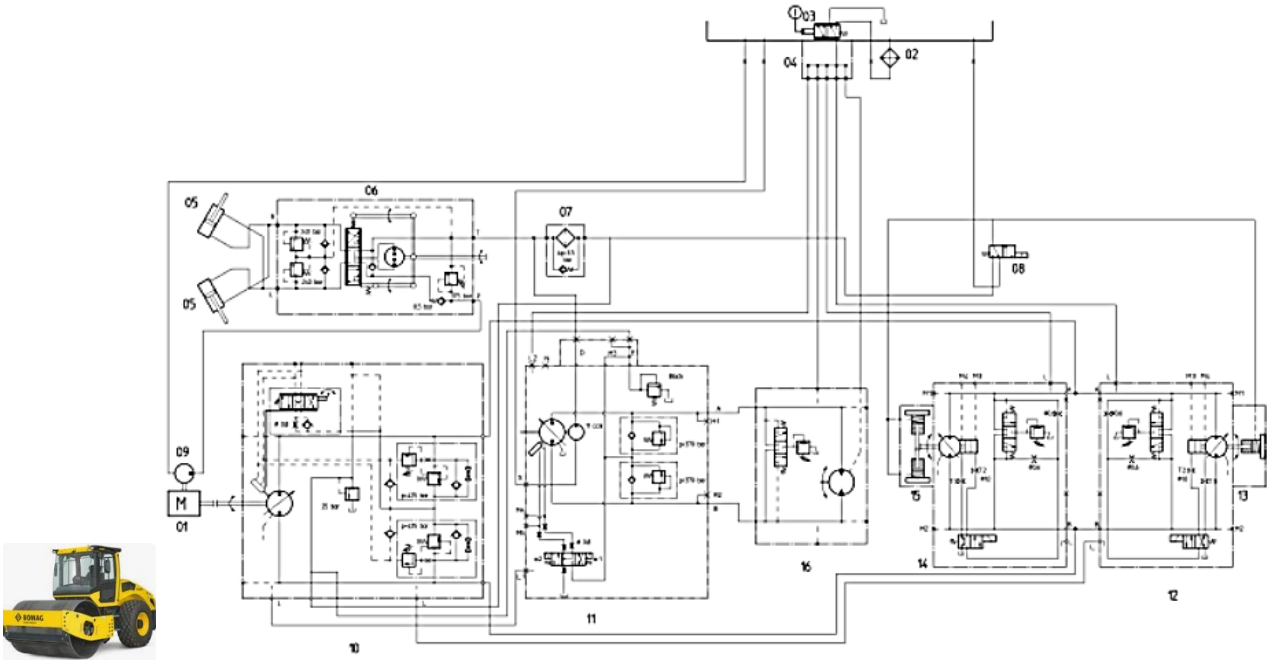

**Fig. 1.** Single drum vibratory roller hydraulic circuit (Bomag Bw 213)

For all types of hydraulic circuits (both open and closed systems), the main components include a hydraulic pump, control valves, actuators (such as cylinders or rotary motors), reservoirs, filters, and piping or hoses, as shown in Figure 2. These components work together to ensure the efficient transfer of hydraulic energy to perform various tasks. This diagram will form the basis for the development of the study in this paper.

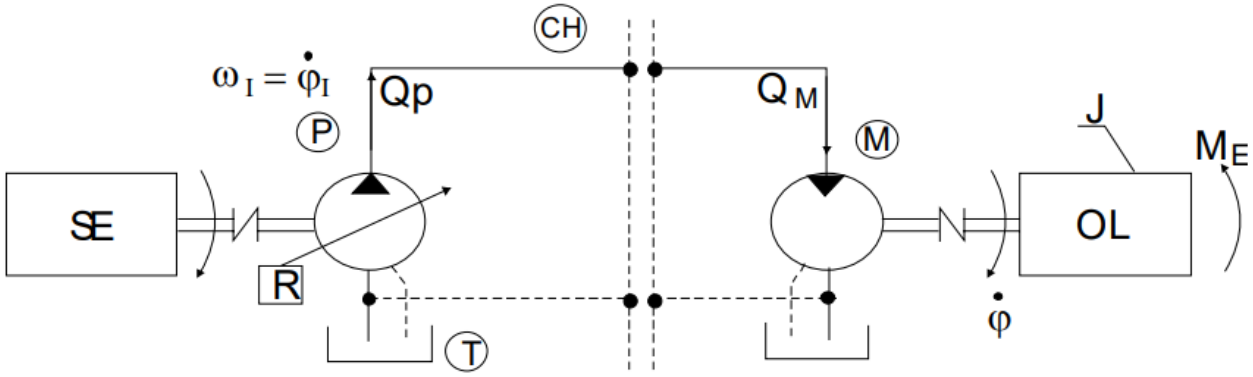


**Fig. 2.** The drive system model:
SE - energy source; P - pump; CH - hydraulic circuit; M – hydraulic motor; OL - rotative working tool; R - pump debit regulator; T - hydraulic tank.

The expression for evaluating the output flow ($Q_P$) from the hydraulic circuit is [10]

$$Q_P = \frac{V_p \omega_I}{2\pi} = \frac{V_{OM} \omega_E}{2\pi} + \alpha_{MR} p + \beta_{MR} \dot{p}, \quad (1)$$

where $V_{OM}$ represents the volume of the hydraulic agent content in the rotative engine, $\omega_E$ is the rotational speed at the axle of the hydrostatic engine (for the working element), $\alpha_{MR}$ is the coefficient of the volumetric losses of the hydraulic agent from the system (proportional to the pressure $p$), and $\beta_{MR}$ is the coefficient that define the hydraulic capacity of the circuit (proportional to the derivative of pressure $p$ with respect to time).

In the circuit, the pump *P* and the hydraulic motor *M* can be considered, of the constructive type with axial pistons, with an inclined block or in disc construction. If the aim is to highlight the effects of the pulsation of the flow rate of the pump $Q_P$ for a set of *m* pistons being in the pumping action, it can be evaluated with expression:

$$Q_P = 2rA_p sin\alpha \sum_{i=1}^{m} sin\varphi_i, \tag{2}$$

where $\alpha$ is the angle of pump block or disk, *r* is the disposition radius of the pump pistons, $A_p$ is the piston area, and $\varphi_i$ represents the angular motion at the spindle pump. In typical cases of axial piston pumps with seven pistons (commonly used in the drive circuits of vibratory rollers), the pump flow rate can be expressed as:

$$Q_p = \frac{q_0 \omega_I}{2\pi} \sin(\omega_I t + \varphi_0), \tag{3}$$

where

$$q_0 = 2rA_p sin\alpha \cdot \frac{sin\frac{m\pi}{7}}{sin\frac{\pi}{7}}, \tag{4}$$

and

$$\varphi_0 = \frac{(m-1)\pi}{7}. \tag{5}$$

Therefore, the equation of dynamic balance at the motor shaft, deduced by the kineto-static method, is [10]

$$M_I = J\ddot{\varphi} = \frac{V_{0M}\dot{\varphi}}{2\pi} - \chi_{MR}\dot{\varphi} - M_E, \tag{6}$$

where $J$ represents the mechanical moment of inertia of all movable elements (reduced to the axis of the rotary engine), $\varphi$ is the angular motion at the engine shaft, $\chi_{MR}$ is the adjustment factor of the cylinder volume of the motor, and $M_E$ is the resistance moment developed to the working tool by the external medium (which must be kept constant regardless of the roller's response to the continuous variation in the degree of soil compaction). To simplify the mathematical model, moment losses caused by dynamic flow forces, Coulomb friction forces, and aerodynamic friction forces, etc., are neglected.

### 3. Mathematical modeling

Processing the terms of the Eqns. (1), (3) and (6) leads to the mathematical modelling of the hydrostatic circuit with rotary motor.

$$\ddot{p} + a_1\dot{p} + a_2 p = a_3 M_E + a_4\omega_I^2 cos(\omega_I t + \varphi_0) + a_5\omega_I sin(\omega_I + \varphi_0), \tag{7}$$

where $a_1 = \frac{\alpha_{MR}}{\beta_{MR}} + \frac{\chi_{MR}}{J}$, $a_2 = \frac{1}{J\beta_{MR}}\left(\frac{V_{0M}^2}{4\pi^2} + \alpha_{MR}\chi_{MR}\right)$, $a_3 = \frac{V_{0M}}{2\pi J\beta_{MR}}$, $a_4 = \frac{q_0}{2\pi\beta_{MR}}$, $a_5 = \frac{\chi_{MR}q_0}{2\pi J\beta_{MR}}$.

By incorporating the expressions for the dynamic factors and simplifying the terms on the right-hand side of the preceding equation, the resulting expression is obtained as follows [11]

$$\ddot{p} + 2\zeta_{MR}\omega_{MR}\dot{p} + \omega_{MR}^2 p = H_{MR} + \Pi_{MR} sin(\omega_I t + \Phi), \tag{8}$$

with the description of the involved parameters in the Table 1.

In Eq. (8) it is considered transient flows that represents the intermediate flow conditions when the flow is changed from one steady state to another. Thus, depending upon the characteristics of the system and of the excitation, a disturbance in a piping system may be amplified with time instead of decaying and may result in severe pressure and flow oscillations (phenomenon called resonance). In addition, the periodic dynamic force of the excitation generated by the vibration system incorporated into the roller's drum causes the pressure and flow in the entire system to oscillate at the period of the excitation, being named steady-oscillatory flow.

**Table 1:** Parameters identification from Eq. (8)

| Description of the parameters | Symbol | Formula |
|---|---|---|
| Natural pulsation of the hydro-mechanic system | $\omega_{MR}$ | $\frac{V_{oM}}{2\pi}\sqrt{\frac{2}{JC_h}}[s^{-1}]$ |
| Damping factor | $\zeta_{MR}$ | $\sqrt{\frac{J}{C_h}}\frac{2\alpha_{MR}+\chi_{MR}}{\frac{V_{0M}}{\pi}\sqrt{2}}$ $[-]$ |
| Disturbing factor due to the resistant torque at the working tool | $H_{MR}$ | $\frac{V_{0M}}{2\pi}\frac{M_E}{J}\frac{2}{C_h}$ $[N/m^2s^2]$ |
| Excitation magnitude | $\Pi_{MR}$ | $\frac{q_0\omega_I^2}{\pi C_h}\sqrt{1+\left(\frac{\chi_{MR}}{J\omega_I}\right)^2}$ $[N/m^2s^2]$ |
| Initial phase of the excitation | $\phi$ | $\phi=\varphi_0+arctg\frac{J\omega_I}{\chi_{MR}}$ $[rad]$ |

An analytical solution of the differential equation (8) has the expression

$$p = p_1 + p_2 = p_0 e^{-\zeta_{MR}\omega_{MR}t} sin\left(\omega_{MR}\sqrt{1-\zeta_{MR}}t\right) + p_s + p_0 sin(\omega_I t + \phi_0) \tag{9}$$

but, for the phenomenon analyzed in this paper presents interest only pressure that described the behavior of the working steady state, and then we used the analytical solution as the next form

$$p = p_s + p_r \sin(\omega_I t + \phi_0) \tag{10}$$

where $p_s$ is the static state system pressure and, respectively, $p_r$ is the overpressure due to the resonance phenomenon.

$$p_s = \frac{2\pi M_E}{V_{0M}}, \tag{11}$$

$$p_r = \frac{q_0}{\pi C_h}\frac{\mu^2\sqrt{1+\varepsilon^2}}{\sqrt{(1-\mu^2)^2+(2\zeta_{MR}\mu)^2}}. \tag{12}$$

We denote the relative damping of the hydro-mechanic system as $\varepsilon = \frac{\chi_{MR}}{J\omega_I}$ and the initial phase of the pressure as

$$\phi_0 = arctg\frac{tg\varphi_0\left[\varepsilon(1-\mu^2)+2\zeta_{MR}\mu\right]+(1-\mu^2)-2\varepsilon\zeta_{MR}\mu}{\varepsilon(1-\mu^2)+2\zeta_{MR}\mu tg\varphi_0[(1-\mu^2)-2\varepsilon\zeta_{MR}\mu]}. \tag{13}$$

## 4. Numerical scenarios simulation

The pressure resonance phenomenon, as highlighted by Eq. (12), corresponds to a similar phenomenon observed in mechanical systems. It is characterized by a sudden increase in pressure beyond the steady-state working value when the angular speed of the pump spindle matches the natural pulsation of the hydro-mechanical system, respectively: $\omega_I = \omega_{MR}$ when $\mu = 1$ and $\zeta_{MR} = 1$.
The pressure amplification is incorporated into the evidence through the magnitude factor

$$\Omega_p = \frac{p_r}{p_0} = \frac{\mu^2\sqrt{1+\varepsilon^2}}{\sqrt{(1-\mu^2)^2+4\zeta_{MR}^2\mu^2}}. \tag{14}$$

where $p_0 = q_0/(\pi C_h)$ represents the static pressure developed by a single piston in the pump.

Since the denominator in Eqn. (13) is the sum of squares, the magnitude factor $p_1$ remains finite for any value of the relative pulsation $\mu$. Pressure magnitude resonance occurs when the $\Omega_p$ factor reaches its maximum value. The resonance pulsation value is determined by nullifying the derivative of the $p_1$ magnitude factor with respect to $\mu$, leading to the following result:

$$\omega_I = \omega_{MR} \frac{1}{\sqrt{1-2\zeta_{MR}^2}} \text{ for } \zeta < \frac{1}{\sqrt{2}}. \tag{15}$$

In this case, the magnitude factor of the pressure resonance is

$$\Omega_{prez} = \frac{1}{2\zeta_{MR}} \sqrt{\frac{1+\varepsilon^2}{1-2\zeta_{MR}^2}}. \tag{16}$$

For $\mu$=1, as derived from Eqn. (13), the phase resonance can be defined as

$$\phi_0 = arctg \frac{a_0 - \varepsilon}{1 + a_0 \varepsilon}, \tag{17}$$

independent of the damping factor $\zeta_{MR}$, but influenced by the relative damping $\varepsilon$ and the $a_o$ factor. Figures 3 to 5 illustrate the variation laws for the $p_1$ magnitude factor, the magnitude factor at resonance, and the phase resonance, all corresponding to different values of the specific parameters: $\mu = 0 - 3$ ; $\varepsilon = 0 - 1{,}5$; $\zeta_{MR} = 0 - 0.5$; $a_0 = arctg(5\pi/7)$.

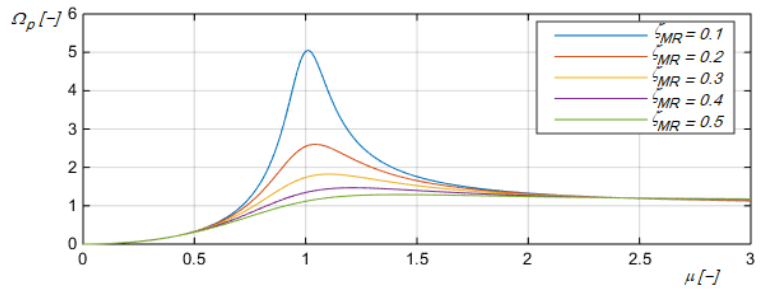


**Fig. 3.** The variation of $\Omega_{prez} - \mu$

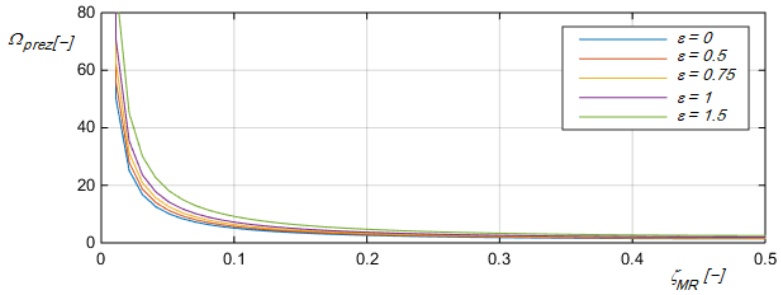


**Fig. 4.** The variation of $\Omega_{prez} - \zeta_{MR}$

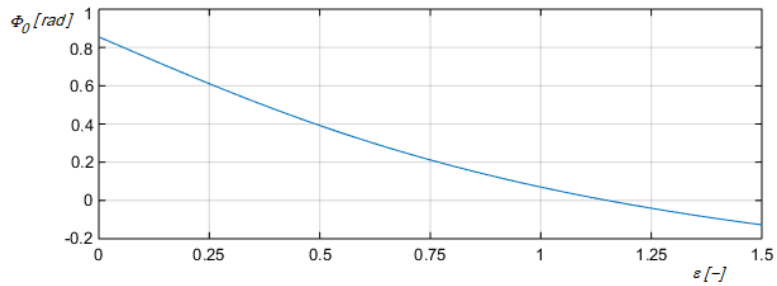


**Fig. 5.** The variation of $\phi_0 - \varepsilon$.

## 5. Conclusions

Based on the analysis of the "pressure resonance phenomenon" in hydraulic driving systems with rotary motors, the following conclusions can be drawn:

a) The observed phenomenon highlights the functional instability of hydraulic driving systems with rotary motors, particularly in predominant dynamic operating states, such as movement-driving systems for technological equipment and working tools. This instability arises due to variations in the hydraulic pump flow of the system. The primary source of this instability cannot be effectively identified using conventional methods provided by automated system analysis theory, which are commonly applied for stability evaluations of such driving systems.
b) The analysis reveals that the system's pressure gain factor can exceed twice the value of the static pressure for typical damping factor values ($\zeta_{MR}$: 0.1 to 0.3), which are common in standard hydraulic driving system components (see Figure 3). In a system operating with stable pressure values of 250–300 bar, the resonance phenomenon can briefly generate peak pressure values ranging from 750 to 1500 bar. These extreme pressure levels pose significant risks, leading to overloading of hydraulic components, reduced lifespan and durability, and ultimately, premature failure of the hydraulic system components.
c) Another effect of the analyzed phenomenon is the increased acoustic level of the pump. During very short time intervals (0.01–0.02 seconds), the pump operates under pronounced overloads, approximately 3 to 4 times the nominal load. During these periods, the system's overload protection elements are activated, further contributing to the rise in noise levels.
d) The resonance gain factor ($\Omega_{prez}$), shown in Figure 4, representing the maximum pressure magnitude of the system, can easily reach values 20 to 50 times greater than the static pressure for damping factors below 0.1. These values show slight variation with the relative damping ($\varepsilon$) of the hydro-mechanical system. This highlights the resonance phenomenon, bringing it into the typical operating range of a hydraulic driving system.
e) The phase resonance illustrated in Figure 5 are minimal impact on the operating state of the system.

The study concludes by highlighting the instability phenomenon in hydraulic driving systems caused by flow variations within system components. Effective methods to reduce or eliminate this harmful phenomenon will be proposed in future studies conducted by the author.

**References**

[1] Palikhe, Sunit, Jianxu Zhou, and Khem Prasad Bhattarai. "Hydraulic Oscillation and Instability of a Hydraulic System with Two Different Pump-Turbines in Turbine Operation." *Water* 11, no. 4 (2019): 692.
[2] Lea, James F., Henry V. Nickens, and Mike R. Wells. *Gas Well Deliquification*. 2nd Edition. Gulf Professional Publishing, 2008. "Chapter 9 - Hydraulic pumping", pp. 241-281.
[3] Akers, Arthur, Max Gassman, and Richard Smith. *Hydraulic power system analysis*. 1st Edition. Boca Raton, CRC Press, 2006. "Chapter 9 - Axial piston pumps and motors", pp. 241-254.
[4] Zhou, J.X., B.W. Karney, M. Hu, and J.C. Xu. "Analytical study on possible self-excited oscillation in S-shaped regions of pump-turbines." *Proceedings of the Institution of Mechanical Engineers, Part A: Journal of Power and Energy* 225, no. 8 (2011): 1132–1142.
[5] Wylie, E.B., and V.L. Streeter. *Fluid Transients in Systems*. Englewood Cliffs, Prentice Hall, 1993.
[6] Wylie, E.B. "Resonance in Pressurized Piping Systems." *Journal of Basic Engineering* 87, no. 4 (1965): 960–966.
[7] Chaudhry, M.H. *Applied Hydraulic Transients*. Berlin, Springer, 2013.
[8] Suo, L., and E.B. Wylie. "Impulse Response Method for Frequency-Dependent Pipeline Transients." *Journal of Fluids Engineering* 111, no. 4 (1989): 478–483.
[9] Kim, S. "Impedance matrix method for transient analysis of complicated pipe networks." *Journal of Hydraulic Research* 45, no. 6 (2007): 818-828.
[10] Axinti, G., S. Nastac, A. Axinti, and A. Potarniche. "The analysis of the dynamic response of the hydrostatic driving systems in a closed circuit." *The Annals of "Dunarea de Jos" University of Galati*, Fascicle XIV Mechanical Engineering (2002): 11-16.
[11] Axinti, G., S. Nastac, C. Debeleac, and A. Axinti. "About the Presure Resonance Phenomenon in the Hydraulic Driving Systems with Rotative Motor." *Romanian Journal of Acoustics and Vibration* 2, no. 1 (March 2005): 27-32.

# FLUIDAS

## NATIONAL PROFESSIONAL ASSOCIATION OF HYDRAULICS AND PNEUMATICS IN ROMANIA


fluidas@fluidas.ro